

CRUSTAL CALIBRATION OF THE LARGE APERTURE SEISMIC

ARRAY (LASA), MONTANA

by

David H. Warren, John H. Healy, Joyce Bohn, and P. Anthony Marshall

National Center for Earthquake Research  
U.S. Geological Survey  
Menlo Park, California 94025

U.S. Geological Survey

OPEN FILE REPORT 72-444

This report is preliminary and has  
not been edited or reviewed for  
conformity with Geological Survey  
standards and nomenclature.

Worked performed under ARPA Order No. 923, Amendments 3 and 5.

# Crustal Calibration of the Large Aperture Seismic Array (LASA), Montana <sup>1/</sup>

by

David H. Warren, John H. Healy, Joyce Bohn, and P. Anthony Marshall

National Center for Earthquake Research  
U.S. Geological Survey, Menlo Park, California

## INTRODUCTION

The need for crustal calibration of the LASA site was shown by studies of traveltime residuals for teleseismic earthquakes observed at the array. Greenfield and Sheppard (1969) and Chiburis (1966) stated the problem and suggested methods for correcting the arrival times of distant earthquakes. Chiburis tabulated average residuals from 637 earthquakes in different regions. The traveltimes of the events were normalized to the center seismometer of the AO cluster of LASA by subtracting that residual from all residual values. Two points are clear from an examination of these data. First, the magnitude of the largest residuals increases with the distance of the observations from the AO cluster, reaching the largest values in the F ring (Table 1), where the anomalies range from +0.883 to -1.011 sec. Second, the time residuals vary with the azimuth and distance of the seismic event. If the time residuals arose only from variations of crustal structure, a very complex crustal model would be required. But the residuals may arise from a number of causes that can be classified as follows:

1. Structural variations in the upper crust, such as variation in the thickness of sedimentary basins underlying LASA.

---

<sup>1/</sup> Work performed under ARPA Order No. 923, Amendments 3 and 5.

Table 1

Maximum residuals for each LASA station from the data of Chiburis (1966)

<i>LASA Station</i>	<i>Maximum Residuals, Sec</i>	
B1	-0.152	+0.117
B2	-0.296	+0.099
B3	-0.087	+0.119
B4	-0.145	+0.239
C1	-0.193	+0.391
C2	-0.341	+0.187
C3	-0.345	+0.083
C4	-0.226	+0.314
D1	-0.614	+0.380
D2	-0.614	+0.011
D3	-0.403	+0.233
D4	-0.426	+0.830
E1	-0.432	+0.925
E2	-0.600	+0.215
E3	-0.623	+0.180
E4	-0.717	+0.550
F1	-0.537	+0.883
F2	-1.011	+0.123
F3	-0.841	+0.238
F4	-0.923	+0.738

2. Structural variations in the intermediate crust.
3. Variations in total crustal thickness.
4. Structural variations in the upper mantle under LASA.
5. Structural variations in the deep mantle.
6. Structural variations of the upper mantle in the source region.
7. Errors in location or origin time of the seismic events.

The various possible sources of the measured arrival-time residuals cannot be distinguished from the earthquake data alone. In this paper we attempt to identify and separate the sources of error caused by crust and upper mantle structure under LASA.

The crustal structure of Montana was studied by a number of groups between 1956 and 1960, as described by Meyer et al. (1961) and by Asada and Aldridge (1966). The locations of these seismic profiles with respect to the LASA Array are shown in Figure 1. McCamy and Meyer (1964) summarized these results in a fence diagram (Fig. 2). Their summary shows a reasonable agreement in the gross structure of the earth's crust as determined along different profiles, but also reveals marked differences in the internal structure of the crust. McCamy and Meyer were uncertain how to interpret the data because of these differences, which they felt might be related either to changes in crustal properties or to the inadequacy of the method. Our results tend to confirm major features of the interpretation shown in Figure 2 and indicate that the LASA region does have changes in the internal structure of the crust such as those discovered by the 1956-1960 work.

In a 1966 profile recorded in the NE-SW direction across the center of the LASA array (Fig. 1), Borchardt and Roller (1967) found marked

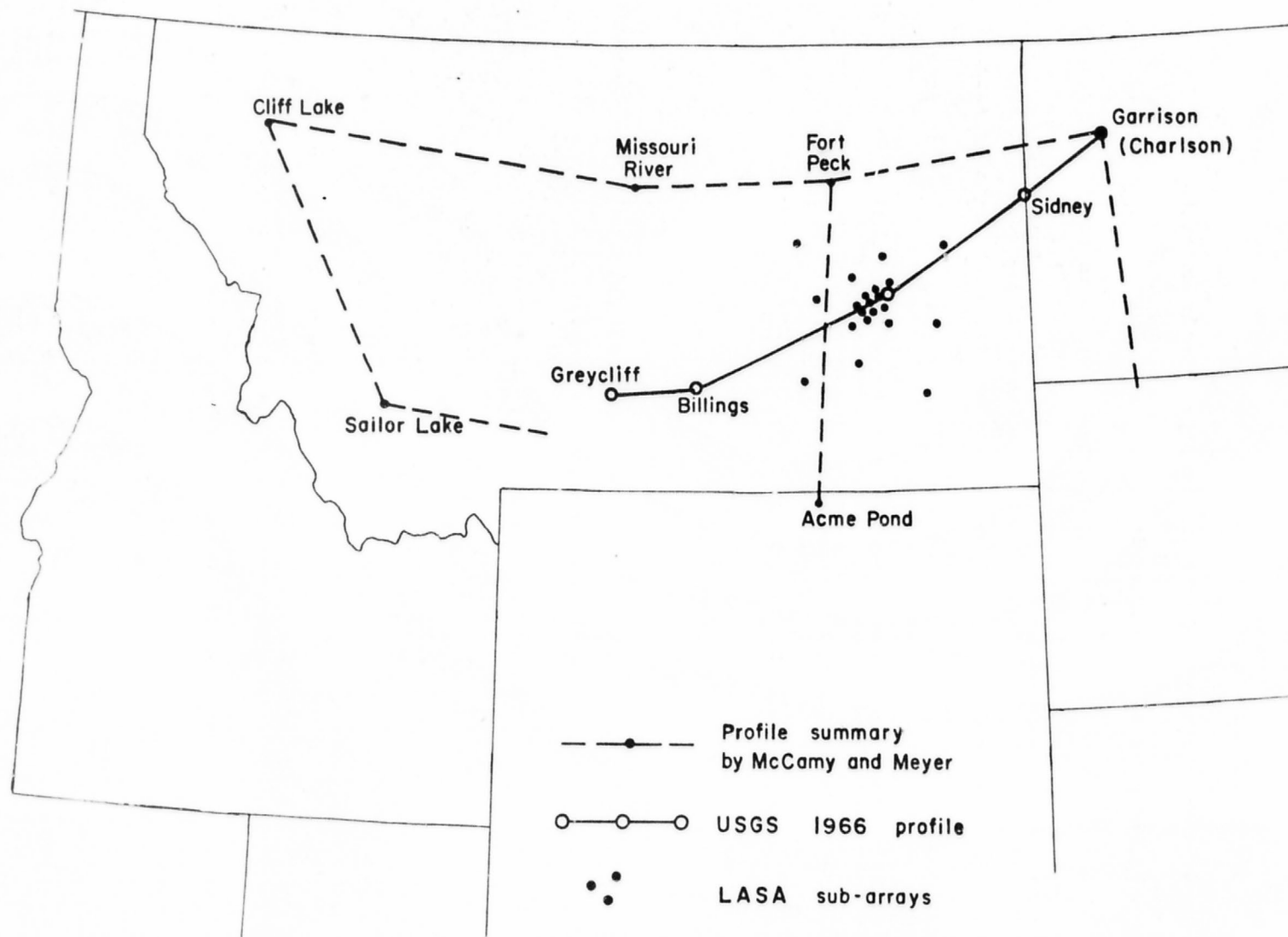


Figure 1. Index map of previous seismic refraction surveys. Shotpoint names are labeled and coded.

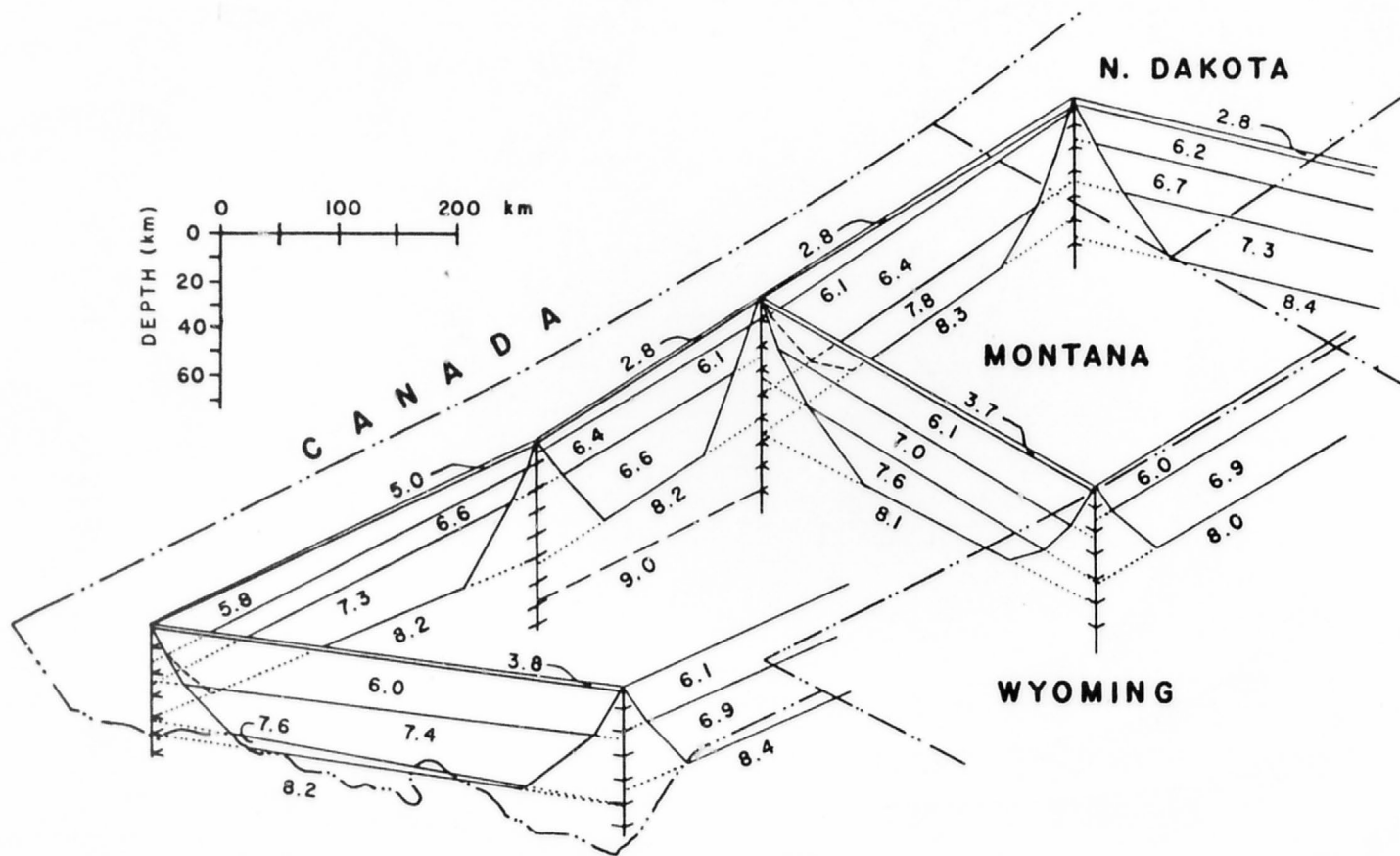


Figure 2. Fence diagram showing summary of crustal models as given by McCamy and Meyer. Values of average "layer" velocity measurements are given in km/sec.

changes in crustal structure within the array (Fig. 3), which confirmed the need for a detailed seismic study of the crust under LASA.

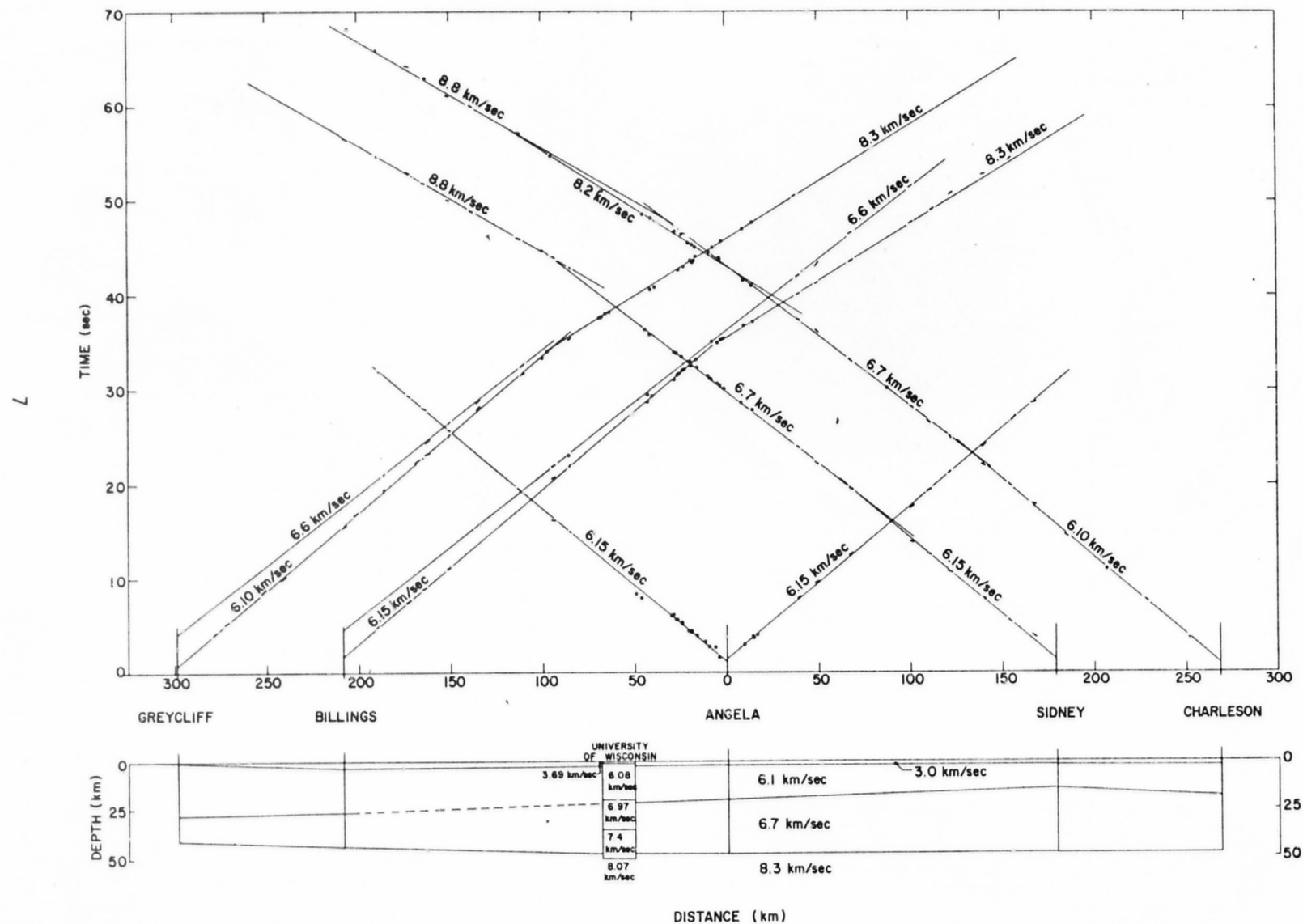


Figure 3. Seismic refraction profile through LASA along a SW-NE line. Survey was run in 1966 by the U.S. Geological Survey. (Borcherdt and Roller, 1966).

## DESCRIPTION OF DATA

Three types of seismic instrumentation were used in this study. The USGS seismic refraction recording trucks described by Warrick et al. (1961) were used to establish short arrays along profile lines, with each truck having six vertical seismometers spaced at 1/2-km intervals along a 2-1/2-km spread and two horizontal seismometers placed near the center of each array. Twenty portable seismic stations (described by Eaton et al. (1970)) having either one vertical or one vertical and two horizontal geophones were laid out in two rings surrounding the LASA array. These instruments were operated for a period of about two months and recorded a number of teleseisms as well as the arrivals from the high-explosive shots fired in the calibration program. The standard LASA array stations were also incorporated into the analysis and were found to be very useful for the identification of secondary phases.

Fifteen high-explosive shots of either 4,000 or 20,000 pounds were detonated in the experiment and recorded on the expanded array of seismic stations (Fig. 4 and Tables 2 and 3). At the time of the 1968 experiment there were 15 geophones at 20 of the LASA clusters and 25 geophones at an expanded cluster, a total of 325 seismic traces. In addition, the 20 portable seismic stations and 13 recording trucks produced 33 seismograms for each shot. Even when only a single geophone was used in each subarray cluster, there were 810 seismograms to be analyzed and correlated. These data provided an unusual opportunity to examine the complexities of crustal structure that are normally left unresolved when only a limited amount of data along a single line is available for analysis.

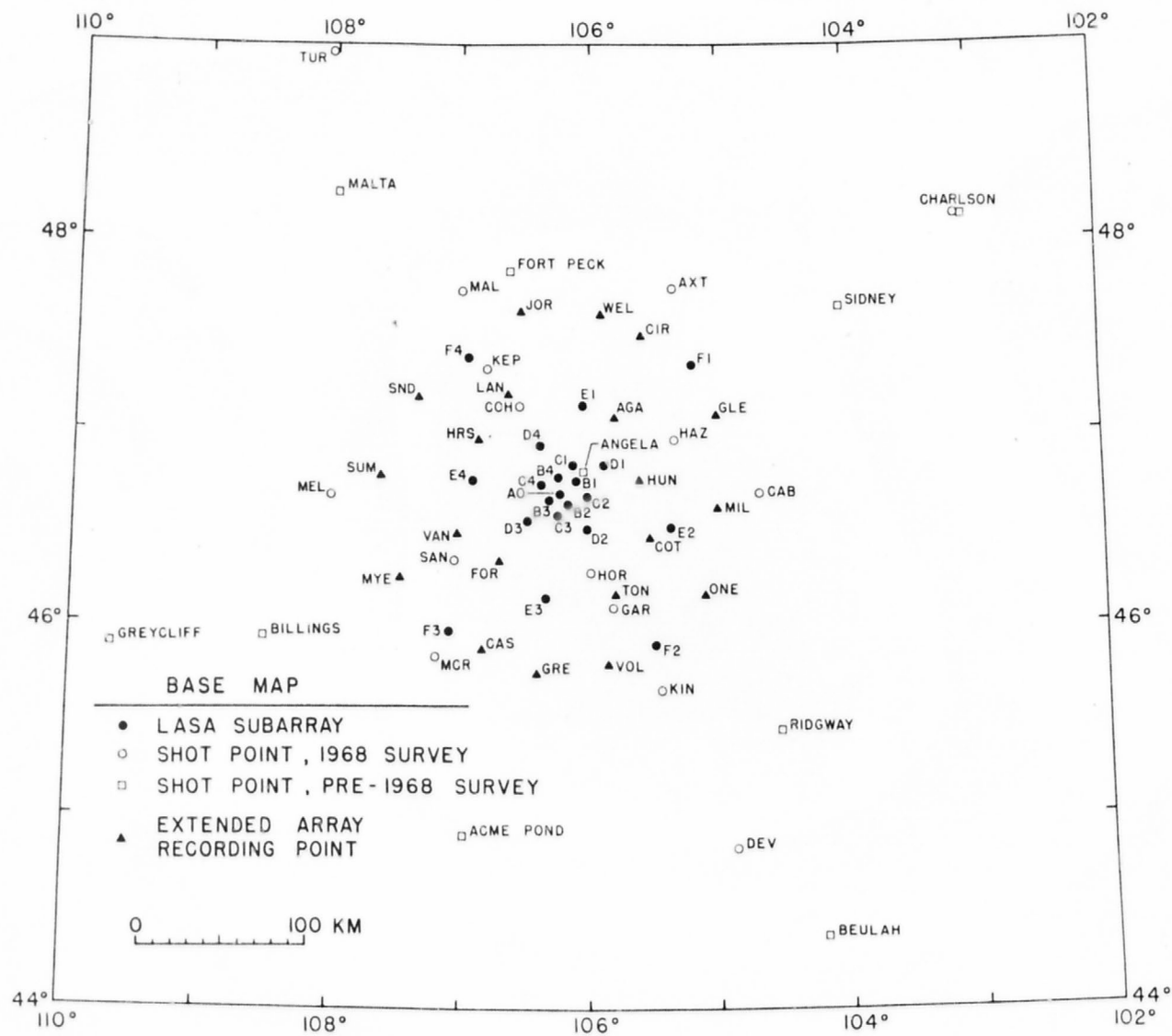


Figure 4. Index map of shotpoints, recording locations, and LASA subarrays.

Table 2

## Shotpoint Data

<i>Shotpoint Name</i>	<i>Abbreviation</i>	<i>Date Sept 1968</i>	<i>Time (MDT)</i>	<i>Lat. N</i>	<i>Long. W</i>	<i>Shot Size (lbs)</i>	<i>Comments</i>
Axtell	AXT	13	05:30:00.20	47°45.26'	105°20.37'	3,960	two 200' drill holes
Cabin Creek	CAB	11	06:30:00.06	46°41.14'	104°40.80'	4,020	two 210' drill holes
Charlson	CHA	13	06:00:09.54	48°07.48'	103°06.22'	20,650	55' water
Cohagen	COH	12	06:30:00.39	47°08.80'	106°32.66'	4,020	two 205' drill holes
Devils Tower	DEV	10	05:00:00.16	44°50.32'	104°52.36'	20,040	ten 210' drill holes
Garland	GAR	12	05:00:00.41	46°05.55'	105°48.89'	4,020	two 210' drill holes
Hazel	HAZ	10	06:30:00.11	46°58.20'	105°20.15'	3,960	two 210' drill holes
Horton	HOR	12	06:00:00.49	46°16.46'	105°59.18'	4,020	two 210' drill holes
Keplerville	KEP	10	05:59:59.81	47°20.36'	106°48.01'	4,020	two 205' drill holes
Kingsley	KIN	11	05:00:00.71	45°39.95'	105°26.64'	4,020	two 210' drill holes
Maloney Hill	MAL	13	06:29:59.40	47°44.78'	106°59.87'	4,040	30' water
McRae	MCR	11	05:30:00.59	45°50.25'	107°11.23'	4,020	two 205' drill holes
Melstone	MEL	12	05:30:00.42	46°40.78'	108°00.49'	4,020	two 205' drill holes
Sanders	SAN	10	05:30:00.64	46°20.34'	107°02.71'	4,020	two 205' drill holes
Turner	TUR	11	05:59:59.73	48°58.26'	108°02.96'	20,040	three 150' drill holes two reopened drill holes

Table 3

## Recording Station Locations

<i>Station Name</i>	<i>Abbreviation</i>	<i>Lat. N</i>	<i>Long. W</i>	<i>Elevation (ft)</i>	<i>Recording Unit*</i>
Axtell	AXT	47°45.26'	105°20.37'	2400	R
Cabin Creek	CAB	46°41.14'	104°40.80'	2550	R
Charlson	CHA	48°07.48'	103°06.22'	1800	S
Cohagen	COH	47°08.80'	106°32.66'	2850	R
Devils Tower	DEV	44°50.32'	104°52.36'	3800	S
Garland	GAR	46°05.55'	105°48.89'	2800	R
Hazel	HAZ	46°58.20'	105°20.15'	2800	R
Horton	HOR	46°16.46'	105°59.18'	2600	R
Keplerville	KEP	47°20.36'	106°48.01'	2700	R
Kingsley	KIN	45°39.95'	105°26.64'	3100	R
Maloney Hill	MAL	47°44.78'	106°59.87'	2230	R
McRae	MCR	45°50.25'	107°11.23'	3600	R
Melstone	MEL	46°40.78'	108°00.49'	2880	R
Sanders	SAN	46°20.34'	107°02.71'	2660	R
Turner	TUR	48°58.26'	108°02.96'	2800	S
Agate Flat	AGA	47°05.12'	105°48.37'	2950	PS
Castle Rock	CAS	45°52.65'	106°49.60'	3400	PS
Circle	CIR	47°30.90'	105°36.26'	2500	PS
Cottonwood Creek	COT	46°27.53'	105°31.06'	2800	PS
Forsyth	FOR	46°20.74'	106°41.79'	2900	PS
Glendive	GLE	47°06.23'	105°00.20'	2800	PS
Greenleaf Creek	GRE	45°45.03'	106°24.02'	3200	PS
Horse Creek	HRS	46°58.12'	106°51.56'	3010	PS
Hunter Creek	HUN	46°45.92'	105°36.06'	2550	PS
Jordan	JOR	47°38.26'	106°32.39'	2750	PS
Langs Fork	LAN	47°12.03'	106°38.13'	2780	PS
Mildred	MIL	46°36.64'	105°00.10'	2600	PS
Myers	MYE	46°15.01'	107°28.04'	2960	PS
O'Neil	ONE	46°09.28'	105°07.74'	2750	PS
Sand Springs	SND	47°11.55'	107°20.18'	3160	PS
Sumatra	SUM	46°46.44'	107°37.42'	3180	PS
Tongue River	TON	46°09.93'	105°47.33'	2500	PS
Vanada	VAN	46°28.52'	107°01.57'	3060	PS
Volborg	VOL	45°48.28'	105°51.04'	3250	PS
Weldon	WEL	47°37.68'	105°54.97'	2650	PS

---

\* R = truck-mounted 8-channel recording system

S = truck-mounted 4-channel recording system

PS = portable 1 or 3-channel magnetic tape recording system

(Cont'd...)

Table 3. Recording Station Locations (Cont'd)

<i>Station Name</i>	<i>Abbreviation</i>	<i>Lat. N</i>	<i>Long. W</i>	<i>Elevation (ft)</i>	<i>Recording Unit*</i>
LASA A0 A0	A0	46°41.32'	106°13.33'	2940	L
LASA B1 A0	B1	46°45.13'	106°05.50'	2980	L
LASA B2 A0	B2	46°38.10'	106°09.77'	2780	L
LASA B3 A0	B3	46°39.55'	106°19.02'	2870	L
LASA B4 A0	B4	46°46.08'	106°14.43'	2850	L
LASA C1 A0	C1	46°50.37'	106°07.65'	2860	L
LASA C2 A0	C2	46°40.17'	106°00.72'	3060	L
LASA C3 A0	C3	46°34.45'	106°14.98'	2740	L
LASA C4 A0	C4	46°44.12'	106°22.43'	3010	L
LASA D1 A0	D1	46°50.37'	105°53.40'	2990	L
LASA D2 A0	D2	46°30.18'	106°00.65'	2770	L
LASA D3 A0	D3	46°32.98'	106°28.82'	3130	L
LASA D4 A0	D4	46°56.52'	106°23.00'	2840	L
LASA E1 A0	E1	47°09.77'	106°03.35'	2750	L
LASA E2 A0	E2	46°30.77'	105°21.88'	2500	L
LASA E3 A0	E3	46°08.97'	106°20.05'	3000	L
LASA E4 A0	E4	46°45.63'	106°54.85'	3130	L
LASA F1 A0	F1	47°22.25'	105°11.25'	2930	L
LASA F2 A0	F2	45°54.57'	105°29.12'	2980	L
LASA F3 A0	F3	45°58.37'	107°04.90'	3250	L
LASA F4 A0	F4	47°24.67'	106°56.60'	2820	L

---

\* L = recording element of LASA

## SEISMIC PHASES

An important step in the interpretation of seismic refraction data is the identification of the phases whose traveltimes can be used to determine the crustal and upper mantle structure. This involves the recognition of bursts of seismic energy that can be correlated from record to record and can be described in terms of an arrival time-distance-graph. Record sections referred to in the following paragraphs are in the Appendix.

Surface Layer. We have only limited information on the seismic waves propagating within 10 km of each shot-point. These data can be predicted from the available well-velocity information with sufficient accuracy for our purposes, and we will not discuss these phases further.

Phase  $P_g$ . The most prominent and best correlated phase on the seismograms is the  $P_g$  phase, which is first observed at about 10 km and which can be followed out to distances of 50 or 100 km from a shot-point. Frequently, a single peak or trough can be traced across this entire distance range with little ambiguity. This phase is used to determine seismic delays introduced by near-surface layers, and its properties will be discussed in detail in the sections dealing with that part of the interpretation.

Phases PP, PPP, and PPPP. A prominent series of arrivals follow  $P_g$  in the range between 20 and 60 km. They are similar to PP, PPP, and PPPP of earthquake seismology. These arrivals repeat at a little more than one-second intervals for as many as six times. They are very clearly illustrated on the section from Horton 25, and are consistent with a

multiply reflected phase traveling in the lower part of the sedimentary section at the top of the crystalline rocks. At any given distance each successive repetition has a slightly slower apparent velocity, which is expected if each of these phases represents penetration to a slightly shallower depth (Fig. 5).

To test this interpretation, we picked the first prominent trough and determined an apparent velocity and intercept time using the data on four sections: Horton 25, Horton 26, Axtell 3, and Cohagen 14. A structural model was computed for each set of intercept times and apparent velocities (Table 4, Fig. 6). Surficial layering of 2.0, 3.0, and 4.0 km/sec was assumed. Major features of the models agree reasonably well with the structure taken from four velocity surveys in deep wells (Fig. 7) (Brown and Poort, 1965). These phases probably account for most of the compressional wave energy on the seismogram in the distance range between 20 and 60 km and obscure any phases that might be reflected from deeper crustal layering in the region.

Phase  $S_g$ . A prominent  $S_g$  phase can be observed on a number of record sections close to the shot-point. The onset of  $S_g$  travels with a speed of about 2.8 km/sec and is followed by a complex series of arrivals lasting for 4 to 10 seconds. Some portions of this phase have a dispersed character suggesting a type of surface-wave propagation. We tried to produce group and phase-velocity dispersion curves for these data, and we attempted to match these dispersion curves with lower-mode Rayleigh waves calculated from models appropriate for the seismic velocities at LASA. The group- and phase-velocities predicted by the model are much lower than those suggested by the experimental data. We therefore conclude that this phase cannot be

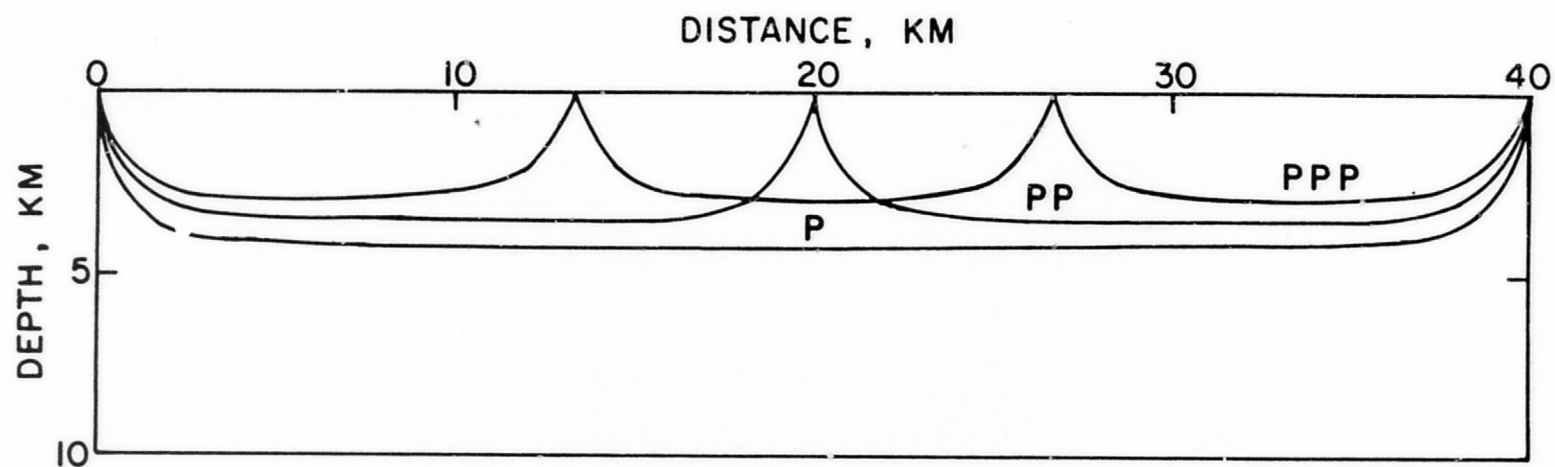


Figure 5. Ray paths for multiply refracted phases in uppermost crust. The paths are shown for P, PP, and PPP.

Table 4

## Shallow Structure from Multiply-Refracted Events

<u>Layer No.</u>	<u>Intercept</u>	<u>Apparent</u>	<u>Computed</u>	
	<u>(sec)</u>	<u>Velocity (km/sec)</u>	<u>Thickness (km)</u>	<u>Depth (km)</u>
Assumed Surficial Layers				
1	0.00	2.0	0.80	0.00
2	0.60	3.0	0.69	0.80
3	1.00	4.0	-	1.49
Horton No. 25 N25°W				
3	1.00	4.0	0.12	1.49
4	1.17	5.42	0.13	1.61
5	1.19	5.57	0.25	1.74
6	1.22	5.70	-0.08	1.99
7	1.23	5.82	1.73	1.91
8	1.39	6.0	2.50	3.64
9	1.81	6.4		6.14
Horton No. 26 N15°E				
3	1.00	4.0	-0.05	1.49
4	1.11	5.35	-0.39	1.44
5	1.09	5.42	0.72	1.05
6	1.13	5.51	0.18	1.76
7	1.19	5.82	1.44	1.94
8	1.39	6.17		3.39
Cohagen No. 14 S25°E				
3	1.00	4.0	0.45	1.49
4	1.30	5.63	0.36	1.95
5	1.35	5.85	3.68	2.30
6	1.52	5.90	0.37	5.98
7	1.96	6.39		6.35

Table 4 (cont'd)

## Shallow Structure from Multiply-Refracted Events

<u>Layer No.</u>	<u>Intercept (sec)</u>	<u>Apparent Velocity (km/sec)</u>	<u>Computed</u>	
			<u>Thickness (km)</u>	<u>Depth (km)</u>
Axtell No. 3 S5°W				
3	1.00	4.0	0.64	1.49
4	1.35	5.45	0.94	2.14
5	1.44	5.59	0.08	3.08
6	1.54	5.95	2.06	3.15
7	1.85	6.35		5.21

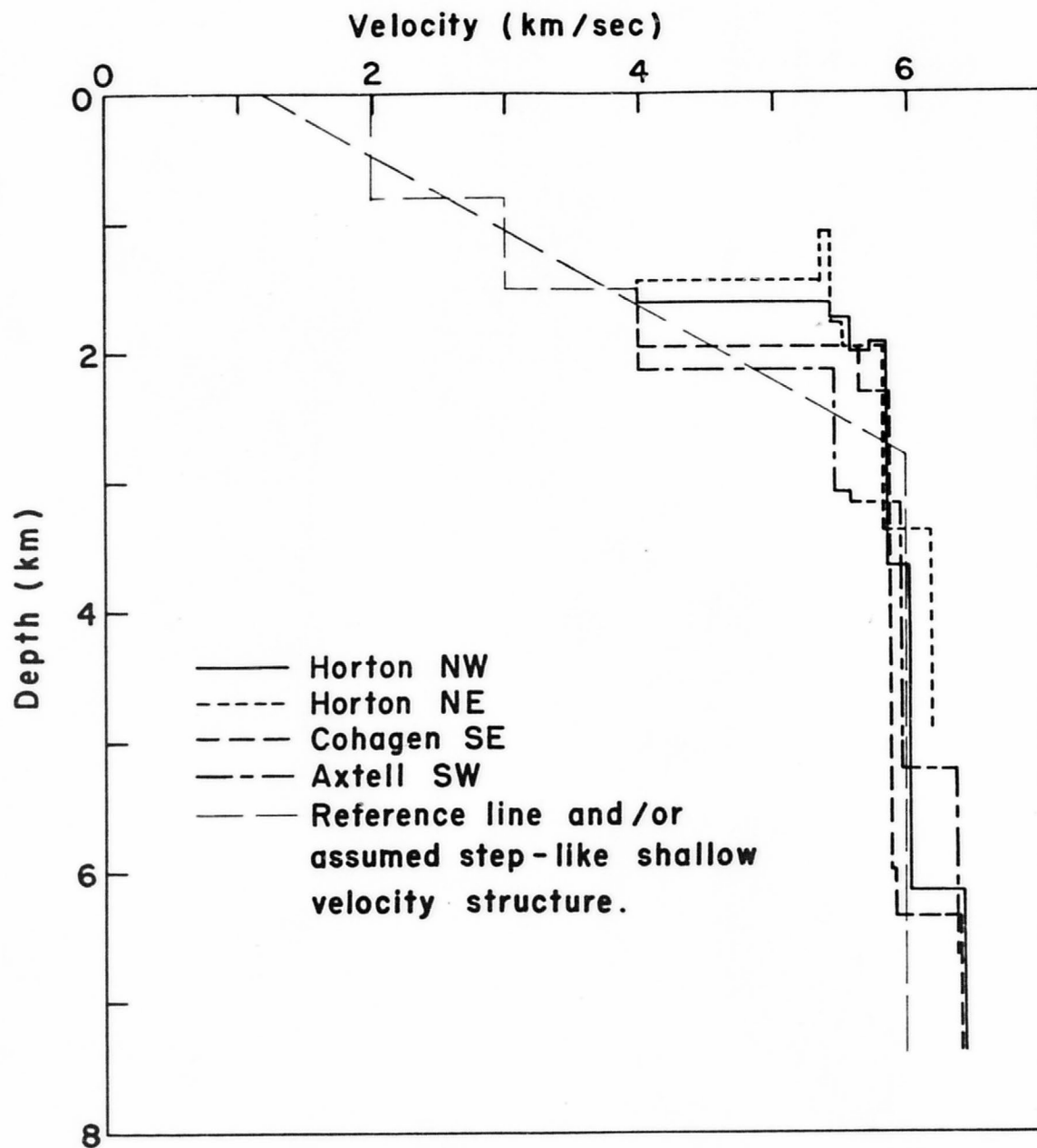


Figure 6. Shallow crustal structure as deduced from multiply refracted phases. Possible transitions from lower sedimentary rocks to granitic basement are shown for several shotpoints.

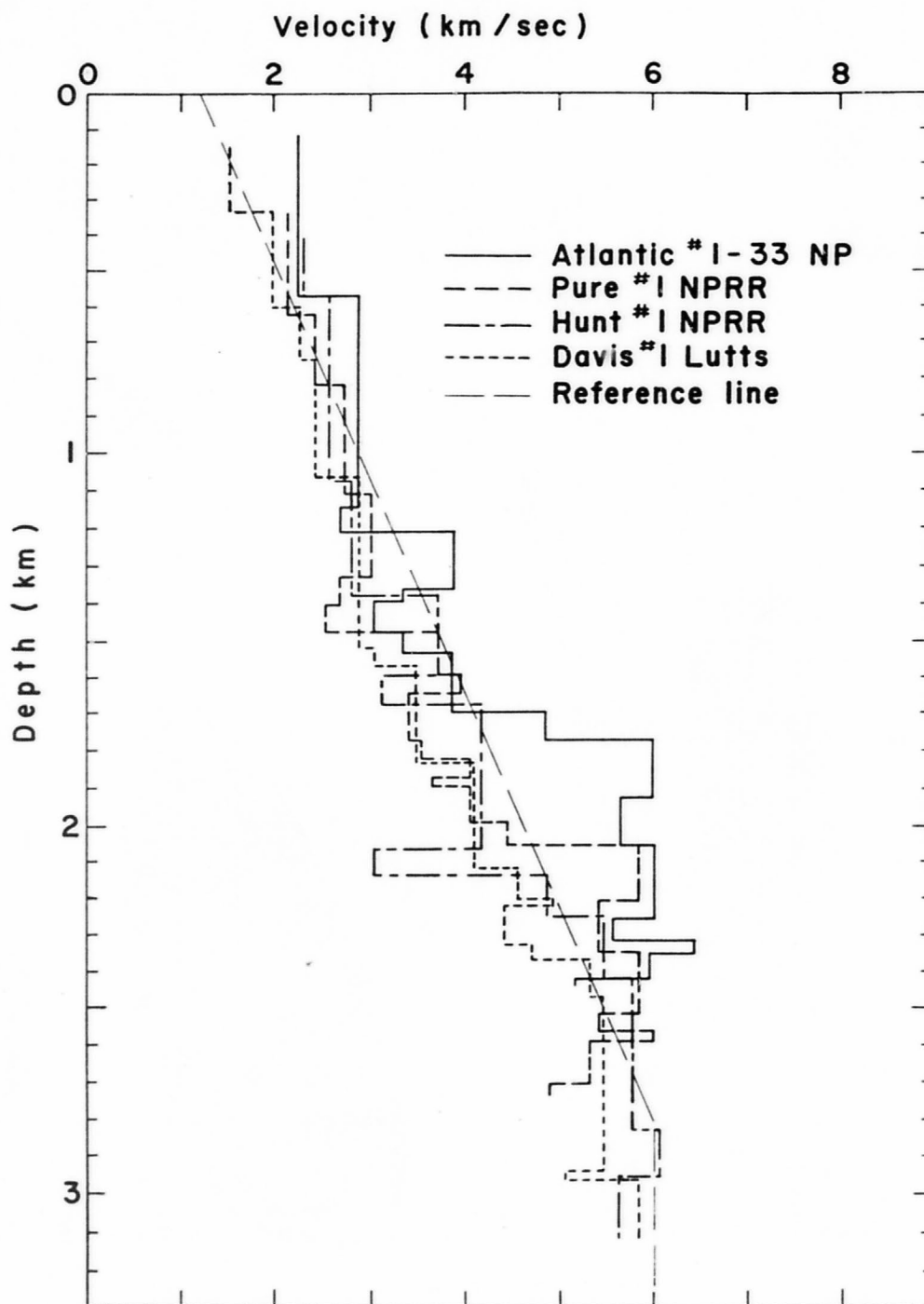


Figure 7. Velocity logs of sedimentary rocks. Four oil wells were surveyed to produce these velocity measurements. The reference lines are the same as in Fig. 6.

explained by lower-mode Rayleigh wave propagation.

Lines drawn through the leading edge of the phase and through the origin on the record sections for Cohagen and Horton result in velocities of 2.70 and 2.85 km/sec, respectively. If these velocities are associated with the first high-velocity P phase (refracted along the lower sedimentary rocks with velocity of 5.8 km/sec), Poisson's ratio can be calculated from

$$\sigma = \frac{C^2 - 2}{2(C^2 - 1)},$$

where C is the ratio of compressional to shear wave velocity. The values of  $\sigma$  are 0.36 from Cohagen and 0.34 from Horton, which are not uncommon for limestone sedimentary rocks, as pointed out by Geyer and Martner (1969).

Phase P\*. From deeper in the crust a phase with a velocity ranging from 6.6 to 7.0 km/sec emerges as a first arrival. The reflected branch  $P_i P$  is occasionally prominent near the critical angle. See, for example, record sections Cabin Creek 7 and Kingsley 30.

Sometimes the transition from the  $P_g$  to  $P^*$  phase is not clear. Measurements of the apparent velocities of first-arrivals (described later) show values of about 6.4 km/sec in some locations (Fig. 13). Good examples are seen on the record sections Axtell 1, Axtell 3, and Maloney Hill 34. There are two possible interpretations for this high apparent velocity: the velocity in the upper crust may approach 6.4 km/sec above the transition to lower crust; or, these velocities may represent structural undulation in the top of the intermediate layer, which rises to shallower depths. In either case, the variation of the apparent velocity of this

phase implies lateral change in velocity structure within the mid-crust.

Phase  $P_m$  - Reflection from the M discontinuity. This phase is a prominent secondary arrival on the seismograms at distances greater than 100 km, and it is used extensively in the interpretation. Its amplitude increases abruptly with distance from the shot-point and then breaks into two branches: the  $P_n$  arrival refracted below the M discontinuity (M), which is difficult to follow, and a wide-angle reflection traveling in an intermediate layer with velocity between 6.6 and 7.0 km/sec. This wide-angle reflection is beautifully displayed on the sections from Turner 48 and Charlson 11. The reflection near the critical point is apparent on many of the record sections, and it has been used to map the M discontinuity.

Phases from the Upper Mantle. The  $P_n$  phase is a weak first arrival at distance ranges greater than about 200 km, as illustrated by the Charlson, Devils Tower, and Turner shotpoints.

There is some evidence of a second transition zone below that horizon which would be normally identified as the M discontinuity. Two lines of evidence suggest this transition: the velocity of rocks immediately below the 6.7 layer are apparently lower than 8 km/sec, but the velocities indicated by distant events suggest velocities considerably higher than 8 km/sec for the upper mantle. On a few of the sections there is a suggestion of a reflected phase which sometimes seems appropriate for a deeper transition. For example, the sections from Devils Tower 17a and 19 show a prominent secondary phase in the distance range 250 to 350 km. To distinguish, the arrivals have here been called  $P_{n1}$  and  $P_{n2}$ .

## AVERAGE CRUSTAL MODEL

To illustrate the phases just described, we now introduce an average crustal structure which will be deduced in succeeding sections (Fig. 8), together with traveltimes calculated for this average model and a ray path diagram showing the propagation paths in this idealized model (Fig. 9).

## INTERPRETATION OF FIRST ARRIVALS

The arrival time of the first phase to appear on the seismogram is the least ambiguous part of the data. Questions may arise about the exact time of arrival if the phase is weak, but this is not as serious as the ambiguity in the identification and timing of secondary phases. A complete description of the analysis of first arrivals is contained in the report by Healy et al. (1969). We use the first arrivals to delineate the gross structure and then use the secondary phases to modify the details of the structure.

A composite plot of all first-arrival data (Fig. 10) reveals a fairly tight alignment of arrival times in the distance range 0 to 110 km followed by a gradually increasing scatter of data about the average arrival times between 110 and 200 km. A large increase in the scatter of arrival times occurs at distances greater than 200 km, where  $P_n$  emerges as the first arrival. Some of the arrival times shown on Figure 10 are obviously "bad." All picks were rechecked and represent real arrivals, but some are from a source other than the intended shot-point. We chose to include all objective picks at first so as not to bias the statistics by subjective judgments; but the poor picks were removed later in the computer program used to analyze the data.

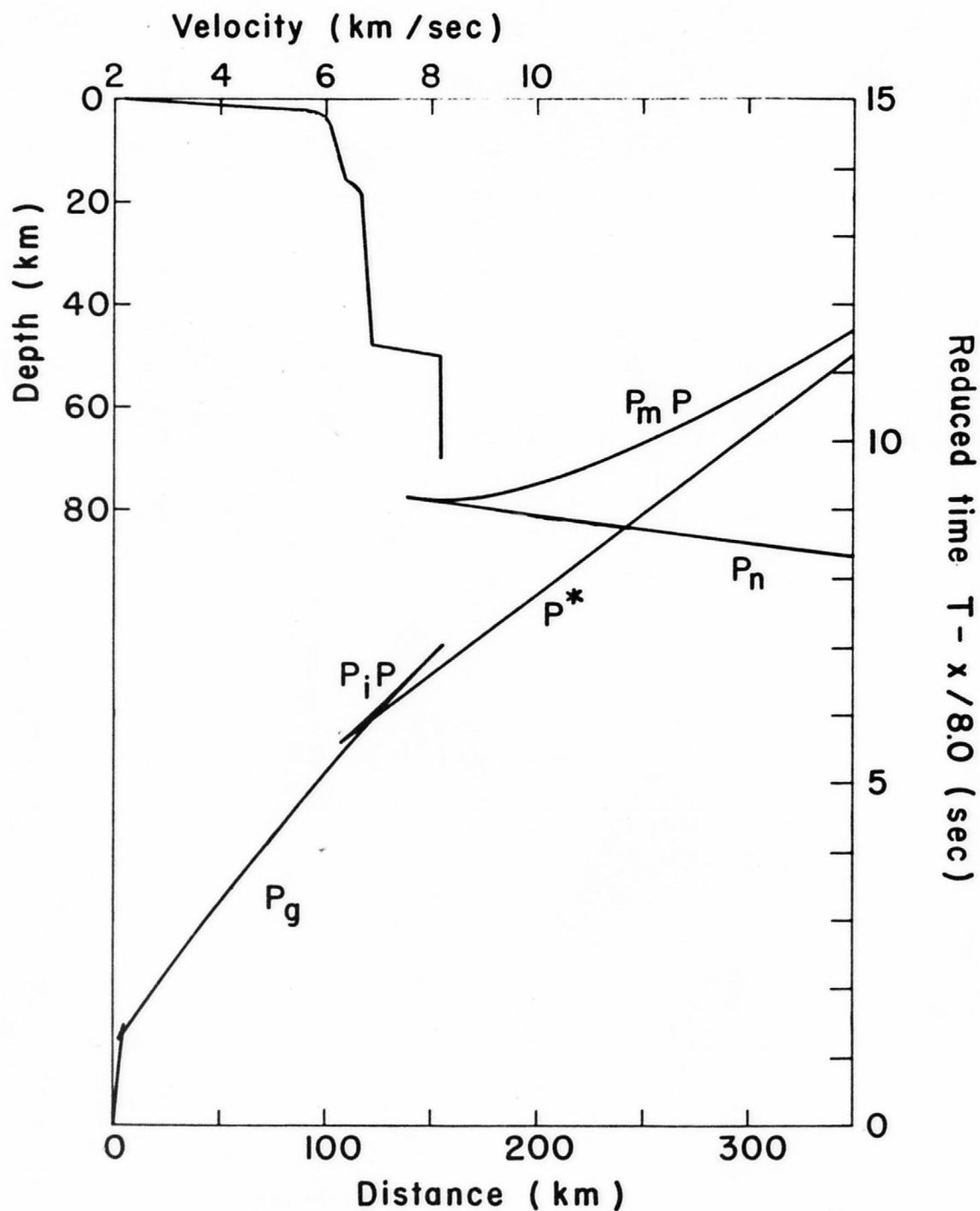


Figure 8. Average crustal model. The complete average traveltime curve is shown in reduced form, and the velocity-depth function that produces the curve is shown in the upper left corner.

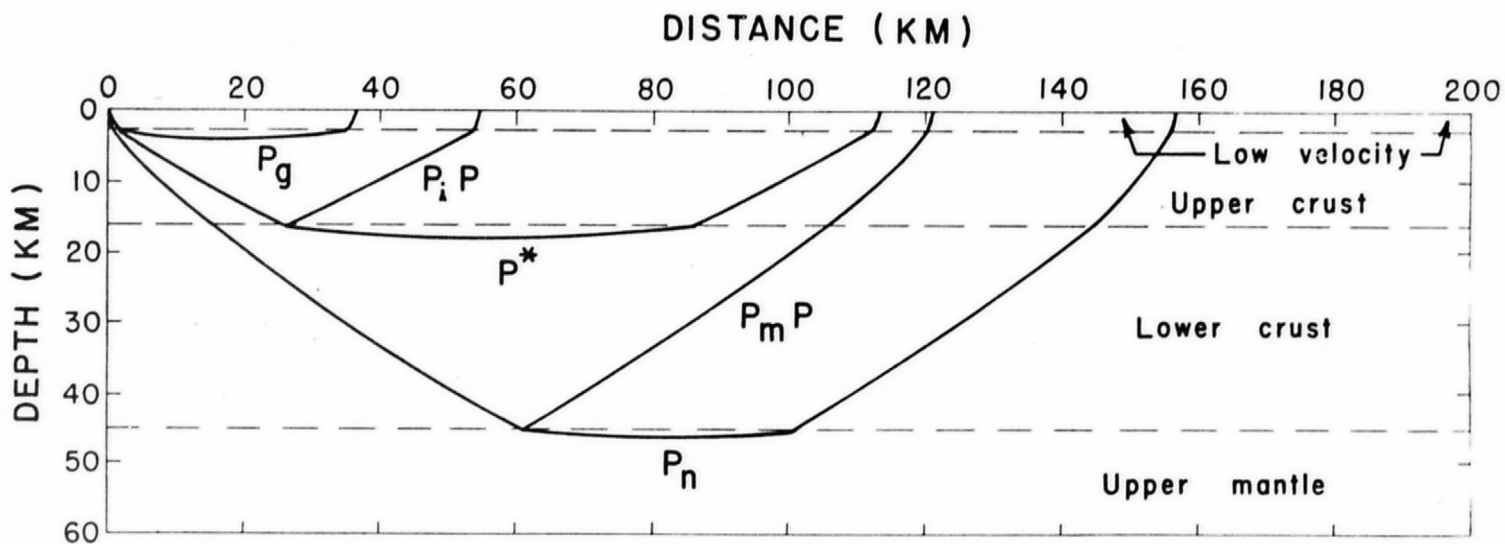


Figure 9. Ray paths for crustal refraction and reflection phases. Each ray represents a seismic phase, as shown.

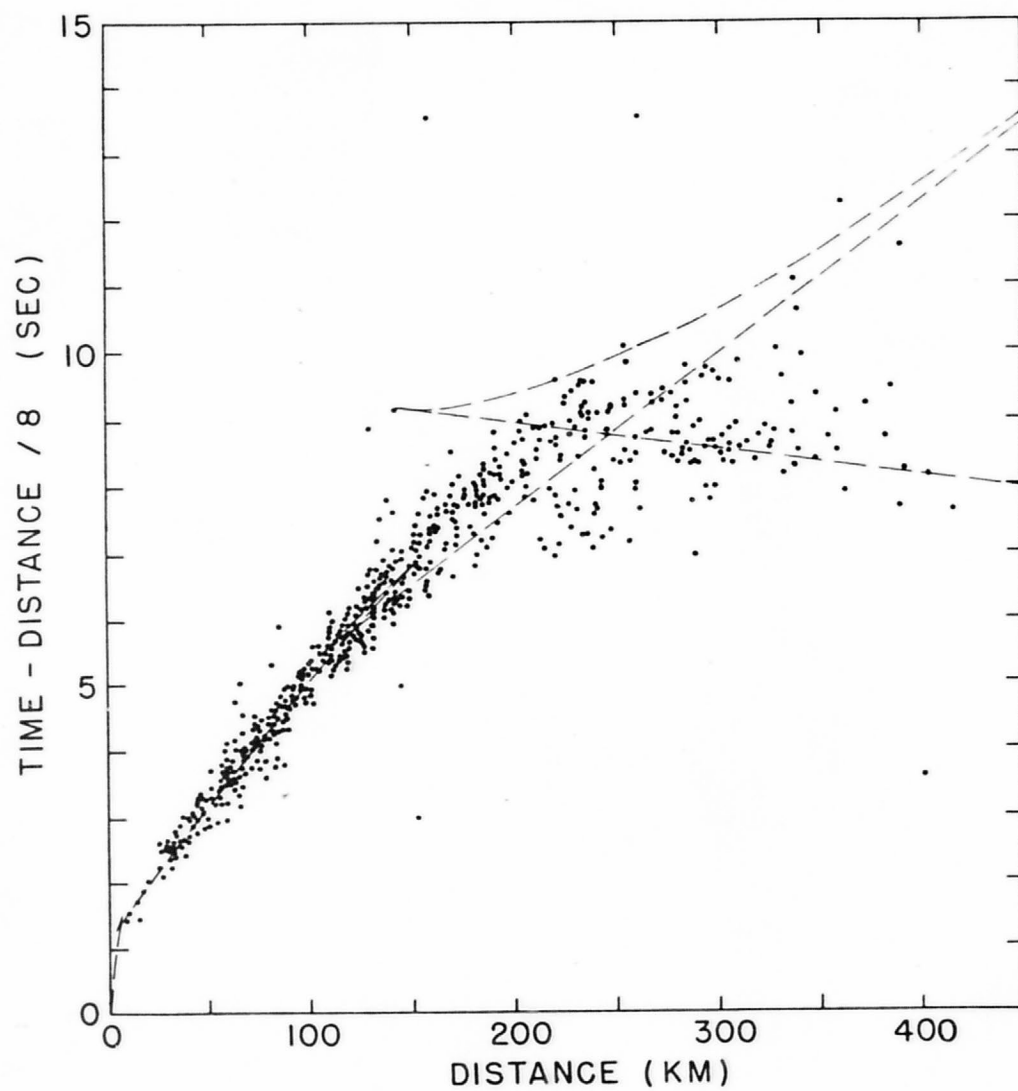


Figure 10. Reduced traveltime plot of first arrivals from all shotpoints. Dashed line is traveltime curve for average crustal model.

The composite first-arrival data were inverted to obtain a velocity-depth structure (Fig. 11). Also, an individual velocity structure was calculated from the data for each shot-point (Fig. 12) and a plot of apparent velocity vs distance was constructed (Fig. 13). This analysis helped to reveal the character of the anomalies at LASA. The most important anomalies appear to be in the lower part of the crust and possibly in the top of the mantle. The upper crust below the sediments has a velocity of 6.1 km/sec, which increases gradually with depth, reaching a velocity of 6.4 to 6.5 km/sec at depths ranging from 10 to 20 km. Low-velocity zones would not be revealed in the analysis and limited velocity reversals could be present but the overall increase of velocity with depth would still be required to explain the traveltime data.

The velocity structure of the lower crust cannot be accurately determined from first arrivals, but it appears to increase gradually with depth with no clear evidence for abrupt changes in the velocity-depth function.

#### TIME-TERM MAPS

We attempted to map the structure of the crustal layers using the time-term method. An outline of the analysis follows:

1. Data from each shot-point were plotted on a reduced traveltime plot and all of the data were fit by a single least-squares line. All points with a residual of more than 2.5 sec from this line were rejected.
2. Data from 10 to 100 km were selected from the set, and time-terms were calculated using a program described by Berry and West (1966).

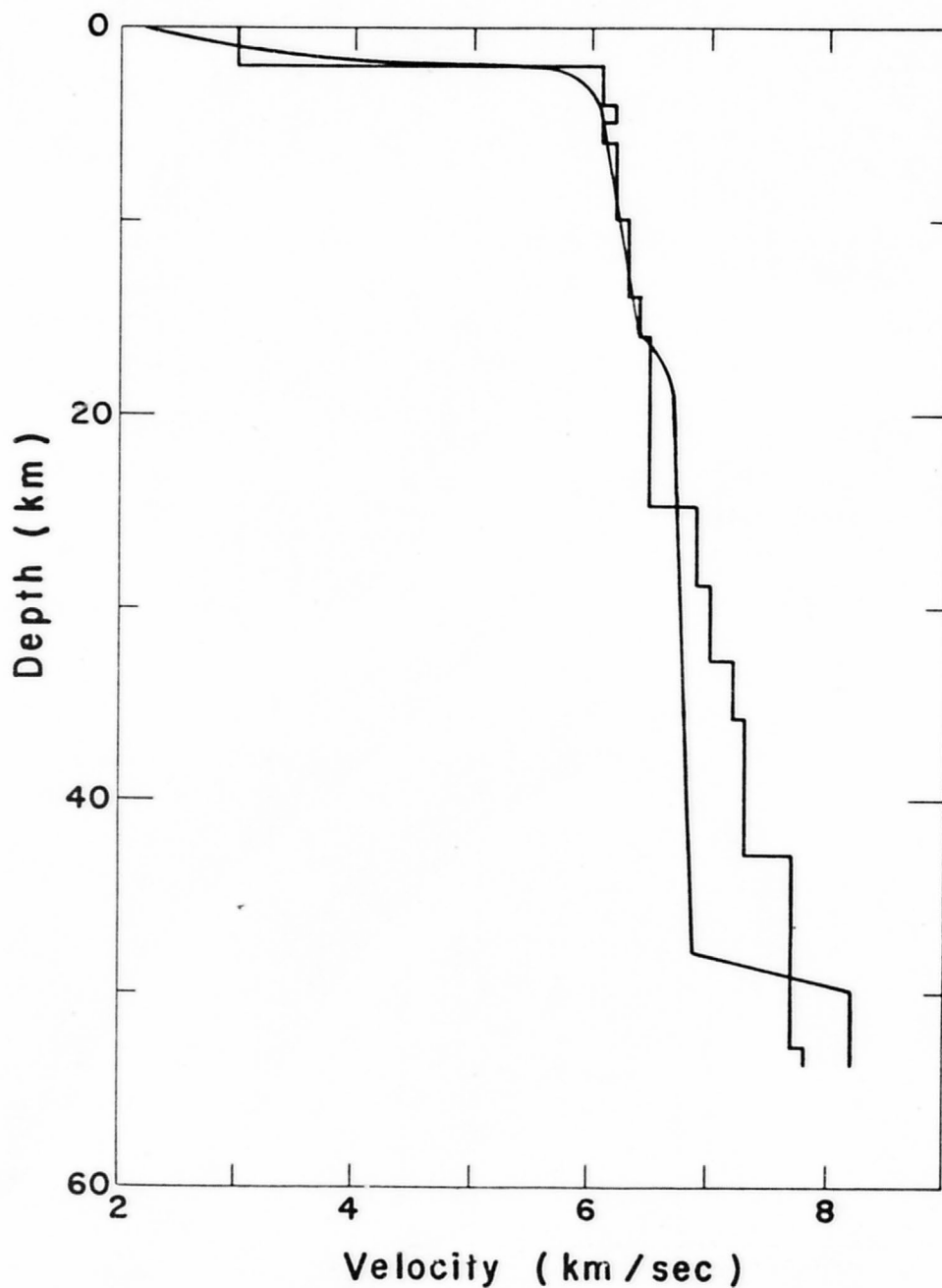


Figure 11. Comparison of average crustal velocity-depth functions. Step function is multilayer model from analysis of first arrivals; smooth curve is model of Fig. 8.

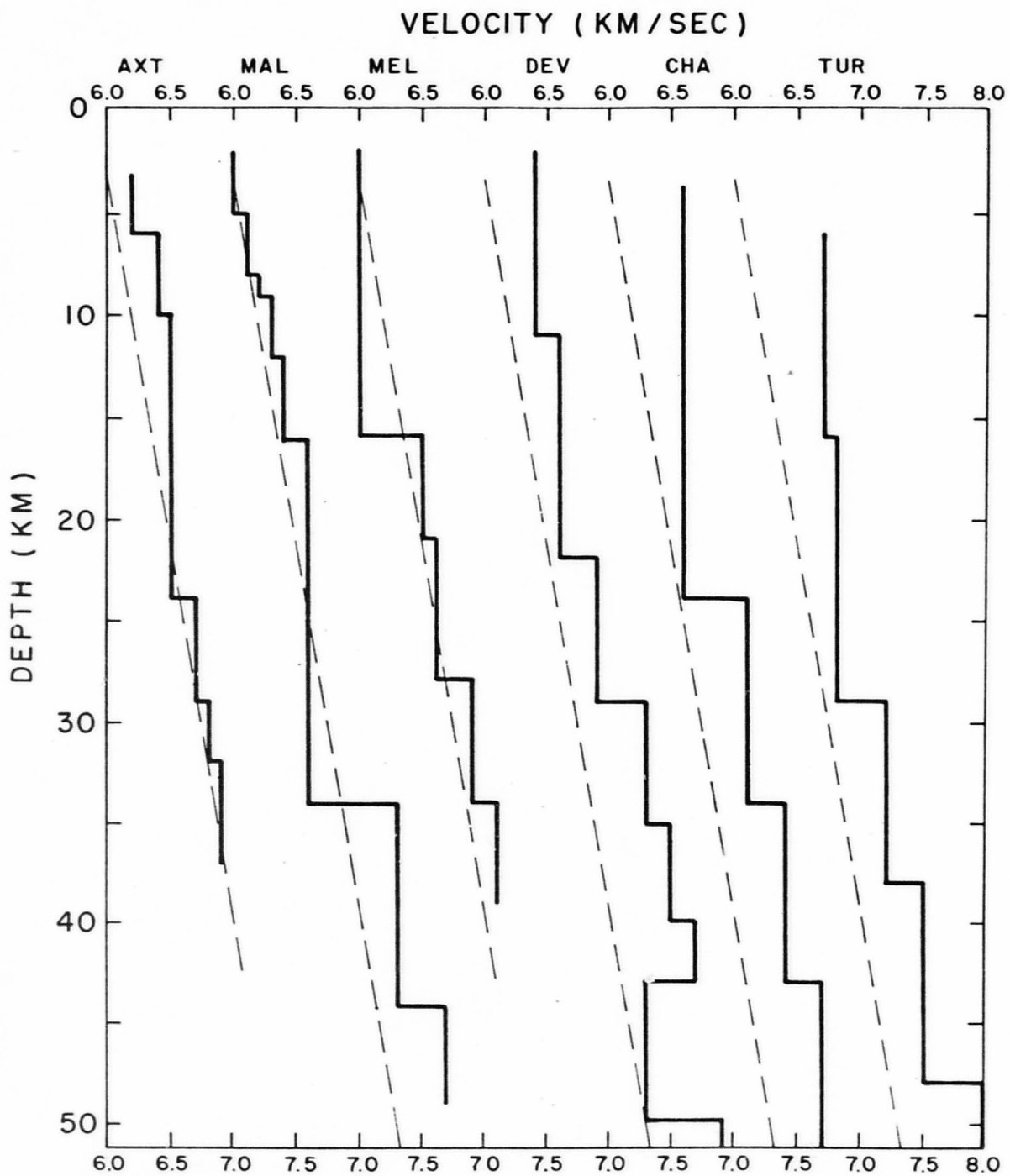


Figure 12. Multilayer crustal models, one for each shot. Only first arrivals were used. The same reference line is shown dashed on each plot.

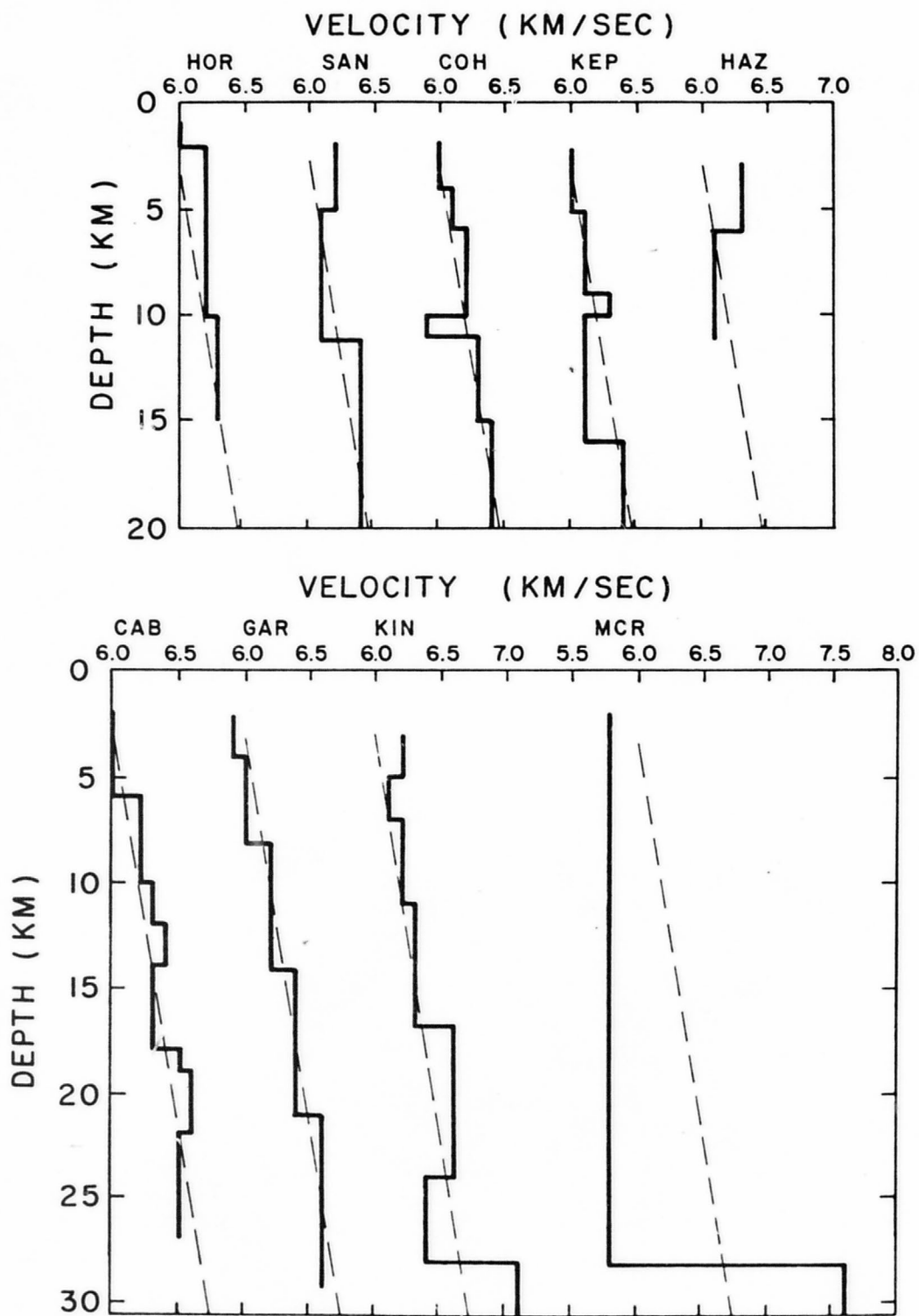


Fig. 12A. Continuation of Figure 12.

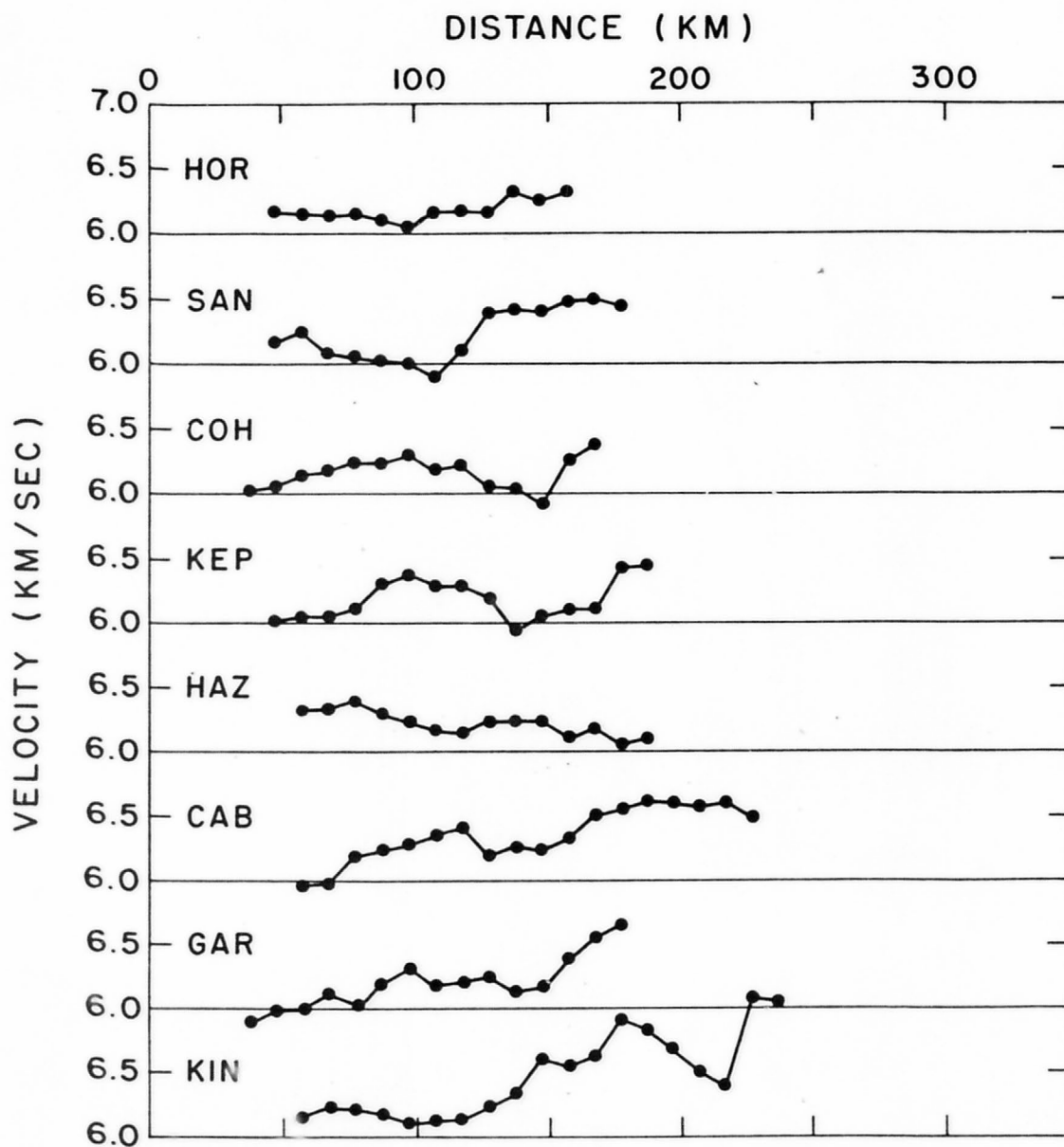


Figure 13. Apparent velocity of first arrival vs distance for each shot.

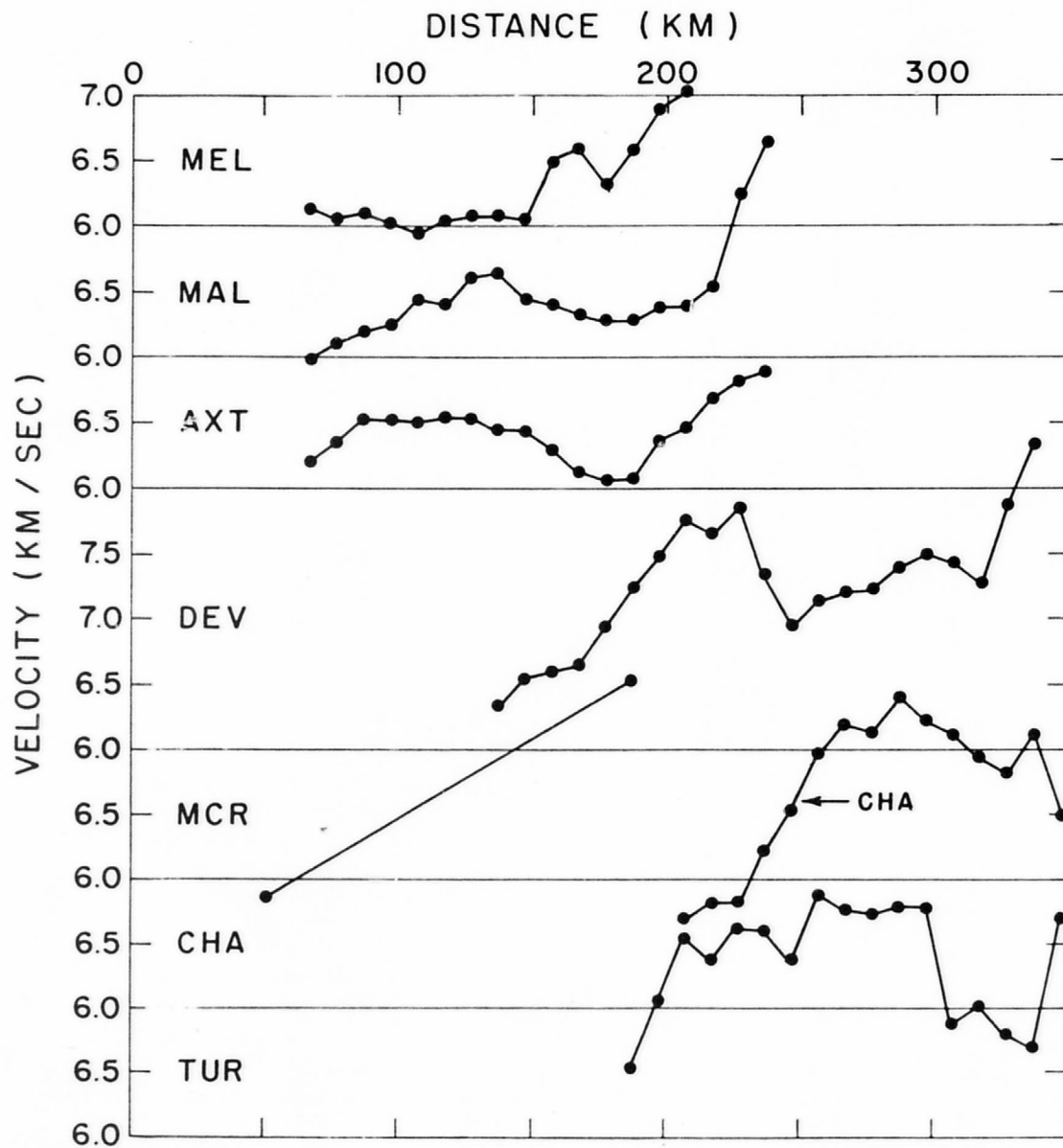


Fig. 13A. Continuation of Figure 13.

Time-terms involve the following parameters:

$$t_{ij} = \frac{\Delta_{ij}}{v} + a_i + a_j$$

$$R_{ij} = T_{ij} - t_{ij}$$

where  $t_{ij}$  = calculated traveltime between  $i^{\text{th}}$  and  $j^{\text{th}}$  sites

$T_{ij}$  = observed traveltime between  $i^{\text{th}}$  and  $j^{\text{th}}$  sites

$R_{ij}$  = residual between measured and theoretical traveltimes

$\Delta_{ij}$  = distance separating  $i^{\text{th}}$  and  $j^{\text{th}}$  sites on the surface

$a_i$  and  $a_j$  = time-terms at the  $i^{\text{th}}$  and  $j^{\text{th}}$  sites, respectively

$v$  - velocity of the base refractor

3. All times  $T_{ij}$  having a residual  $R_{ij}$  greater than 0.5 sec were deleted from the data and time-terms were recalculated.
4. Then, times  $T_{ij}$  having a residual calculated in the second run to be greater than 0.4 sec were rejected.
5. The process was repeated: time-terms were calculated, all times having a residual greater than 0.3 sec were rejected, and time-terms were calculated a fourth time. Each time-term value was saved and designated as time-term 1 (Fig. 14).

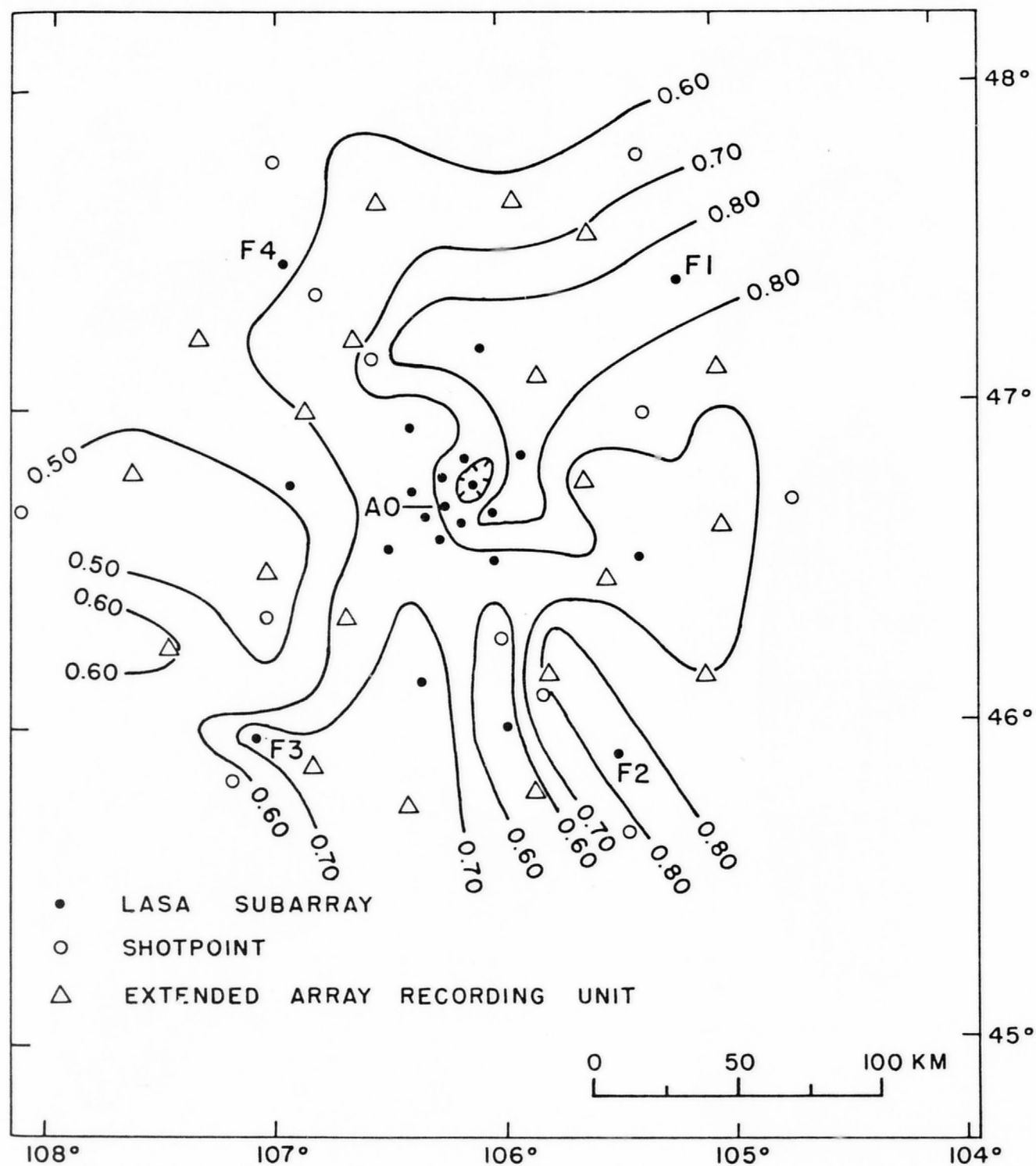


Figure 14. Contour map of time-term 1. Time-terms are from Pg first arrivals in distance range of 10-100 km from shotpoints. Contour interval is 0.1 sec.

6. The appropriate  $a_1$  and  $a_j$  (time-terms 1) were subtracted from all traveltimes data. The data were replotted for each shot-point on a map display and on a reduced traveltimes plot.
7. An examination of these plots reveals that at a distance of about 110 km, the data depart significantly from the velocity calculated in the time-term program. A segment of data between 110 and 185 km was selected and a second time-term, designated time-term 2 (Fig. 15) was calculated in the same series of steps described above for time-term 1. (Another method was used to check this procedure. A different crossover distance for each shot-point was selected by a least-squares fit of two straight lines to the data, and time-terms were calculated for the data beyond each crossover distance out to 190 km. This procedure gives a result close to the time-terms calculated for a constant crossover distance.)
8. A fairly distinct crossover distance is apparent at about 200 km for all plots with data beyond that distance. A third time-term was calculated for all data available beyond 200 km by the same procedure described for time-terms 1 and 2, except that the rejection levels were increased to tolerate the greater scatter in data beyond 200 km.

The time-terms for the arrivals that traveled a distance of 200 km or more were inconsistent. The average velocity was 7.73 km/sec, and adjacent stations had such markedly different values that the data could not be contoured. These data will be interpreted in a later section of this report.

Time-terms 1 are probably a fair estimate of the near-surface time

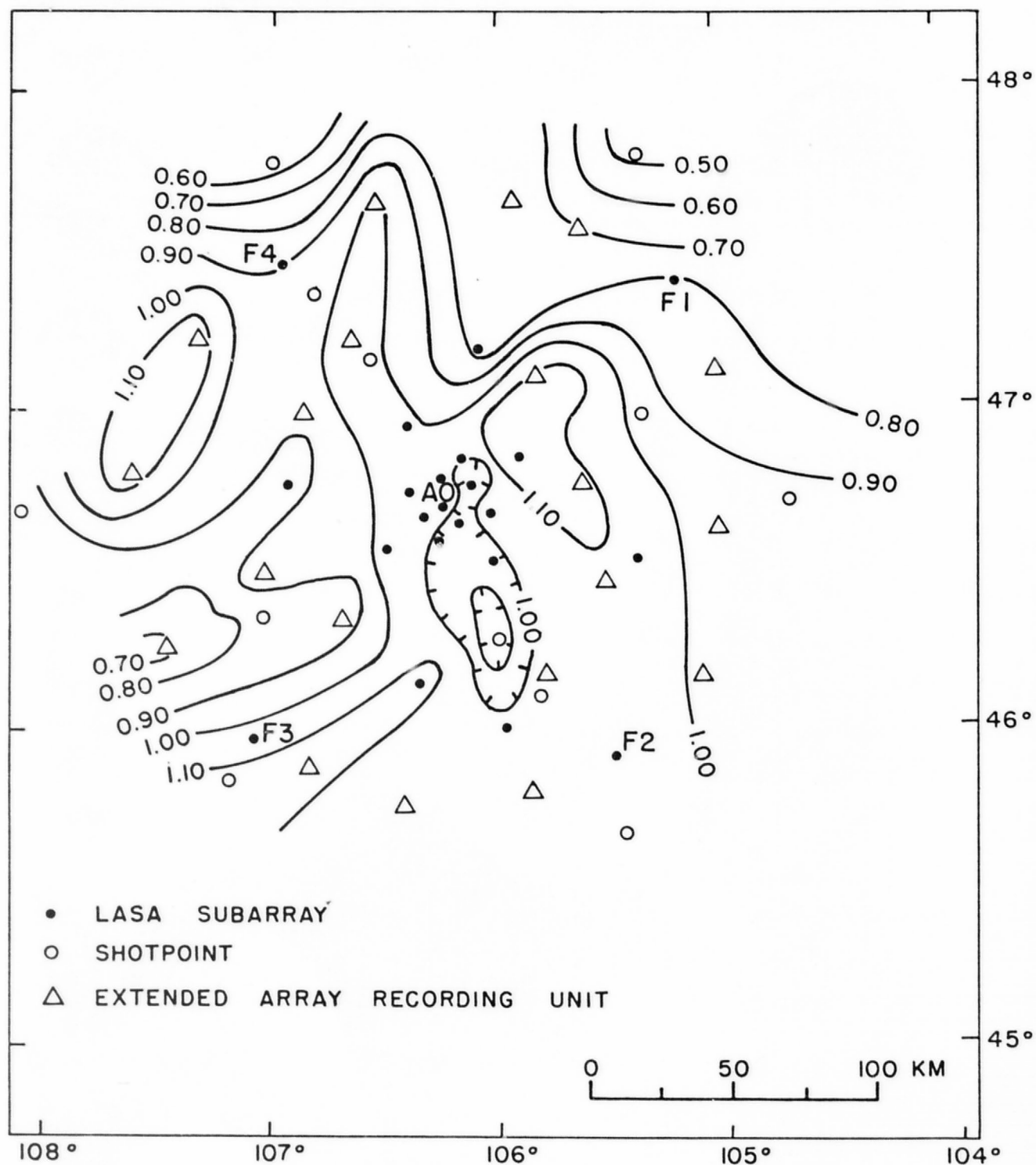


Figure 15. Contour map of time-term 2. Time-terms are from Pg and P\* firstarrivals, in distance range of 110-185 km from shotpoints. Contour interval is 0.1 sec.

delays for waves traveling within the crust. If the average velocity determined in this reduction (6.13 km/sec) and the models of Figure 7 are used, the delay in the top layers can be calculated for waves of any apparent velocity.

Time-terms 2 show the combined effects of variations in refraction velocity and variations in traveltime through overlying layers. The low time-terms in the northeast corner of the array can only be explained if the velocity of the refracting horizon in this area is greater than the average velocity for the time-term 2 refractor, which is 6.30 km/sec.

The total range of values for time-term 1 is 0.4 seconds, which, as we will show later, is about the same magnitude as the total range of time corrections for teleseismic events.

The range for time-term 2 is 0.6 seconds. We believe that these data suggest a compensating mechanism which tends to minimize time residuals for waves passing through the crust. Where near-surface rocks have low velocities they appear to be underlain by rocks of higher than usual velocities.

#### CRUSTAL THICKNESS FROM $P_n$ DATA

As mentioned earlier, the standard time term inversion of the  $P_n$  data did not give consistent values for crustal thickness. Errors in timing of very weak  $P_n$  arrivals combined with a complex structure probably led to instabilities which produced the inconsistent time-term values.

To investigate the structural configuration that could be obtained from  $P_n$  arrivals, a modified time-term approach was used. The travel-

time may be expressed as:

$$T = \frac{x}{V_n} + \frac{h_s \cos \theta}{V_c} + \frac{h_r \cos \theta}{V_c}$$

where  $X$  = distance between shot and receiver

$h_s$  = crustal thickness at shot

$h_r$  = crustal thickness at receiver

$V_c$  = mean crustal velocity

$V_n$  = velocity in upper mantle

$$\theta = \arcsin \frac{V_c}{V_n}$$

The time-terms for shot and receiver are  $\frac{h_s \cos \theta}{V_c}$  and  $\frac{h_r \cos \theta}{V_c}$ , respectively.

The average velocity in the crust is assumed to be  $V_c = 6.4$  km/sec, and the velocity of  $P_n$  is assumed to be  $V_n = 8.2$  km/sec; with these values the time-terms in seconds are very close to one-tenth sec/km times the crustal thickness. Time-term values for each shot were adjusted, by trial and error, to achieve consistent crustal thickness values in the central part of the array.

The depth values were corrected for offset between the emergence point at the interface and the surface recording position, according to  $\Delta x = \frac{h \tan \theta}{V_c}$ . Depth values are plotted at the corrected emergent location on top of the mantle (Fig. 16).

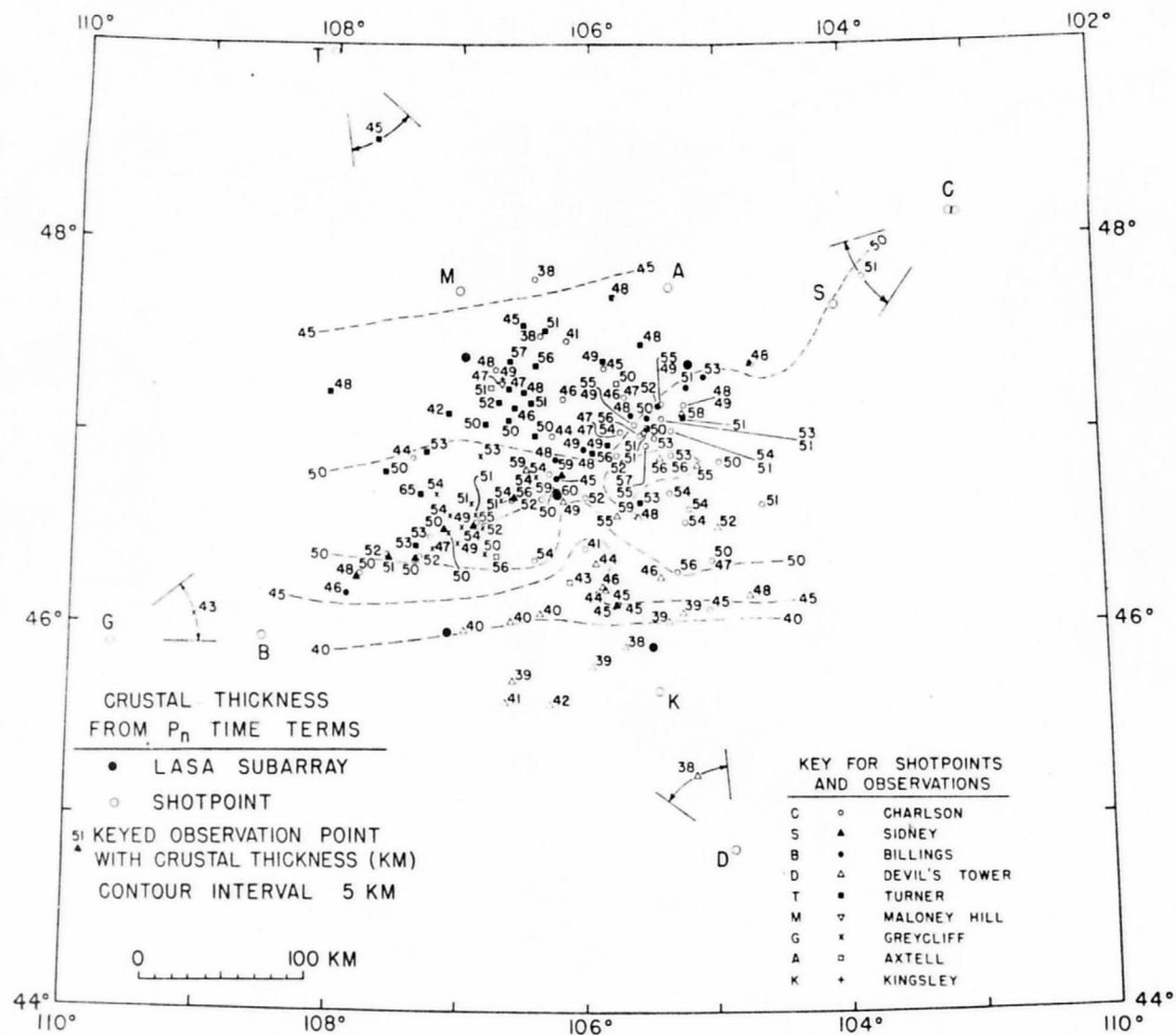


Fig. 16. Map of crustal thickness is determined from  $P_n$  arrivals. Values are in km; contour interval is 5 km.

## INTERPRETATION OF RECORD SECTIONS

Several types of record sections were prepared to display the data. Selected traces from the LASA subarrays were assembled into record sections along profiles extending outwards from each shotpoint. The data from the portable seismic stations and seismic recording trucks were also assembled into similar, but separate, record sections so that they could be used as overlays for the sections prepared from the LASA data.

The sections of data from LASA were plotted by computer from digital data. Sections were prepared from the portable-station data by hand tracing of analog records. Forty-eight individual numbered sections were prepared in this manner (Appendix); each one is labeled with the name of the shotpoint and the approximate direction along which the section was compiled. Even this large number of sections does not display all of the available data, because it was not feasible to use all the traces from each of the LASA subarrays.

The analysis of first arrivals suggests a break in slope of the average traveltime plot at about 110 km. The record sections clarify the change of arrivals with distance. A break occurs at distances between 110 and 150 km, and the apparent velocity increases as the  $P_g$  or  $P_{6.4}$  arrivals are overtaken by  $P^*$  arrivals. The  $P^*$  arrivals are often secondary arrivals at shorter distance ranges. They are marked by dashed lines on the record sections, and apparent velocities measured from them are shown at appropriate distance ranges in Figure 17.

$P^*$  data were used to prepare a map of upper-crust time-terms (Fig. 18). A velocity of 6.6 km/sec was assumed as an average and drawn

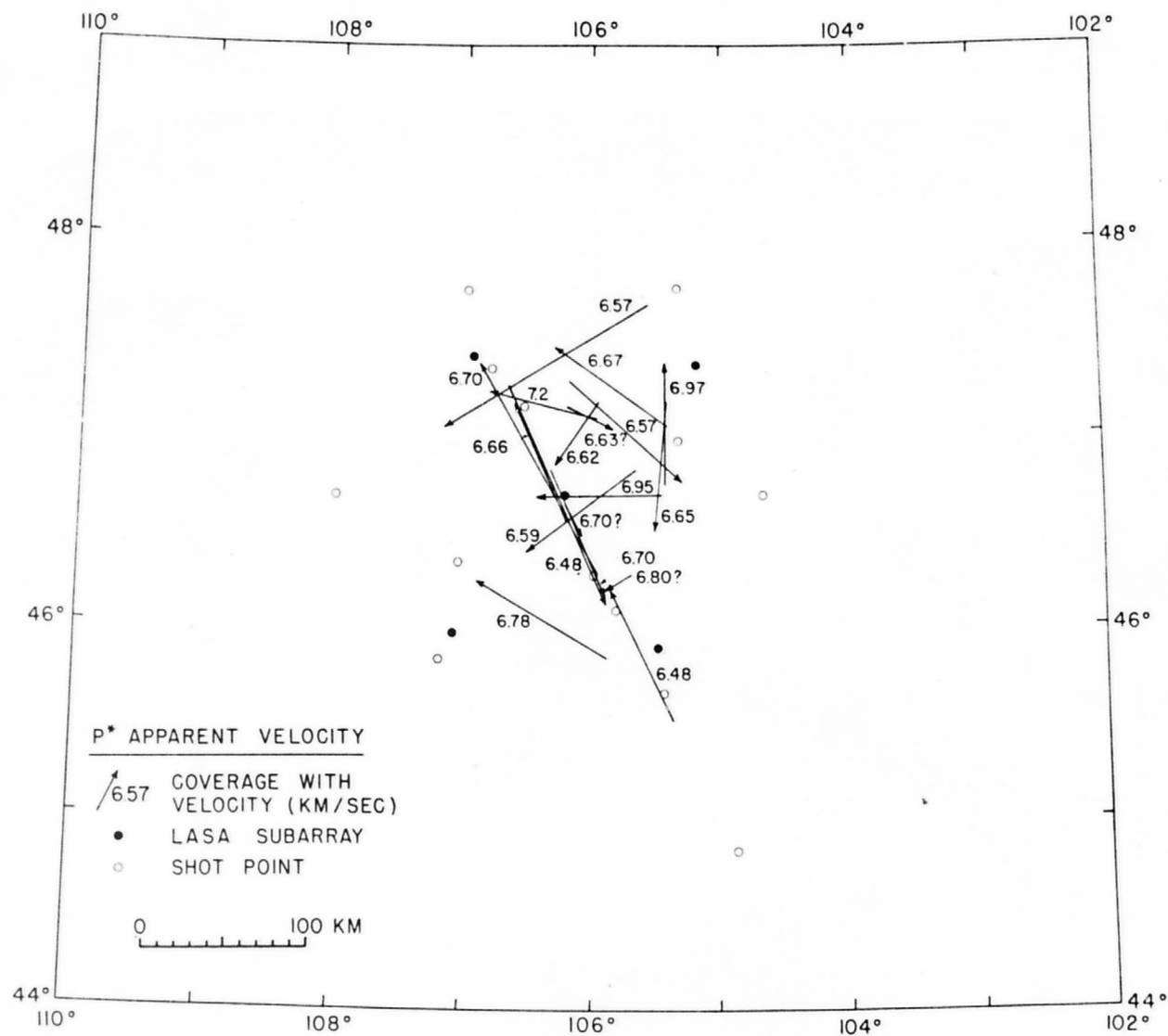


Figure 17. Map of intermediate layer interval velocities. Velocities are given in km/sec., measured over the intervals shown.

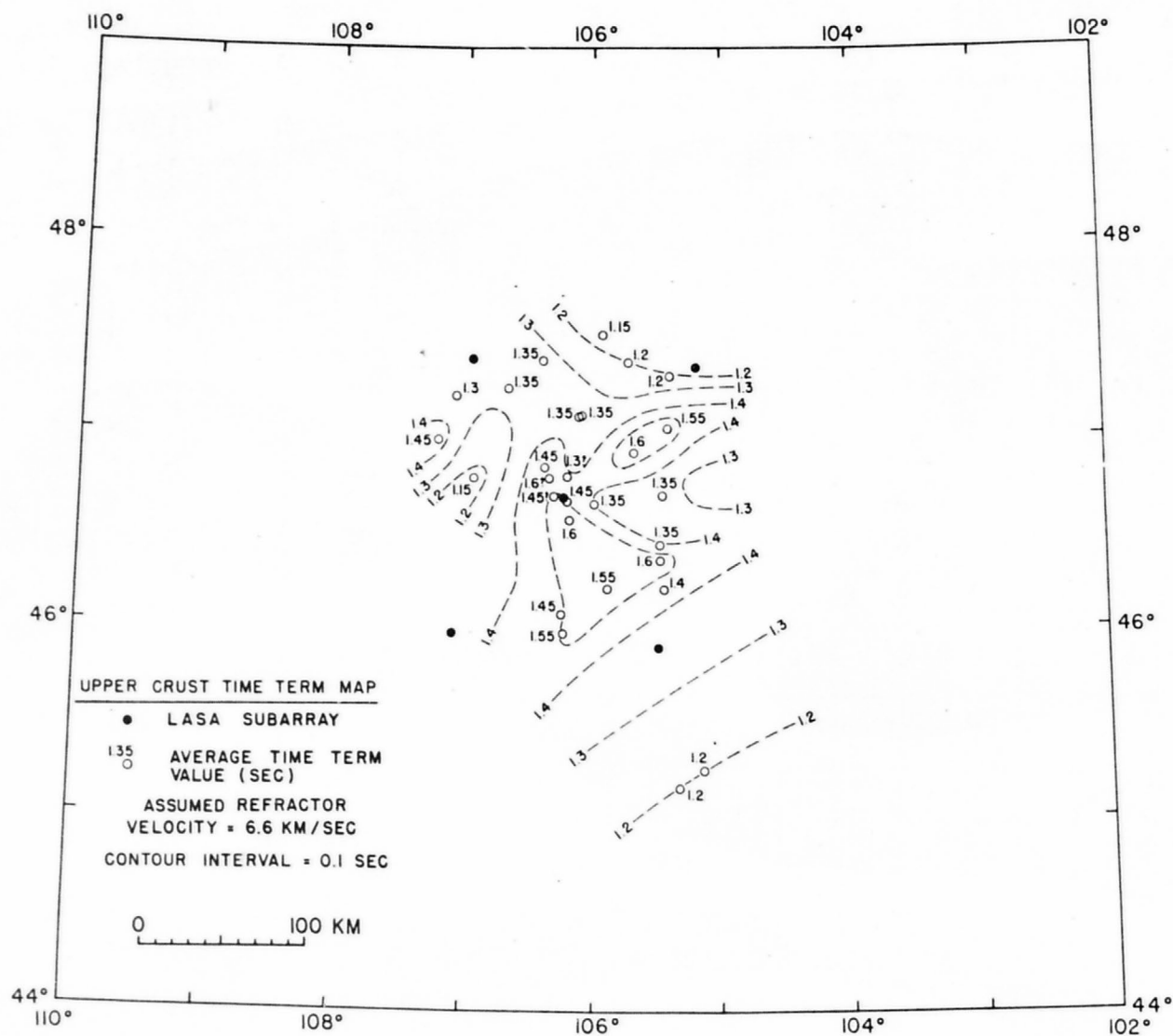


Figure 18. Contour map of upper-crust time-terms, as measured from P\* first and later arrivals on record sections.

to fit  $P^*$  on the record sections. The intercept time was measured, divided by two, and plotted halfway between shotpoint and  $P_g - P^*$  crossover as an average time term. It was not difficult to contour these values by allowing a 0.1 sec scatter. A comparison of this map with that of time-term 2 (Fig. 15) reveals that the pattern of anomalies is similar; the absolute values are slightly greater because the true crossover distances are generally greater than the 110 km assumed for time-term 2.

### $P_m P$ AND CRUSTAL THICKNESS

The reflections from the M discontinuity, phase  $P_m P$ , can be identified on many of the record sections by amplitude build-up and correlation of phase character. Although it is sometimes difficult to pick the exact onset of the phase, it often appears clearly as energy traveling with a higher apparent velocity than the average and can be identified in the distance range between 130 and 180 km. The times of  $P_m P$  are tabulated in Table 5, and the phases are marked on the sections so that the reader can examine each individual pick.

A program by Landisman et al. (1966) was used to compute traveltimes of reflected  $P_m P$  phases as a function of distance, using the average velocity function with different depths to the M discontinuity. As the depth to the M discontinuity was changed, the velocity in the lower crust was changed slightly, so that each model had a constant gradient from a velocity of 6.7 km/sec at the top of the intermediate layer to a velocity of 6.9 km/sec at the bottom of the layer. The velocity then jumps from 6.9 to 8.2 km/sec in a two-km depth interval for all models. The time measurements were reduced and plotted on a nomogram (Fig. 19) on which

Table 5

P<sub>m</sub>P Reflections

Section No.	Shot-Rec.	Traces	Distance (km)	Travel time (sec)	Reduced Traveltime (sec)	Depth (km)	Event No.
4	AXT-COH	6-1	113.2	23.1	4.2	47	7
4	AXT-LAN		115.5	23.3	4.0	47	8
5	AXT-D4	5-21	120.0	23.6	3.6	46	10
3	AXT-E2	5-17	138.3	27.0	4.0	53	5
3	AXT-D2	9-17	148.4	28.3	3.5	54	6
4	AXT-HRS		144.3	27.0	2.9	48	9
1	AXT-B3	17	146.0	27.6	3.3	52	1
1	AXT-C3	12-17	150.0	28.2	3.2	52	2
1	AXT-D3	5-17	159.6	29.4	2.8	52	3
5	AXT-E4	5-21	162.2	29.3	2.3	49	11
2	AXT-TON		179.9	32.2	2.2	53	4
1	AXT-E3	4-21	193.4	34.0	1.7	54	83
4	AXT-VAN		191.3	33.4	1.5	51	84
3	AXT-F2	5-21	205.2	35.8	1.6	56	85
4	AXT-SUM		204.4	35.4?	1.3?	53?	86
-	AXT-MEL	1-5	234.6	38.9	0.7	57	87
1	AXT-F3	5-21	238.8	40.2	0.4	55	88
8	CAB-TON		103.0	22.1	4.9	48	13
9	CAB-F2	9-21	106.6	21.9	4.1	45	16
8	CAB-HOR	6-1	110.2	22.8	4.4	47	14
-	CAB-KIN	1-4	127.4	24.7	3.4	47	80
9	CAB-E3	9-21	140.2	26.0	2.7	45	17
8	CAB-VOL		133.2	25.5	3.3	48	15
6,8	CAB-FOR		159.3	29.2	2.6	51	12
6,8	CAB-SAN		185.6	32.8	1.8	52?	89
9	CAB-F3	9-21	201.4	34.4	0.8	49	90
14	COH-E3	5-13	110.4	23.3	4.9	50	21
13	COH-HOR	2-6	106.2	23.3	5.6	52	18
14	COH-F2	5-17	159.6	29.4	2.8	52	20
13	COH-VOL		158.4	28.8	2.4	49	19

Table 5 (cont.)

P<sub>m</sub>P Reflections

Section No.	Shot-Rec.	Traces	Distance (km)	Travel time (sec)	Reduced Traveltime (sec)	Depth (km)	Event No.
13	COH-KIN	1-4	185.0	32.3	1.5	49	91
17	DEV-F2	17-5	128.6	23.7	2.3	40	22
19	DEV-VOL		131.9	24.2	2.2	40	23
17	DEV-E3	12-5	184.8	32.0	1.2	47	92
18	DEV-CAB	4	205.8	34.7	0.4	46	93
20	GAR-COH	6-1	129.8	25.8	4.1?	51?	24
20	GAR-LAN		138.3	26.8?	3.7?	51?	25
22	HAZ-F2	5-21	118.4	23.4	3.6	45	26
23	HAZ-E4	9-21	122.8	24.9	4.5	50	29
23	HAZ-F4	13-20	130.3	26.0	4.2	51	30
22	HAZ-VOL		135.5	25.6	3.0	46	27
22	HAZ-KIN	1-4	144.9	26.6	2.5	46	28
25	HOR-F4	17-25	145.3	27.7	3.5	52	32
24	HOR-JOR		157.3	29.1	2.9	52	31
28	KEP-F1	21-9	121.6	24.6	4.3	50	33
28	KEP-COT		138.3	27.0	3.9	53	34
28	KEP-E2	25-13	142.6	27.4	3.7	53	35
28	KEP-MIL		159.0	29.5	3.0	54	36
28	KEP-CAB	1-6	177.0	31.9	2.4	54	37
27	KEP-F2	5-17	187.7	32.9	1.7	51	94
32	KIN-FOR		123.0	23.2	2.7	41	43
30	KIN-B2	19	124.0	23.7	3.0	43	38
-	KIN-CAB	1-6	127.8	24.7	3.4	46	81
30	KIN-AO	10-4	128.8	24.5	3.0	45	39
33	KIN-F3	13-25	131.5	24.3	2.4	42	46
30	KIN-B4	10-19	137.4	25.5	2.6	45	40
32	KIN-MCR	6-1	136.9	25.0	2.2	42	44
32	KIN-SAN	2-6	145.0	26.0	1.9	41	45
30	KIN-D4	10-4	159.0	28.7	2.2	48	41
33	KIN-E4	13-25	166.0	28.9	1.2	42	47

Table 5 (cont.)

P P Reflections  
m

Section No.	Shot-Rec.	Traces	Distance (km)	Travel time (sec)	Reduced Traveltime (km)	Depth (km)	Event No.
31	KIN-E1	13-5	173.4	30.3	1.4	45	42
29	KIN-COH	6-1	185.1	32.5	1.6	51	95
31	KIN-F1	17-5	190.8	32.6	0.8	45	96
29	KIN-LAN		193.6	34.5	1.2	49	97
30	KIN-F4	13-4	225.4	38.0	0.5	52	98
29	KIN-SND		223.5	37.6	0.3	50	99
36	MAL-E1	25-13	96.4	21.2?	5.2?	47?	53
35	MAL-AXT	6	124.5	24.2	3.4	46	51
34	MAL-B3	25-13	130.8	26.1	4.3	52	50
36	MAL-D1	5-13	131.0	25.1	3.3	47	54
34	MAL-C3	25-17	141.8	27.2	3.6	52	49
-	MAL-MEL	1-5	140.9	26.3	2.8	47	82
36	MAL-F1	21-13	142.3	26.6	2.9	48	55
35	MAL-HAZ	1-5	152.2	27.9	2.5	48	52
34	MAL-D2	25-17	156.9	29.0	2.9	52	48
37	MAL-SAN	1-4	156.2	29.4	3.4	54	56
34	MAL-E3	5-12	183.8	32.5	1.9	52	100
36	MAL-E2	25-13	184.6	32.1	1.4	48	101
-	MAL-TON		198.4	33.9	0.8	47	102
35	MAL-CAB	1-6	211.6	35.9	0.7	50	103
39	MEL-E4	21-9	83.6	21.7?	7.8?	56?	62
40	MEL-F4	21-9	115.0	24.1	5.0	51	63
-	MEL-COH	1-5	122.8	24.7	4.2	49	64
39	MEL-C4	21-13	125.0	26.0	5.2	55	61
39	MEL-B3	23-9	130.7	26.6	4.8	54	60
39	MEL-A0	21-13	136.7	27.1	4.3	53	59
39	MEL-B2	4-9	142.1	28.1	4.4	54	58
39	MEL-C2	25-9	152.6	29.0	3.6	55	57
-	MEL-WEL		190.5	33.2	1.4	51	104

Table 5 (cont.)

P<sub>m</sub> P Reflections

Sections No.	Shot-Rec.	Traces	Distance (km)	Travel time (sec)	Reduced Traveltime (sec)	Depth (km)	Event No.
-	MEL-CIR		204.8	34.7	0.6	47	105
39	MEL-E2	21-9	203.6	35.0	1.0	51	106
44	SAN-D4	17-5	84.2	20.1	6.0	48	72
42	SAN-B1	21-9	86.6	20.9	6.5	50	68
43	SAN-COH	1-6	97.7	21.7	5.4	49	69
42	SAN-D1	21-9	104.3	22.9	5.5	51	67
44	SAN-F4	17-5	119.2	24.7	4.8	51	73
47	SAN-F2	5-13	130.2	24.3	2.6	42	78
45	SAN-E2	21-9	130.8	25.1	3.3	47	74
46	SAN-KIN	3	144.9	26.5	2.3	44	75
-	SAN-HAZ	5	148.5	28.2	3.4	52	79
46	SAN-ONE		149.2	27.0	2.1	44	76
43	SAN-JOR		149.4	28.1	3.2	52	70
43	SAN-MAL	1-6	157.1	29.4	3.2	54	71
46	SAN-MIL		159.8	28.6	2.0	46	77
42	SAN-CIR		170.7	31.1	2.6	54	66
42	SAN-F1	21-5	182.0	32.4	2.1	53	65
46	SAN-CAB	1-6	185.6	32.3	1.4	49	107

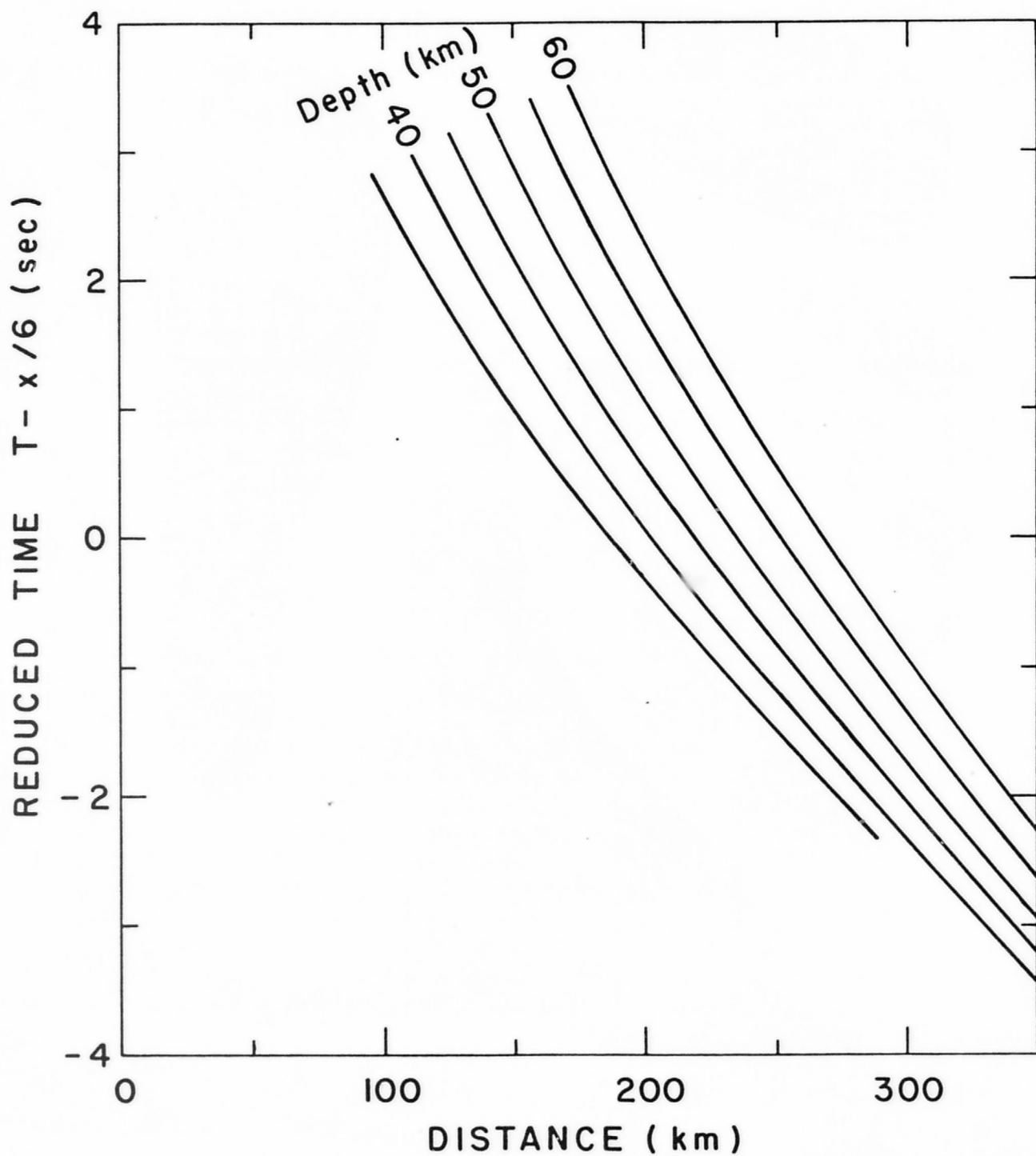


Figure 19. Nomogram for P-P events. A value of crustal thickness is determined from measured distance and reduced traveltime.

the lines represent constant depth. This nomogram can be used to find a value of depth to M for each  $P_m P$  event. Some events at shorter distance ranges are not included in this nomogram, and these events were converted to depth values by extrapolation. The depth values were plotted on a map and contoured (Figs. 20 and 21).

The map of crustal thickness determined from reflections reveals a structure trending approximately N 80 E and having a broad synclinal shape with the axis of the syncline passing approximately through the center of the array. The deepest points indicate an M transition of about 55 km. The shallowest points are in the south where the crust thins to approximately 40 km; the northern part of the array has a crustal thickness of about 45 km.

#### MODIFICATION OF AVERAGE CRUSTAL MODEL

The average model determined from our first-arrival data was perturbed to fit both the first-arrival and the reflection data. We again plotted a composite traveltime curve (Fig. 22), which now includes the reflections. The amplitude and locations of the critical distance of the  $P_m P$  reflection requires a rapid increase of velocity with depth and an indication of the magnitude of this velocity increase comes from a prominent large amplitude phase which follows  $P_n$  in the distance range of 240 to 390 km (see Charlson 11 and Turner 48). We label this phase  $P^*$ , but at larger distances it may be wide angle  $P_m P$  reflections. It is difficult to fit a model with velocities in the lower part of the crust that are substantially higher than the velocity of this phase, about 7.0 km/sec. We conclude that the velocity at the base of the crust must increase rapidly from a value of about 7.0 km/sec to a value near 8.0 km/sec, appropriate for upper-mantle rocks.

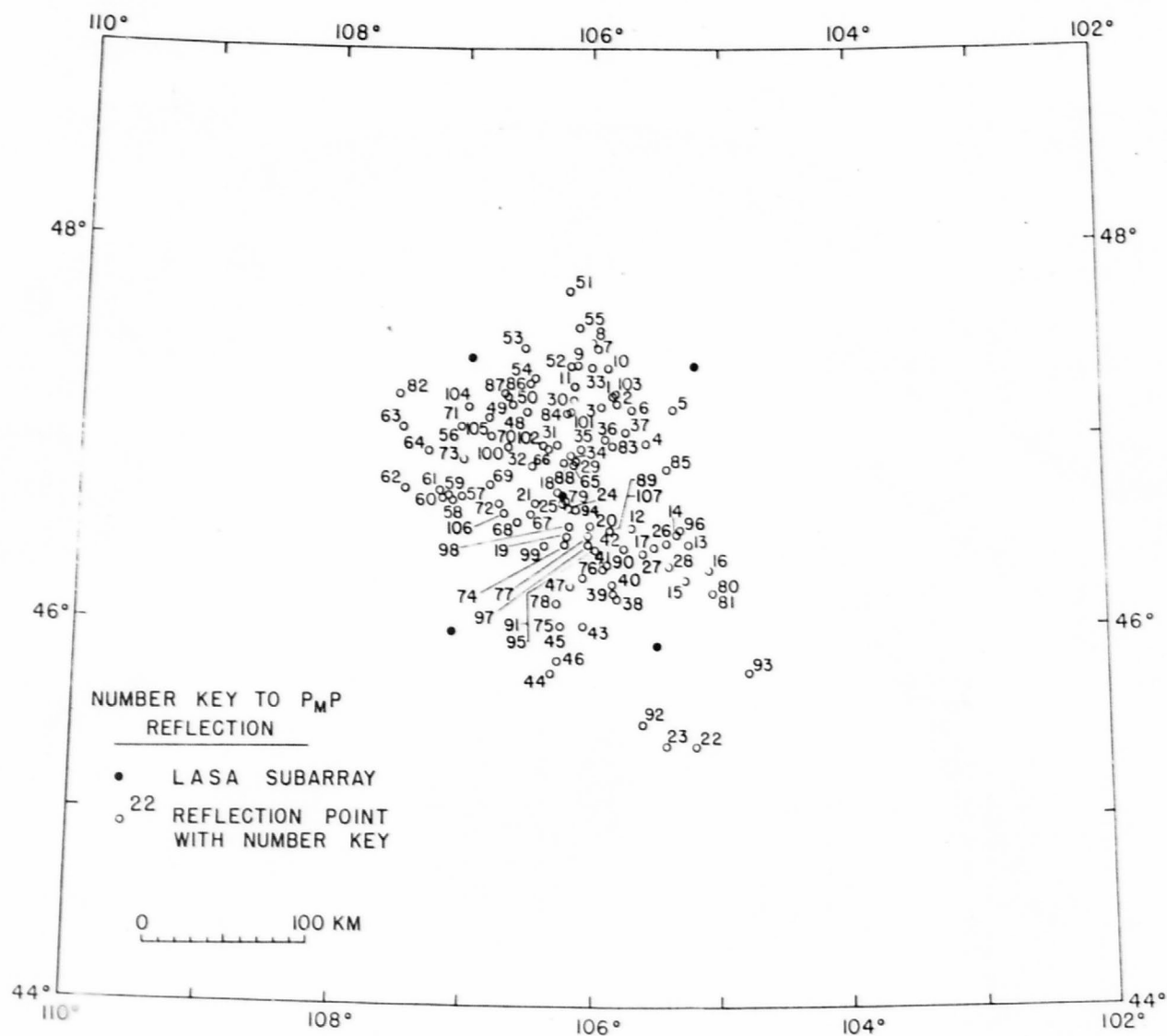


Figure 20. Map of key numbers for  $P_mP$  reflections. Key refers to event numbers listed in Table 5.

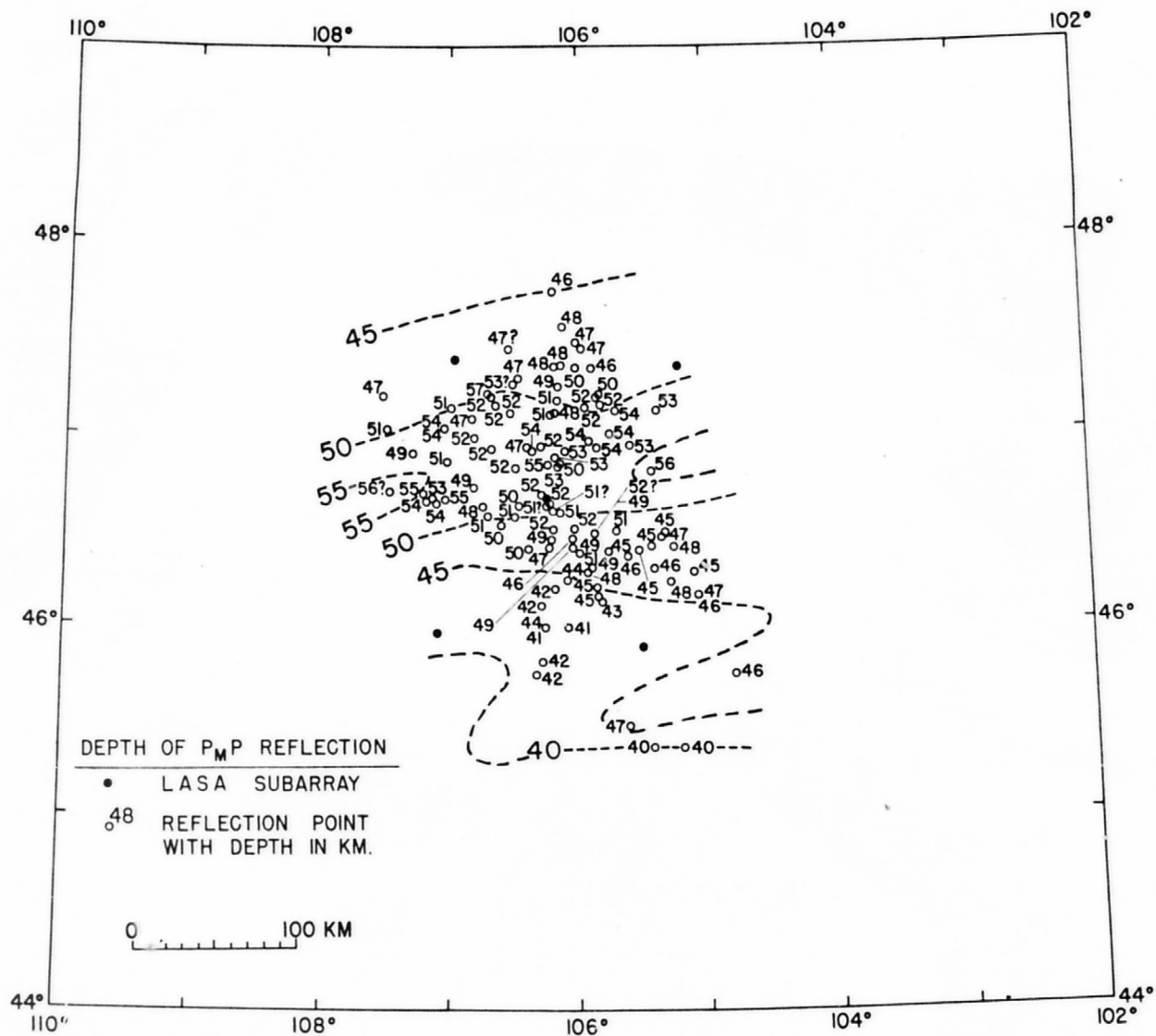


Figure 21. Map of depth of P-P reflections. Crustal thickness values are given in km, and contour interval is 5 km.

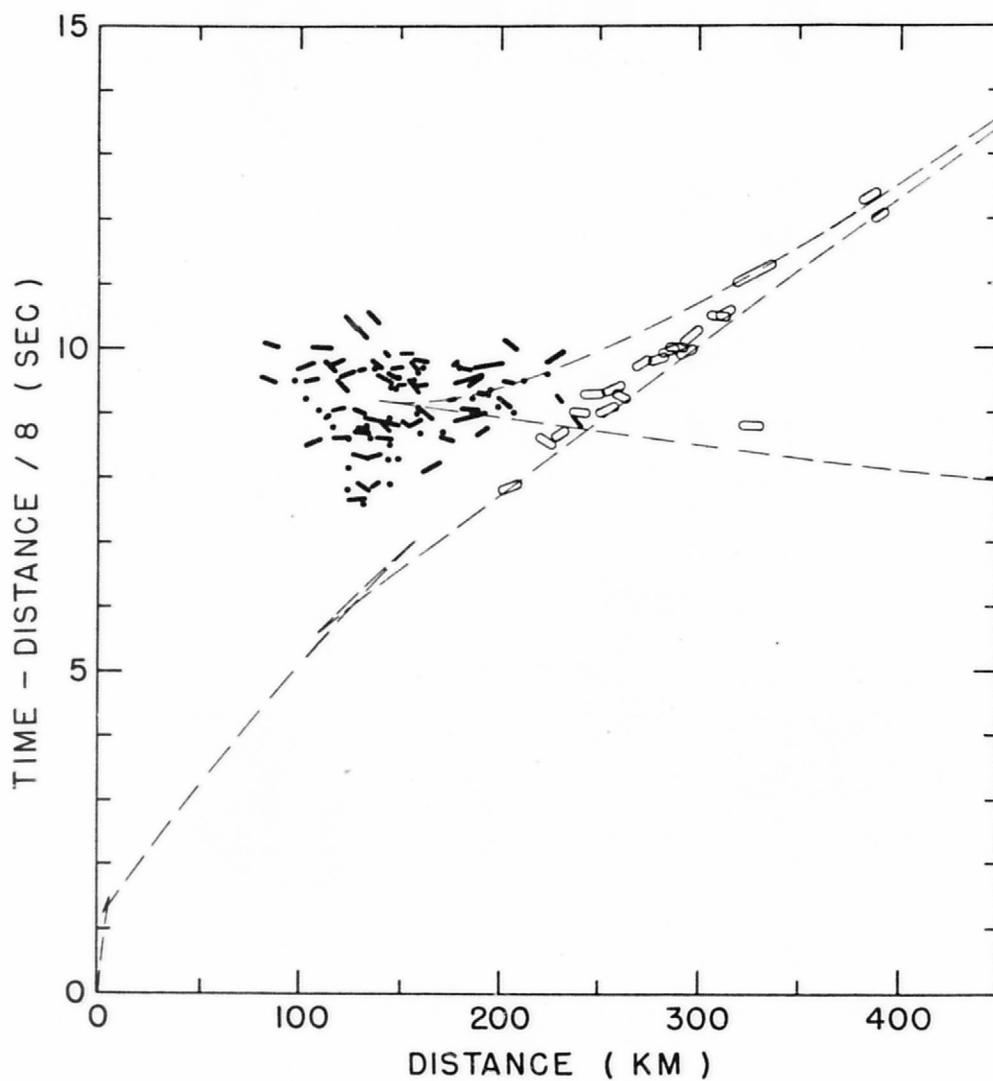


Figure 22. Reduced traveltime plot of average velocity function (dashed) and prominent later phases. P P events are shown by solid bars and dots. The open bars represent a high amplitude phase composed of wide angle P P events and P\* events.

## DISCUSSION

The seismograms recorded for this experiment suggest a degree of crustal and upper mantle complexity that has often been suspected, but has seldom been so well documented. Out of some 50 record sections prepared from the data it is difficult to find two that look alike. These complexities suggest a fine structure that is beyond the resolving power of the seismic techniques we have used. We believe that this complexity is a fundamental property that explains the contradiction between the variety of structure and rock types shown on a good geologic map and the simple layered crustal structures reported by the seismologist. The rocks of the earth's crust tend to separate into zones or layers having similar average physical properties, but within each layer there are rocks with a wide range of composition and structure.

Seismic waves sense the average properties, which are difficult to assess from geologic data. The fact that these averages can be stable and therefore meaningful is clearly demonstrated by the analysis of the  $P_g$  data in this report, which shows that the velocity of rocks below the sediments is usually near 6.1 km/sec. A burst of energy returning from the base of the mantle can be interpreted as a reflection from the crust-mantle boundary, and this boundary can be mapped with fair accuracy, but again the changes in character of the reflection indicate that there are fine details of the structure which cannot be resolved with the available data.

For many purposes the concept of an average model can be very useful. The separation of the crust into layers with characteristic average

properties seems to be a sound statistical procedure and allows us to treat the variation from these average properties as a statistical uncertainty. The time residuals or station corrections computed for the LASA subarrays will have a statistical uncertainty related to the fine structure of the crust, and it is unlikely that the uncertainty in travel-times can be reduced below this level by any practical calibration scheme. Furthermore, the statistical variations found at LASA are not peculiar to this site, and it is likely that all seismic arrays will have similar travelttime uncertainties.

Following this philosophy, we can review the results of this paper as they apply to calibration of LASA. The average model shown first in Figure 8 gives a good approximation of the average crust at LASA. Variations in crustal thickness result primarily from changes at the base of the crust, i.e., with changes in depth of the transition from about 8.0 to about 9.1 km/sec. There are variations in the depth to the velocity change from 6.0 to 6.7, but the travelttime effects of this transition seem to be partially compensated, and it does not appear to affect the overall travelttime through the crust as much as would be expected from the time-terms (Figs. 15 and 18).  $P_n$  data give a reasonable picture of crustal thickness variation (Fig. 16), but we feel that it is not as accurate as the crustal thickness variation determined from reflections (Fig. 21).

A map presenting our best estimate of crustal thickness in the vicinity of LASA was prepared from all the available data (Fig. 23). This map reveals a syncline trending approximately E-W across the array. The greatest depths are about 55 km reached near the center of the array and the shallowest are

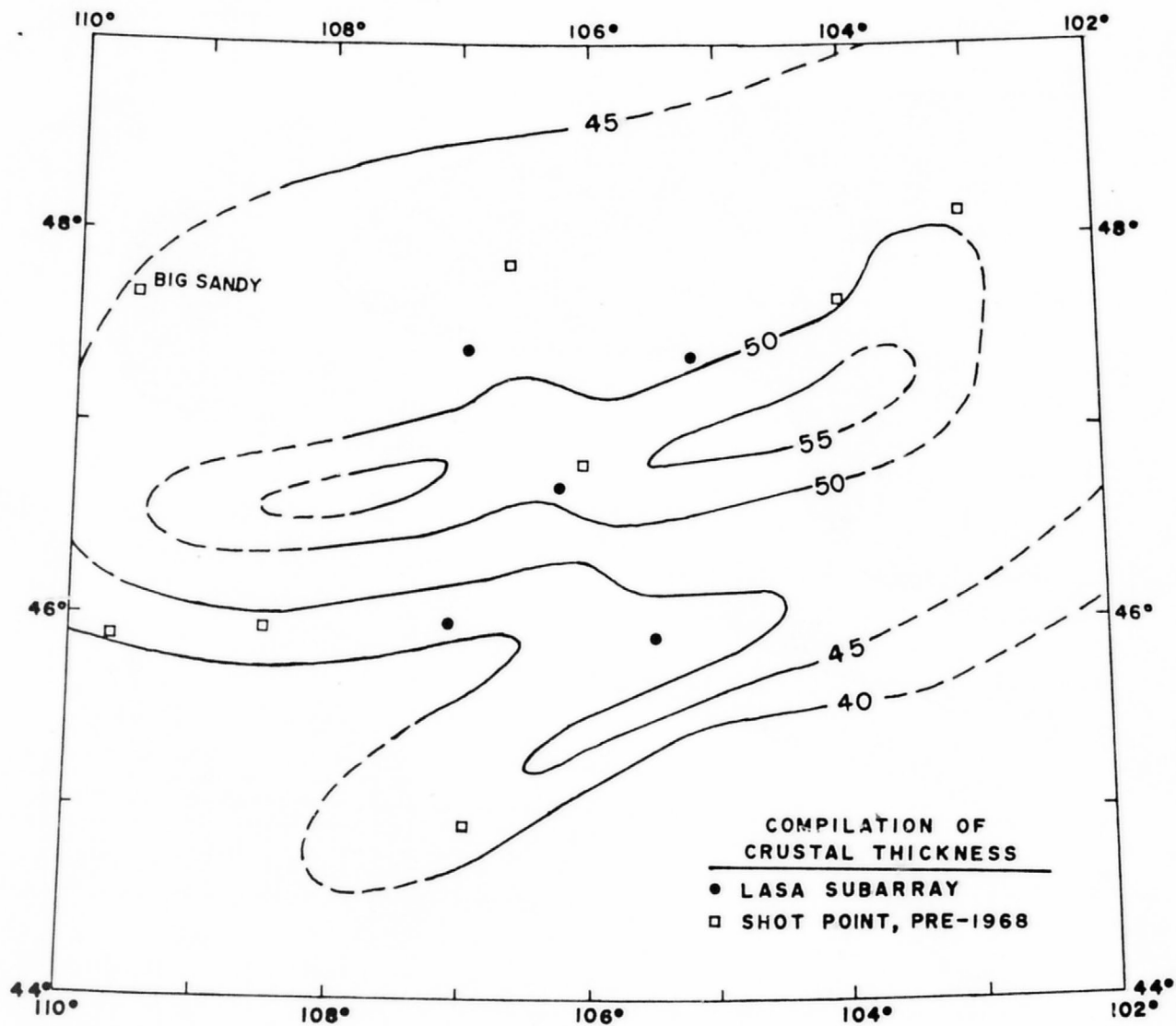


Figure 23. Map of crustal thickness compiled from all available sources.  
Values are in km and contour interval is 5 km.

about 40 km on the southern limb of the syncline.

We have one reservation about this map. It is possible that layering at the base of the crust with velocities between 7.7-7.9 km/sec could have escaped detection. If rocks of this velocity exist at the base of the crust, the map of crustal thickness would approximate the depth to the top of this layer.

The maps showing the thickness of crustal layers can be used to calculate time corrections for earthquakes recorded at LASA as a function of their azimuth and distance. A report on this aspect of the work is in preparation. It appears that corrections for upper layers of the crust do not significantly reduce the time residuals of a representative set of earthquakes, but when the arrival times are corrected for total crustal thickness a significant improvement is achieved.

## REFERENCES

- Asada, T., and Aldrich, L. T., 1966, Seismic observations of explosions in Montana: in The earth beneath the continents, J. S. Steinhart and T. Jefferson Smith, ed., Am. Geophys. Union Mon. 10, Washington, D. C., p. 382-390.
- Berry, M. J., and West, F. G., 1966, An interpretation of the first-arrival data of the Lake Superior experiment by the time-term method: Seismol. Soc. America Bull., v. 56, no. 1, p. 141-171.
- Borcherdt, C. A., and Roller, J. C., 1967, Preliminary interpretation of a seismic-refraction profile across the Large Aperture Seismic Array, Montana; U.S. Geol. Survey Open File Report.
- Brown, T. G., and Poort, J. M., 1965, Subsurface studies and shallow-hole preparation LASA area, eastern Montana: Tech. Report 65-21, Geotech Corp. Garland, Texas.
- Chiburis, E. F., 1966, LASA travel-time anomalies for various epicentral regions: Prepared for Air Force Technical Applications Center, Washington, D. C., by Seismic Data Laboratory of Teledyne, Inc.
- Geyer, R. L., and Martner, S. T., 1969, SH waves from explosive sources: Geophysics, v. 34, no. 6, p. 893-905.
- Greenfield, R. J., and Sheppard, R. M., 1969, The Mohorovičić depth variations under the LASA and their effect on  $dT/d\Delta$  measurements: Seismol. Soc. America Bull., v. 59, no. 1, p. 409-420.
- Healy, J. H., Gibbs, J. F., Bohn, J., and Marshall, A., 1969, Crustal calibration of the large aperture seismic array site, Montana: U.S. Geological Survey report.

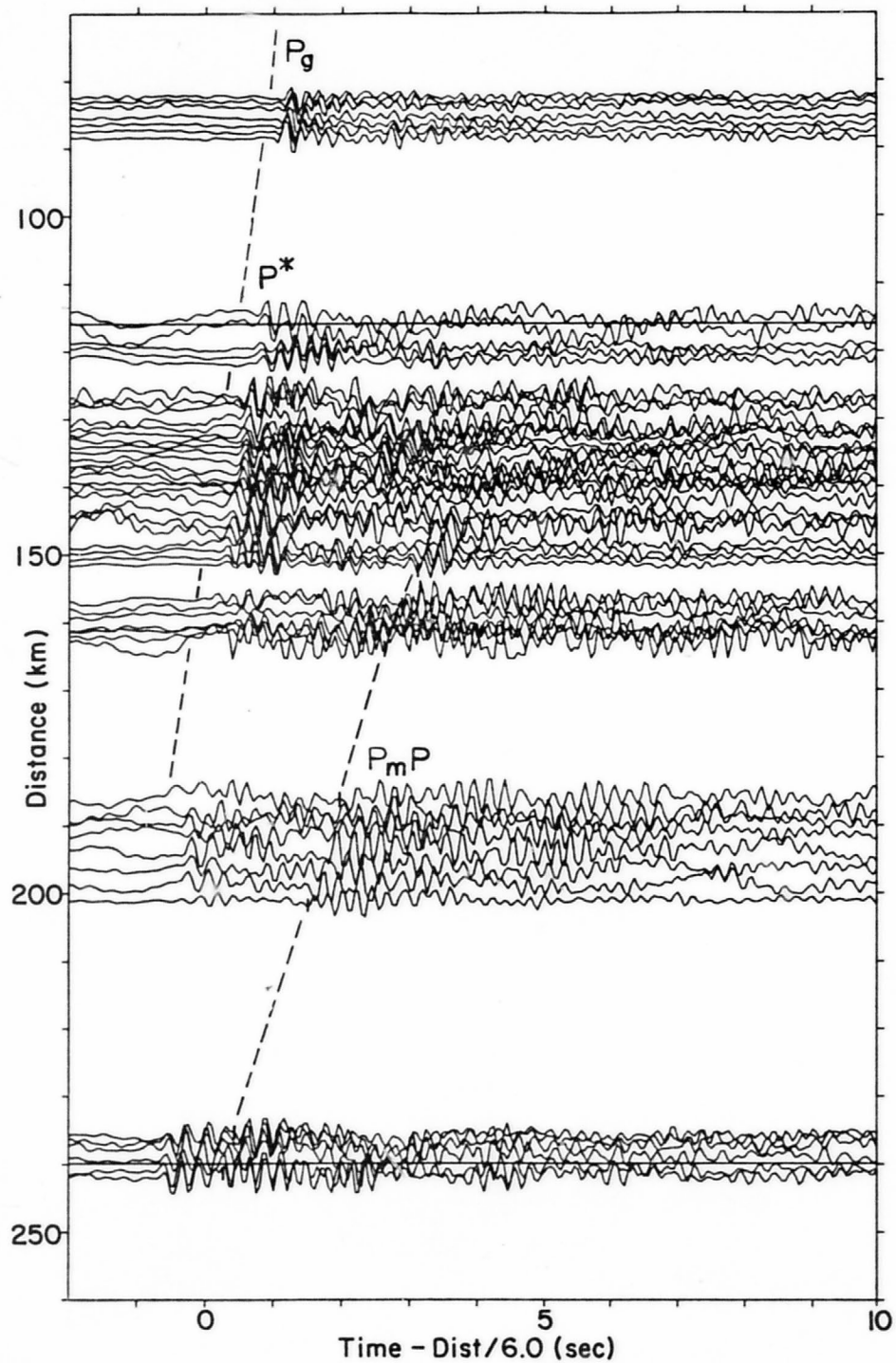
- Landisman, M., Sato, Y., and Usami, I., 1966, Propagation of disturbances in a Gutenberg-Bullen A' spherical earth model: traveltimes and amplitudes of S waves: in The earth beneath the continents, J. S. Steinhart and T. Jefferson Smith, ed., Am. Geophys. Union Mon. 10, p. 482-494.
- McCamy, K., and Meyer, R. P., 1964, A correlation method of apparent velocity measurement: Jour. Geophys. Res., v. 69, no. 4, p. 691-699.
- Meyer, R. P., Steinhart, J. S., and Bonini, W. E., 1961, Montana, 1959: ch. 9, in Explosion studies of continental structure: Carnegie Institution of Washington Publication 622, Washington, D. C., p. 305-343.
- Warrick, R. E., Hoover, D. B., Jackson, W. H., Pakiser, L. C., and Roller, J. C., 1961: The specification and testing of a seismic-refraction system for crustal studies: Geophysics, v. 26, no. 6, p. 820-824.

## Appendix

### Record Sections

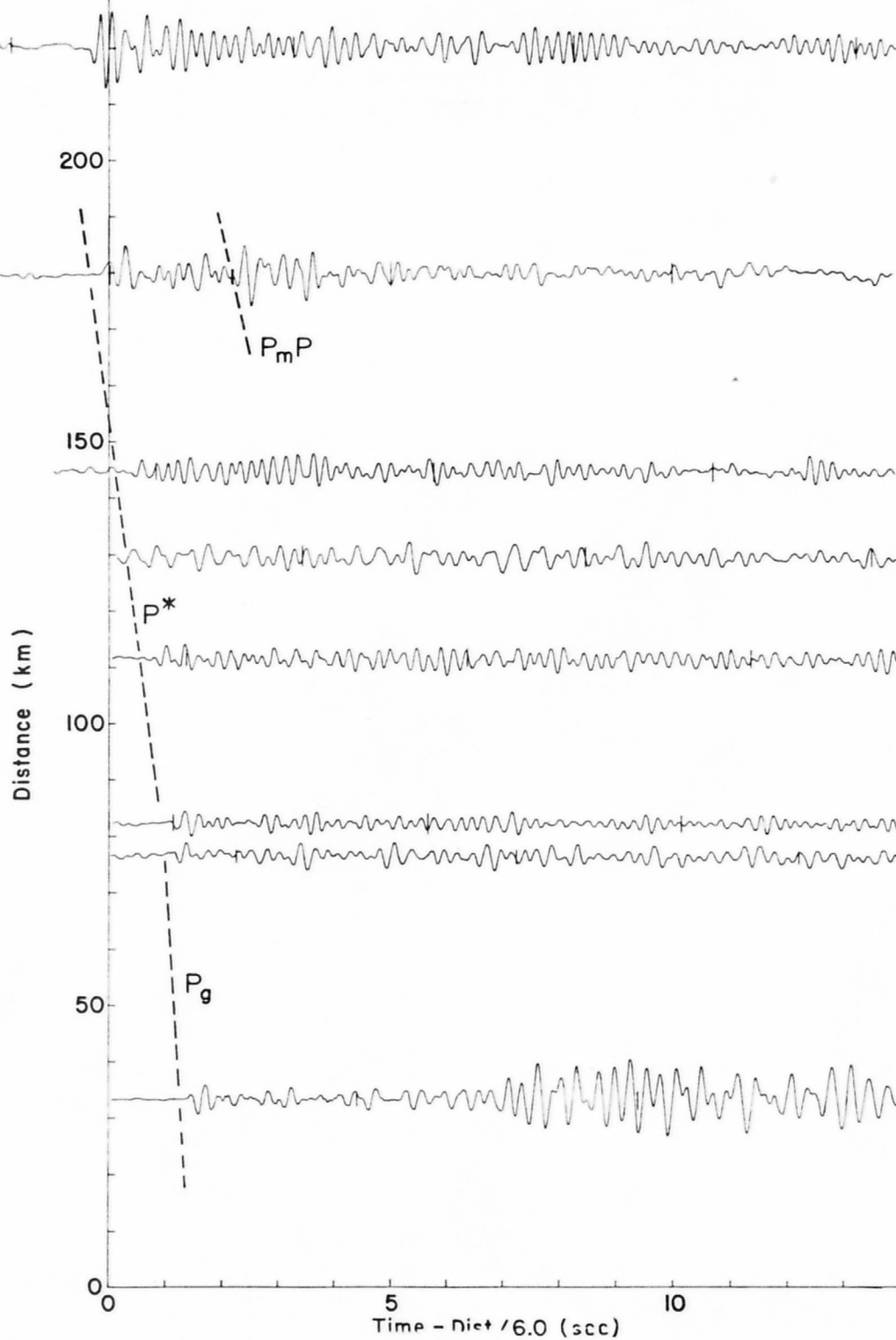
Sections are numbered 1 through 48, followed by tables to identify the traces and picked  $P_m$  arrivals. Phases are marked by dashed lines and labeled. Their nature is described on pages 13-21 of this report, and Figures 5 and 9 show ray diagrams of most phases. Upper-mantle phases are divided into two parts,  $P_{n1}$ , and  $P_{n2}$ , on sections 17, 17A, and 18.

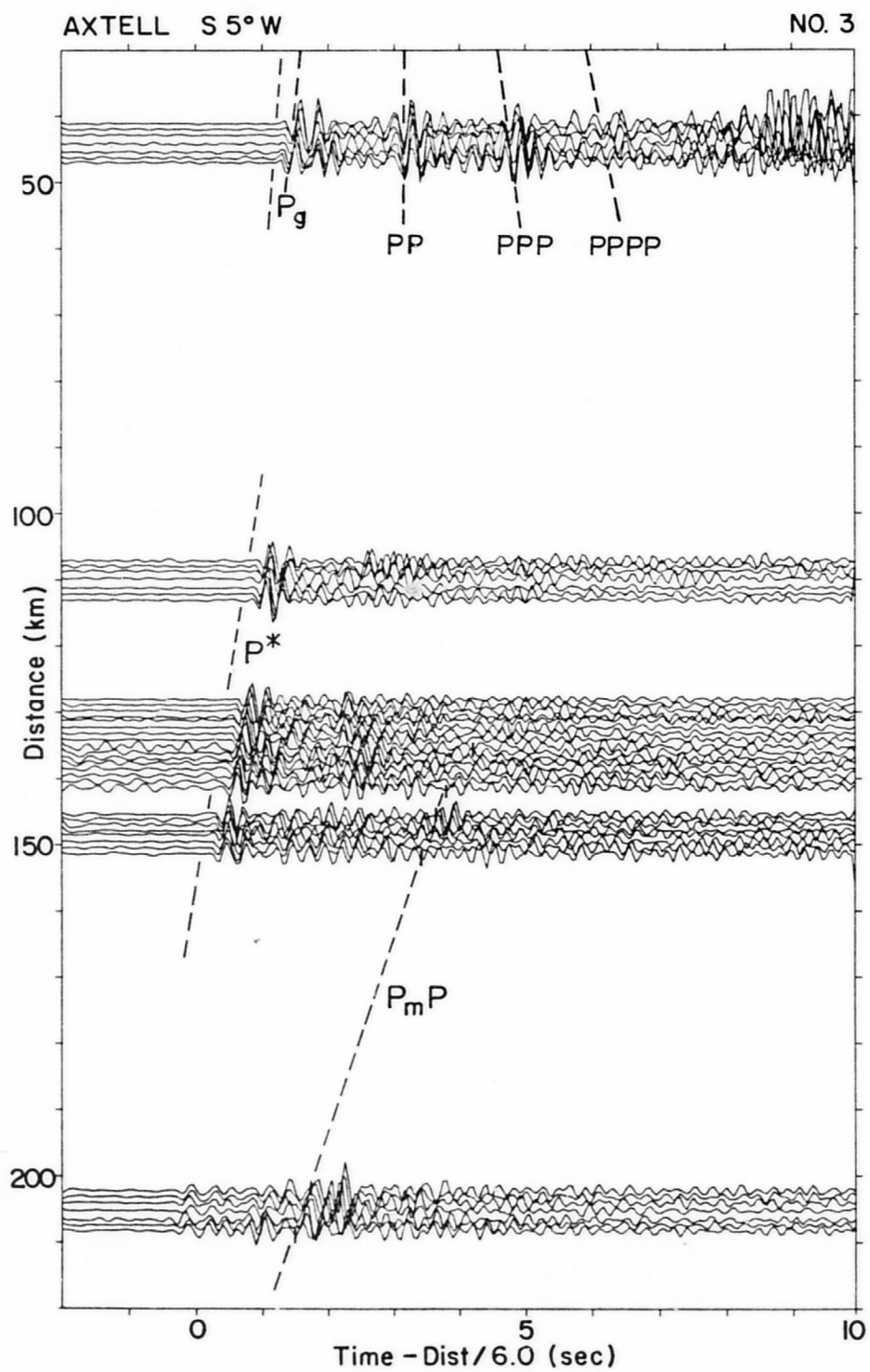
These record sections are composed of data from three recording systems. LASA recordings were obtained on digital computer magnetic tape, while the two USGS systems were recorded on analog magnetic tape. LASA recordings were plotted on a digital computer, after selection of approximately six of the 21 traces available in each subarray. USGS recordings were hand traced onto sections from analog playbacks; one trace from a portable station and one, two, or three traces from a recording truck array.

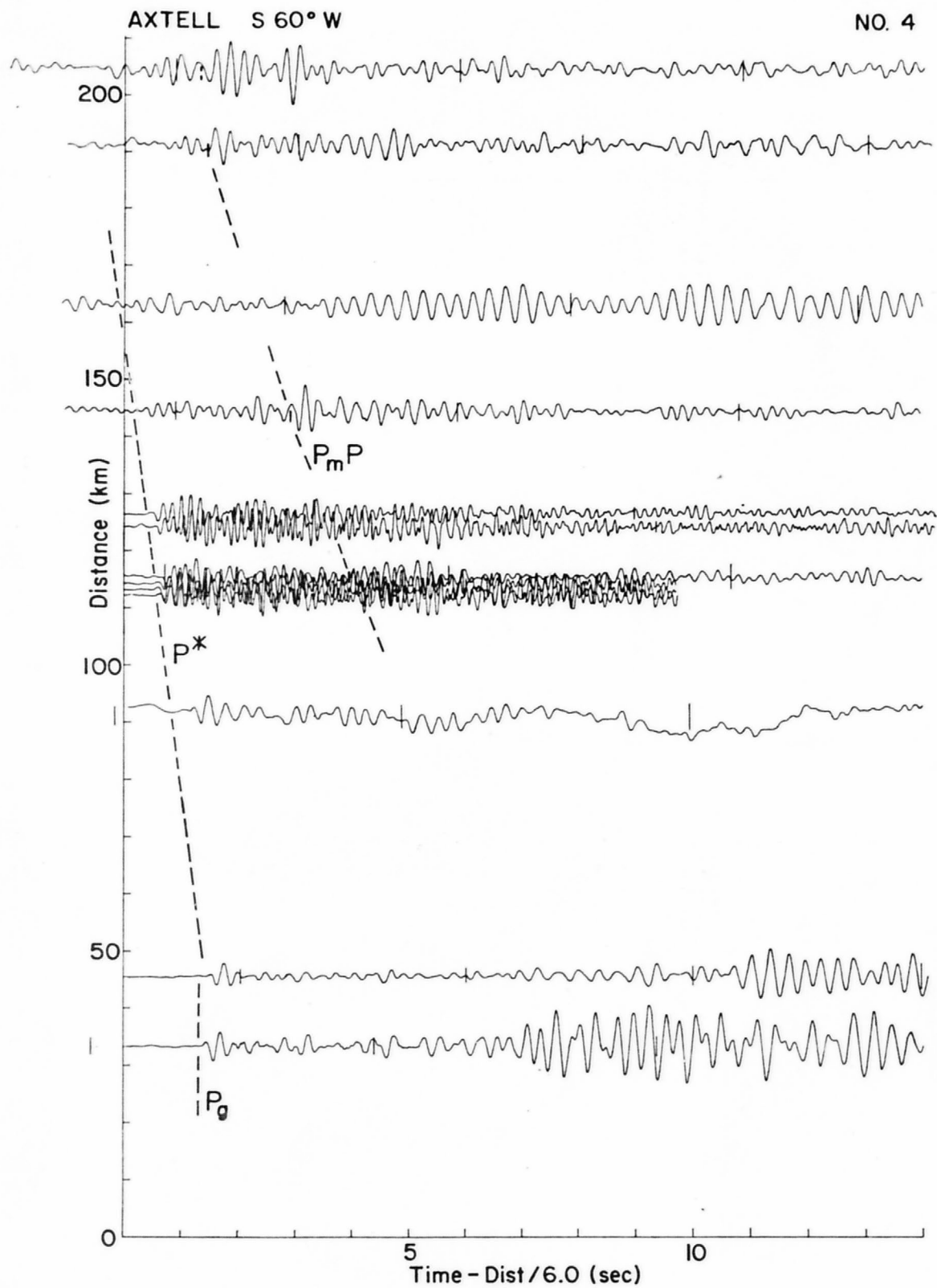


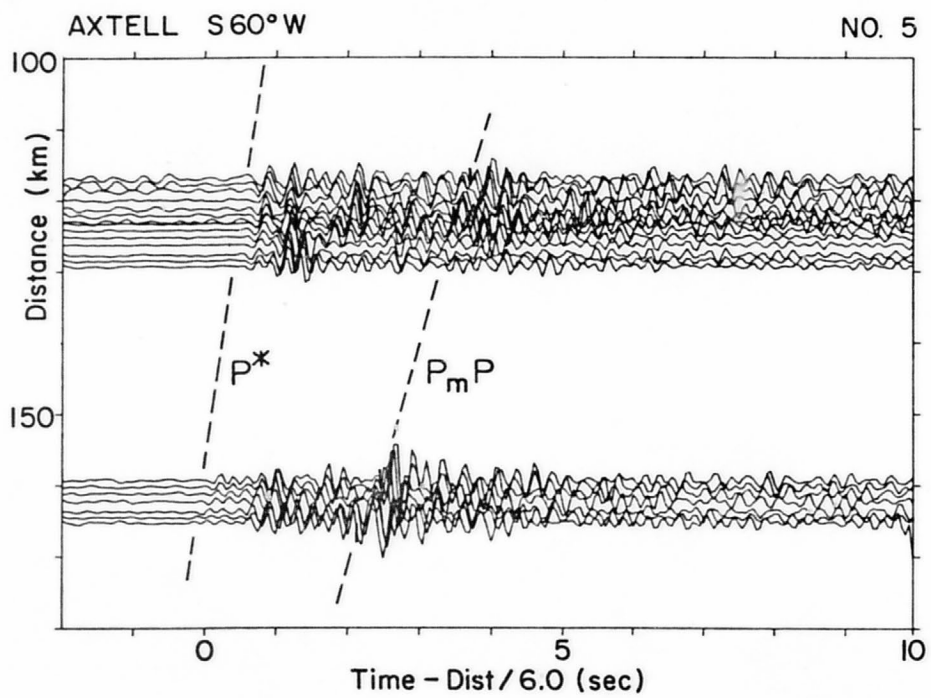
AXTELL S 5°W

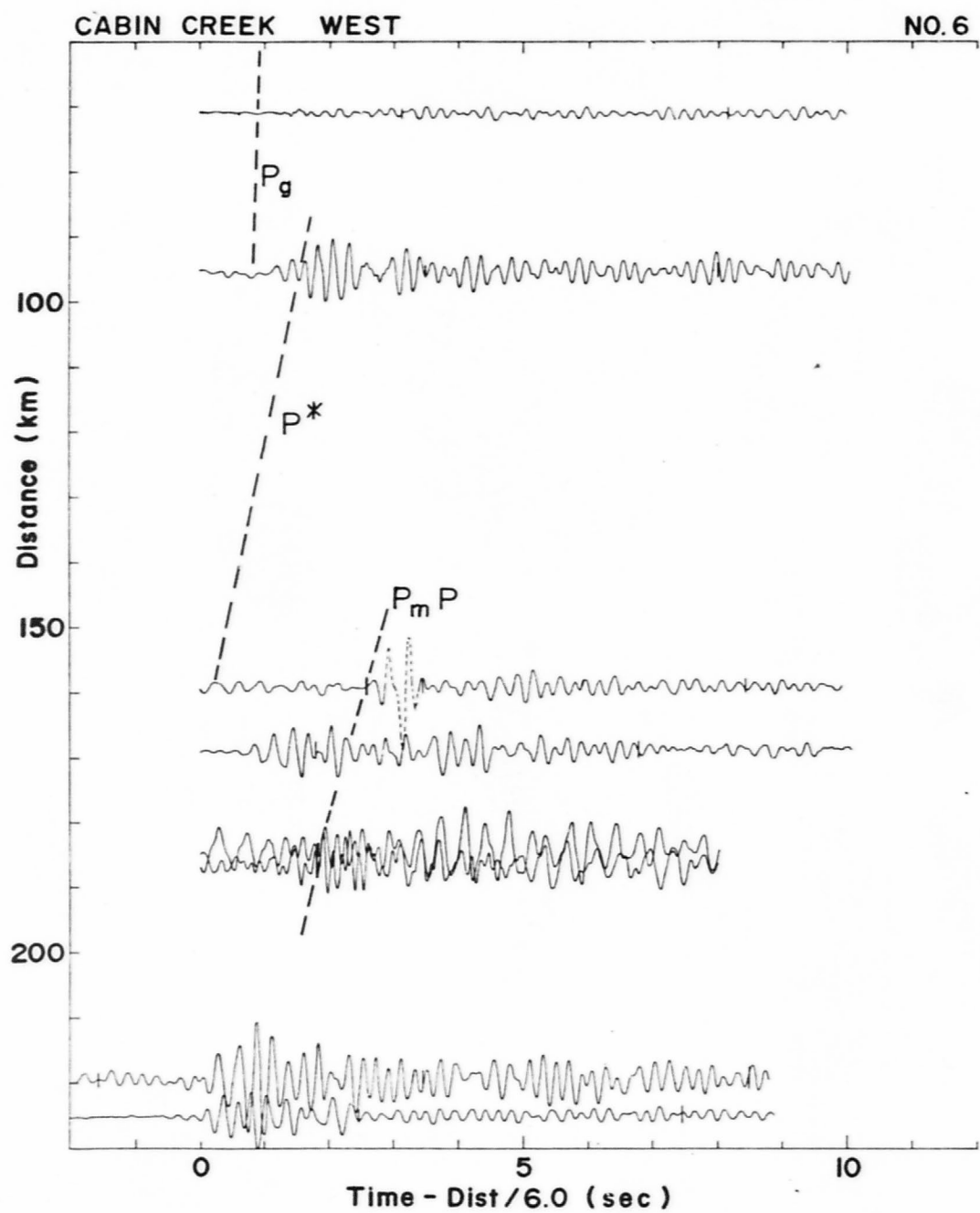
NO. 2

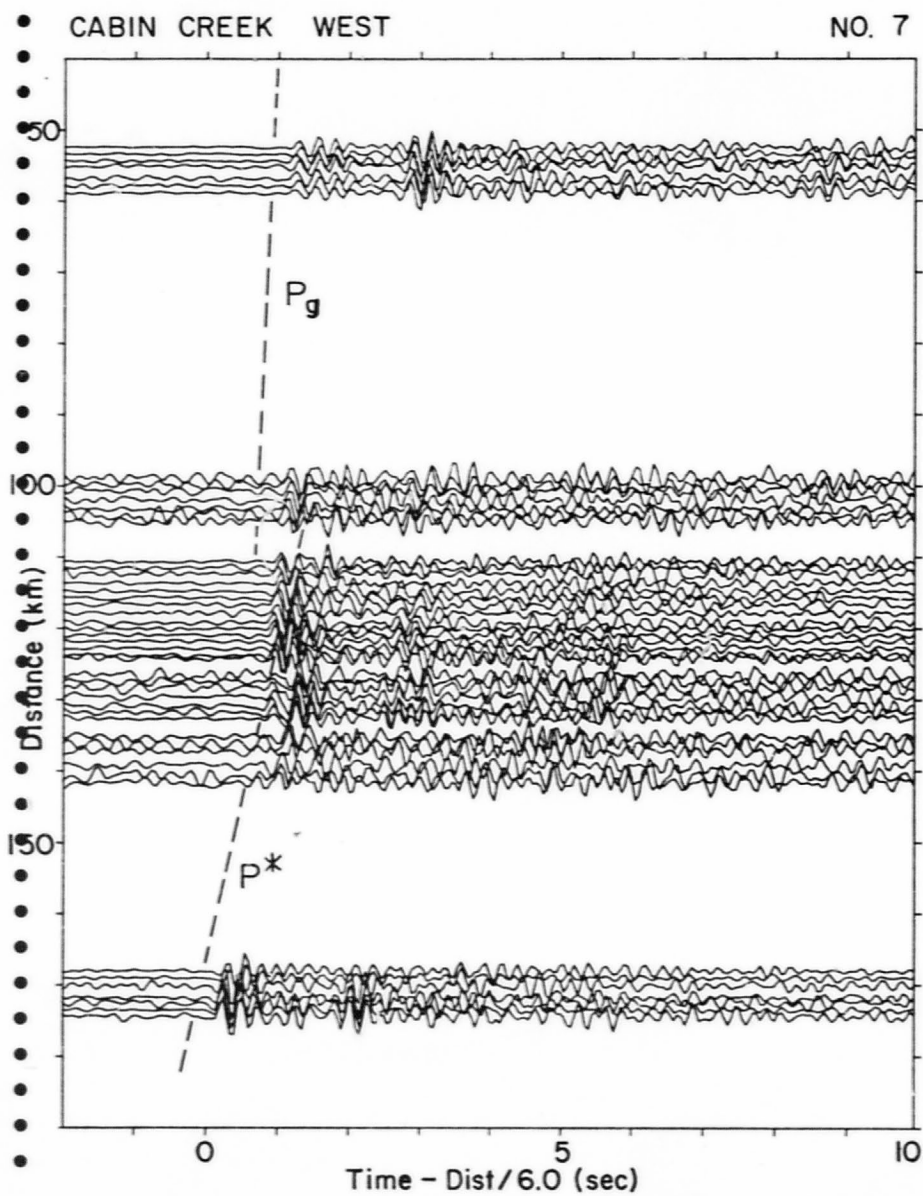


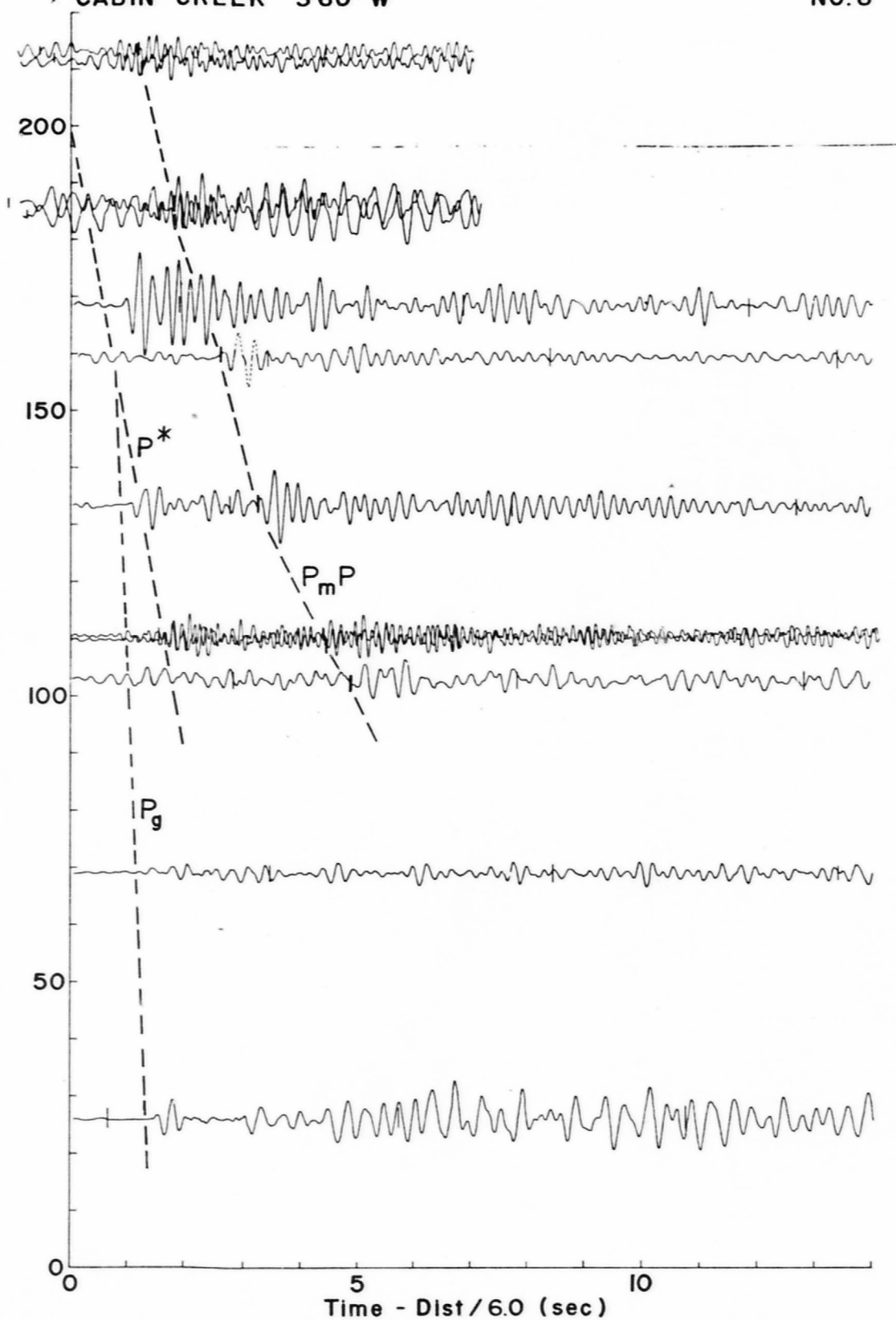


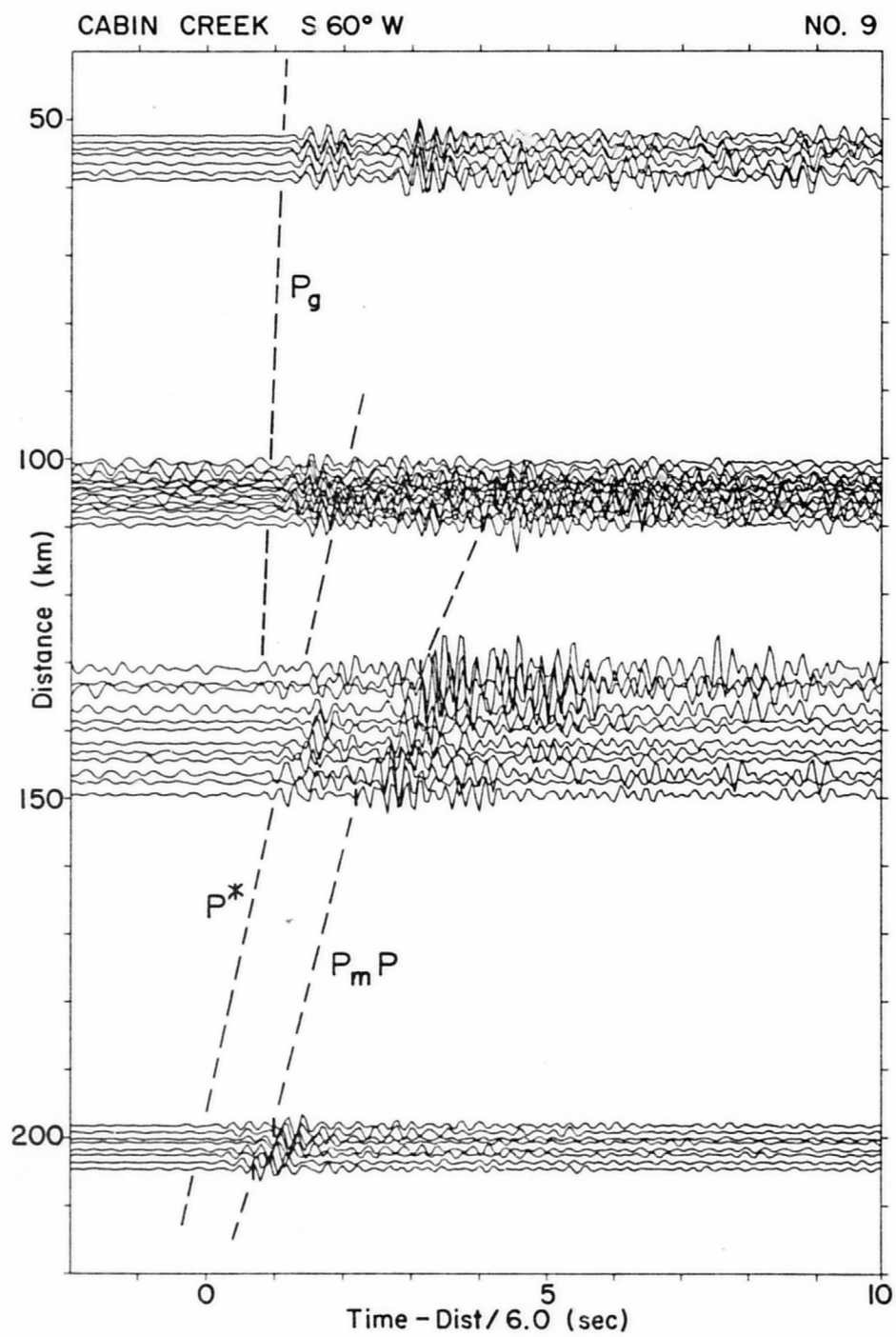






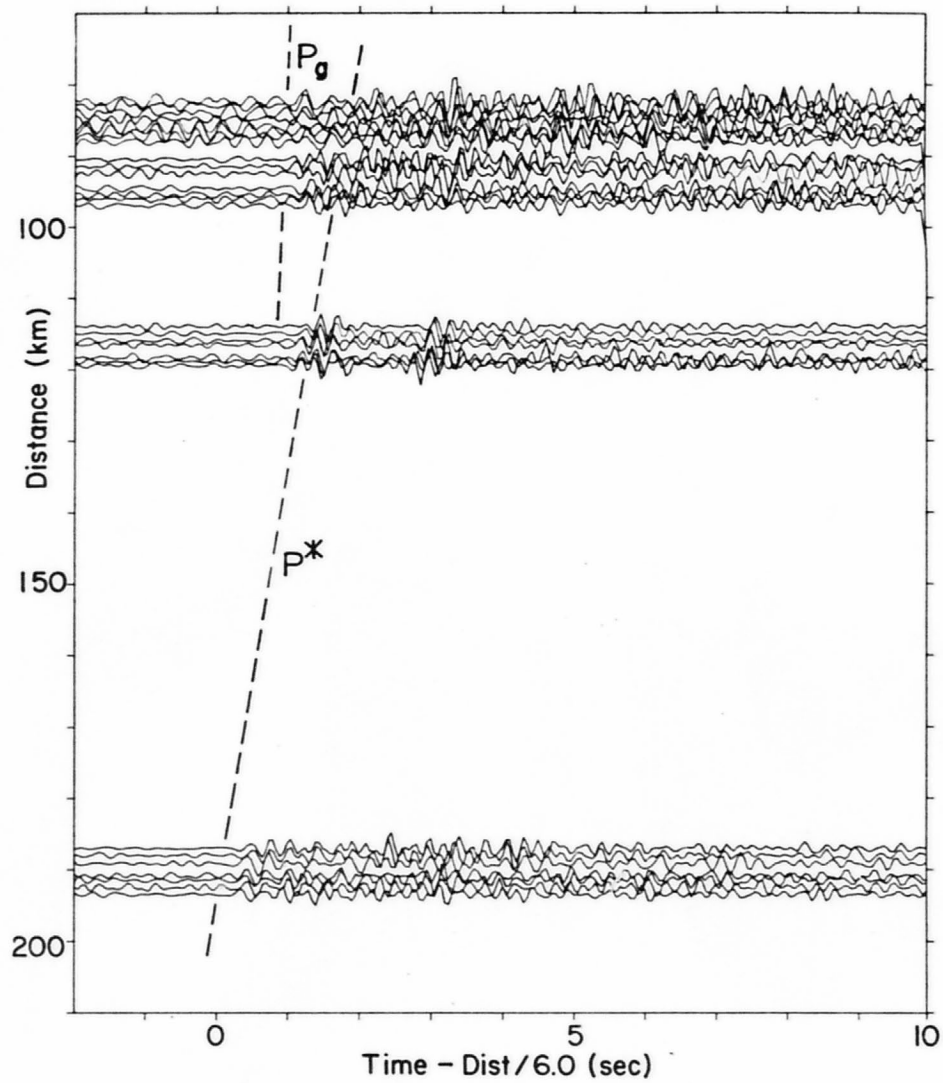


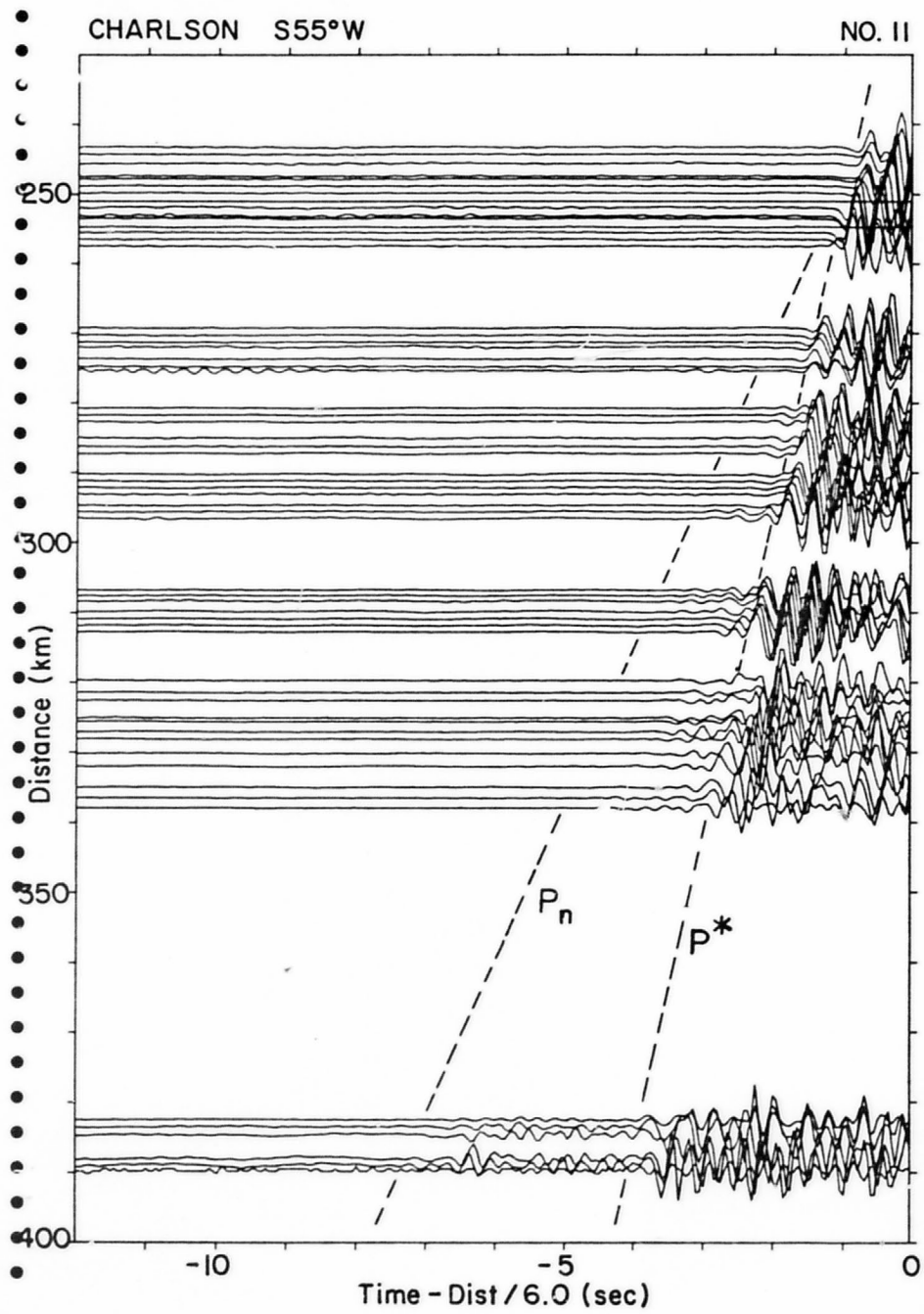


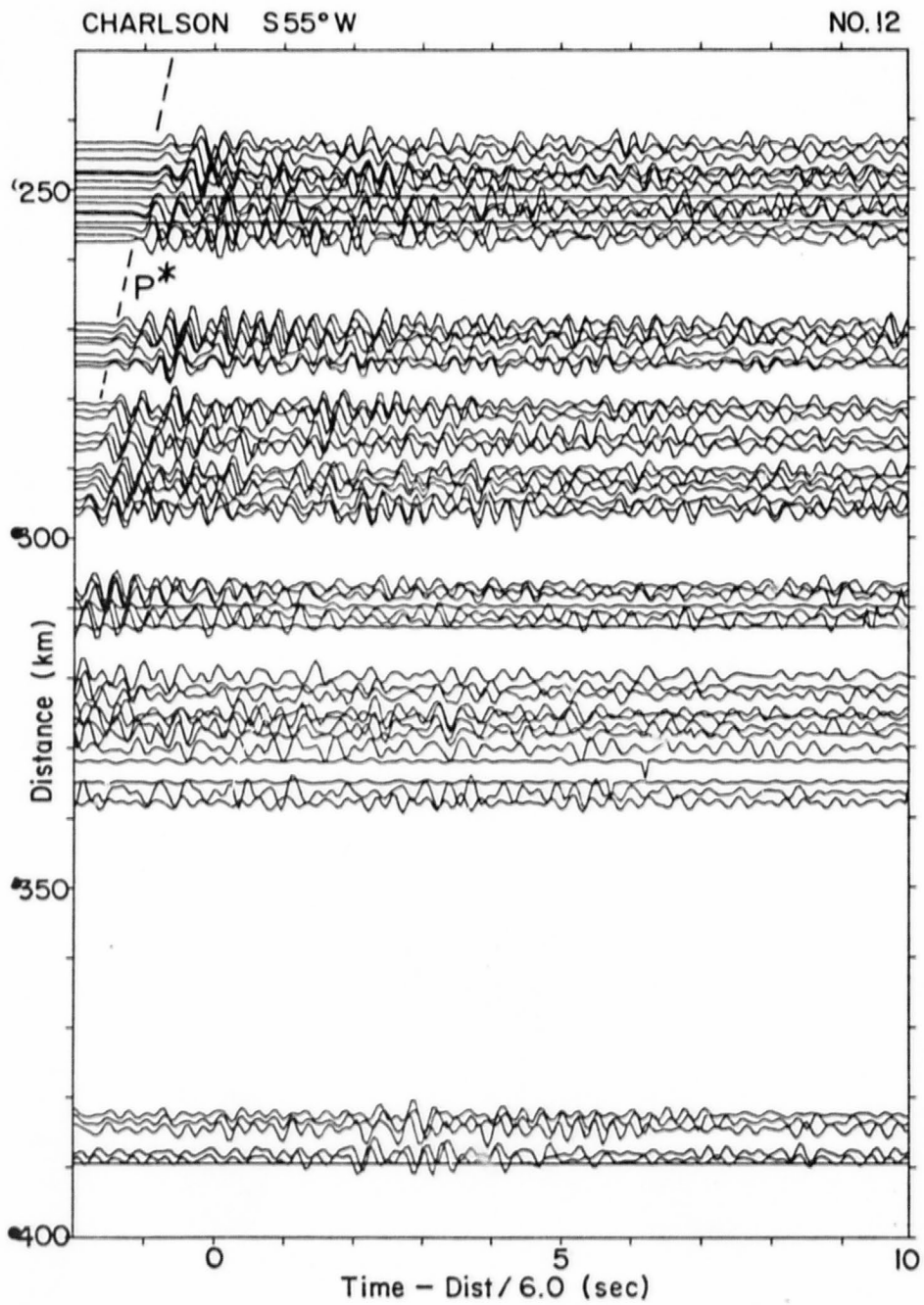


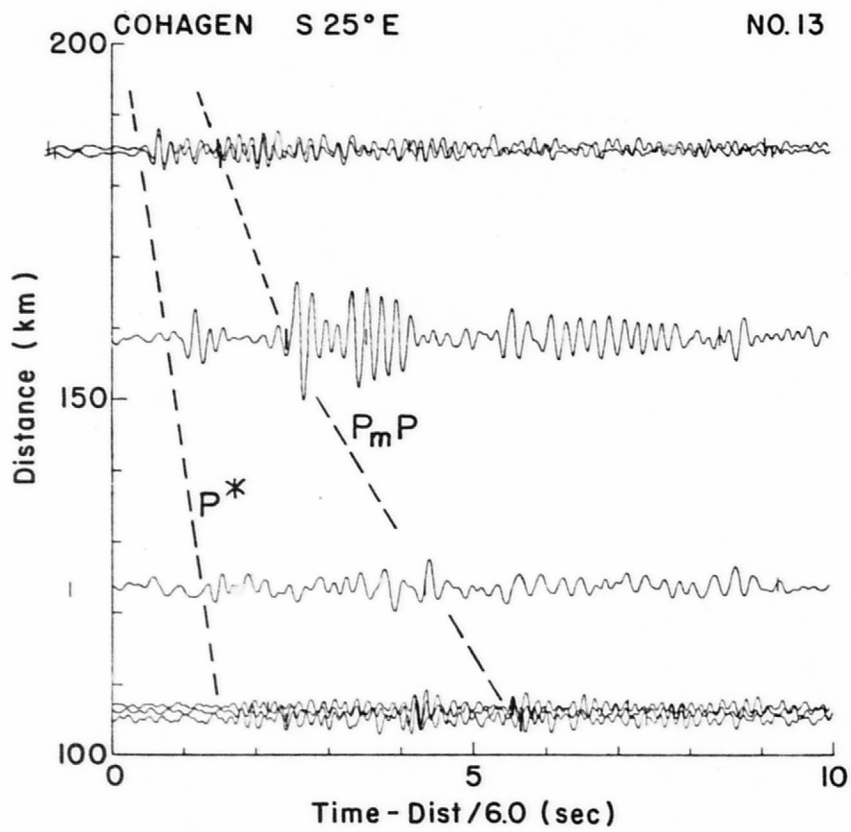
CABIN CREEK N55°W

NO. 10

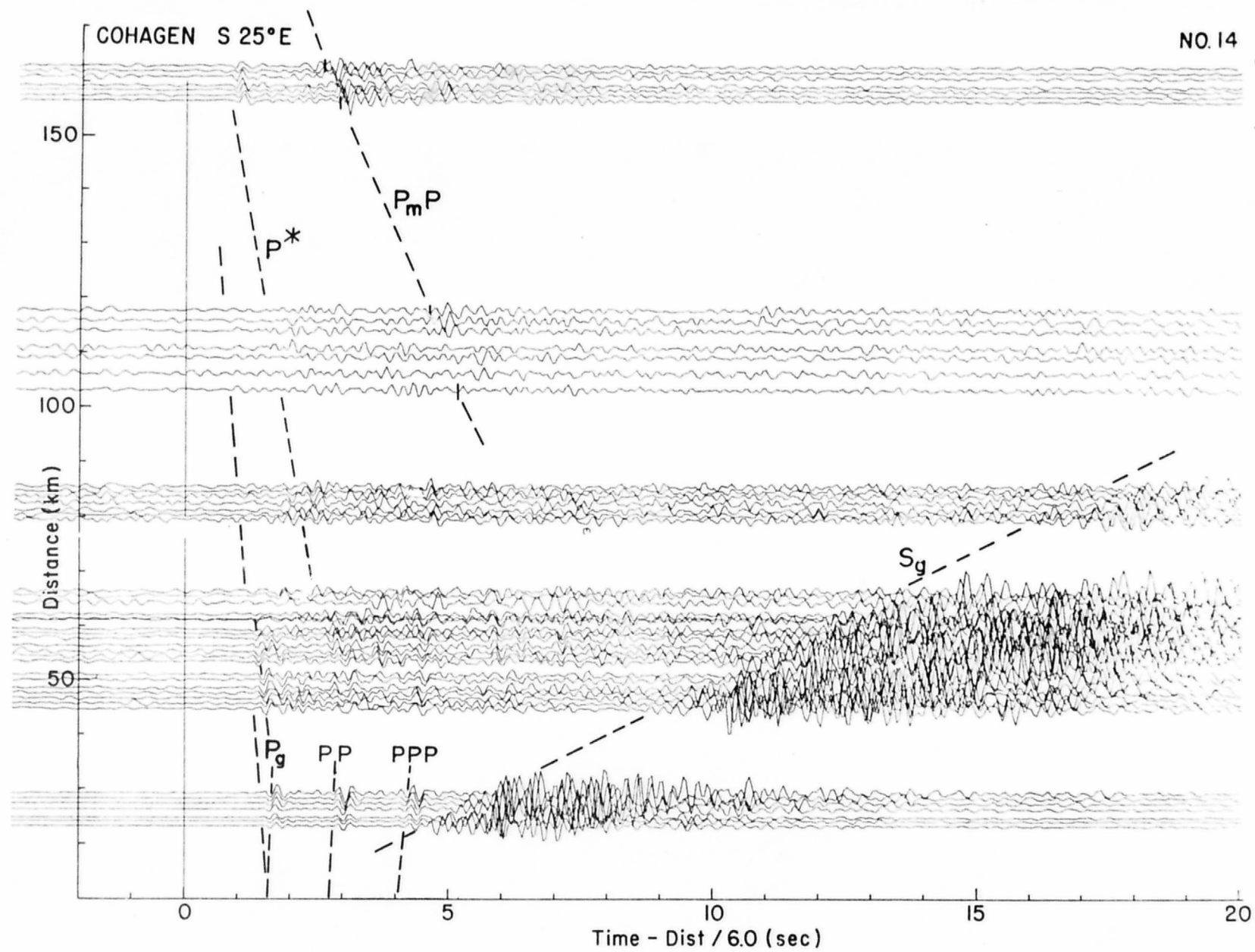


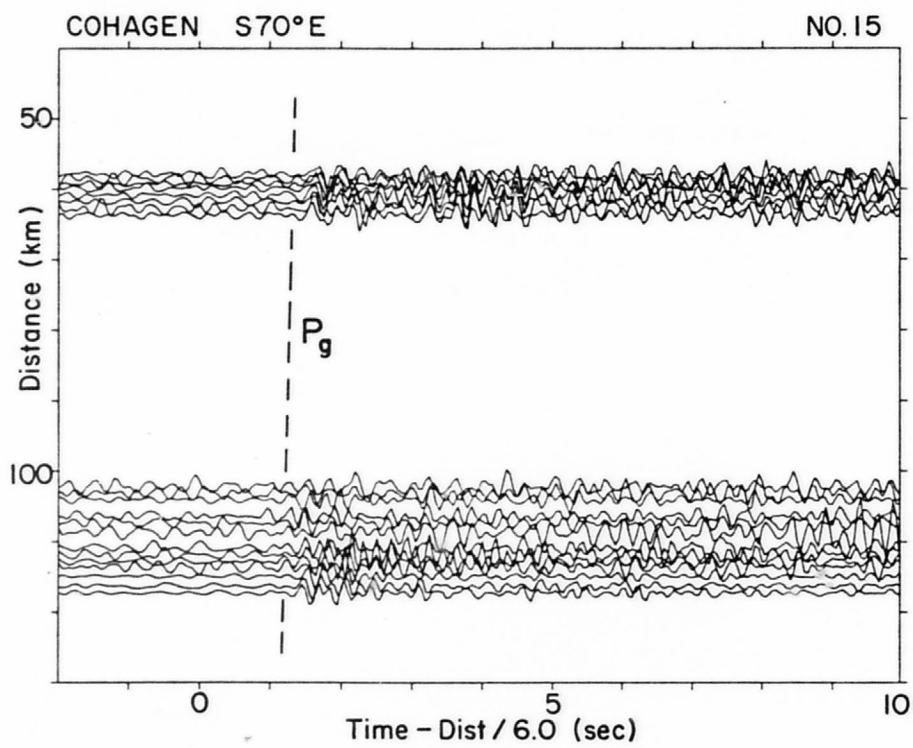


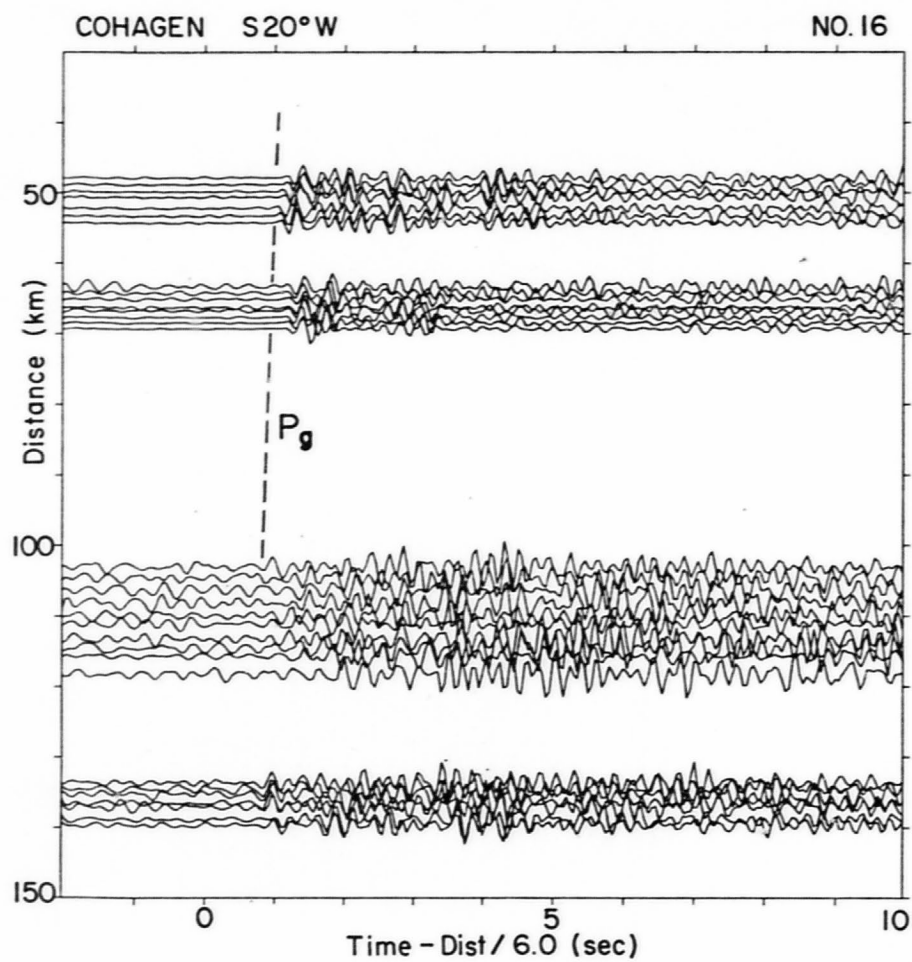




A-14

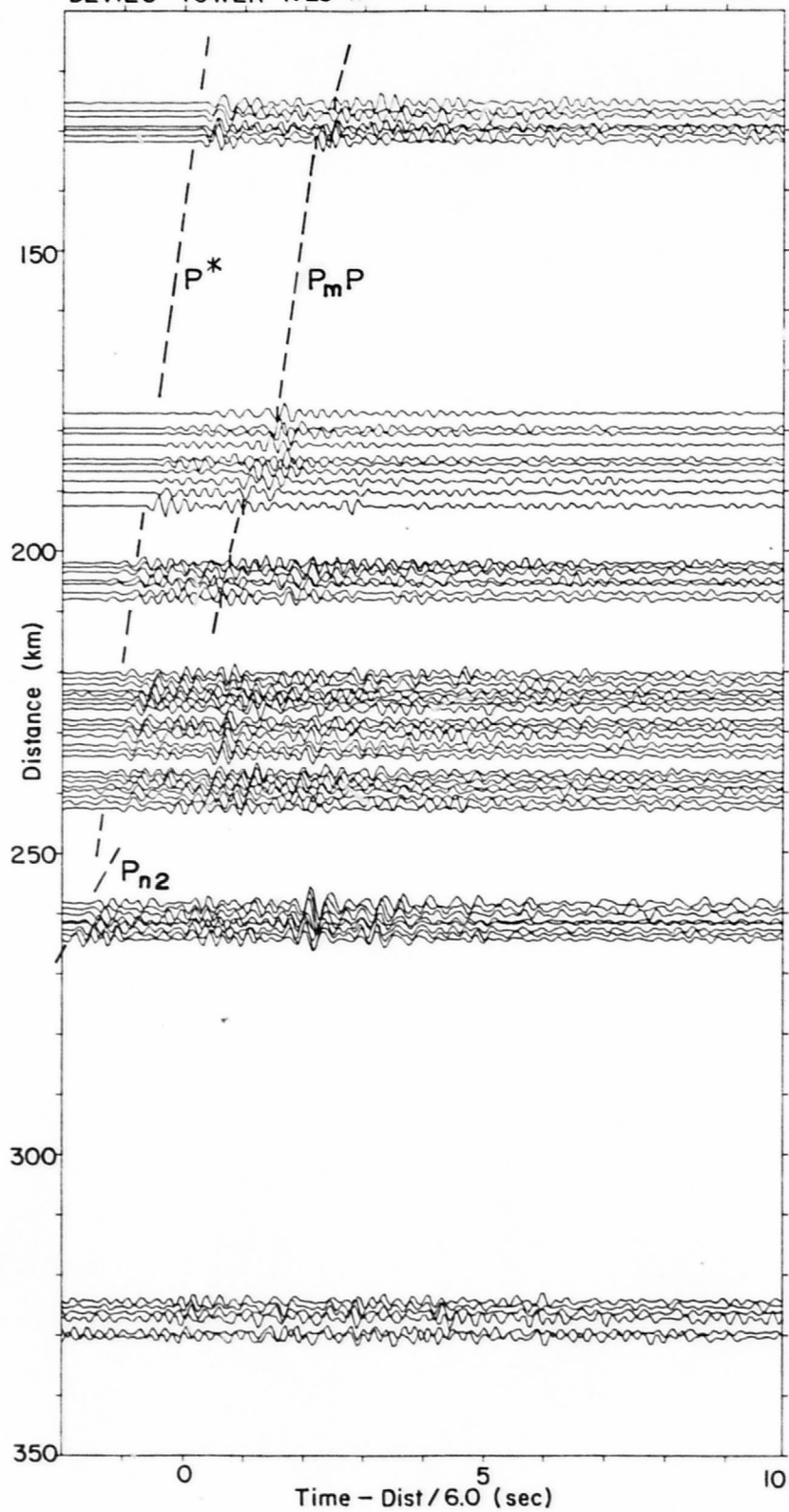


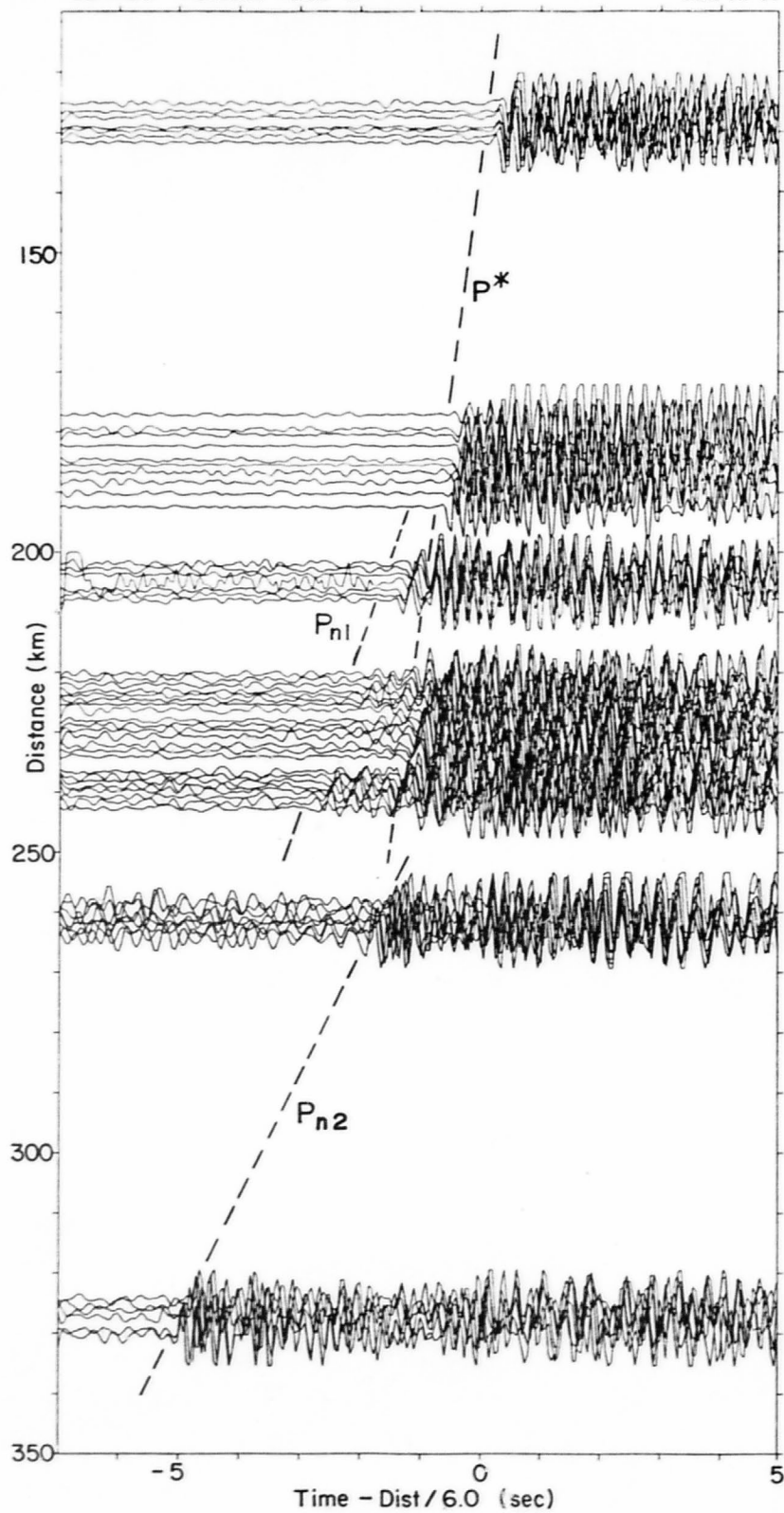


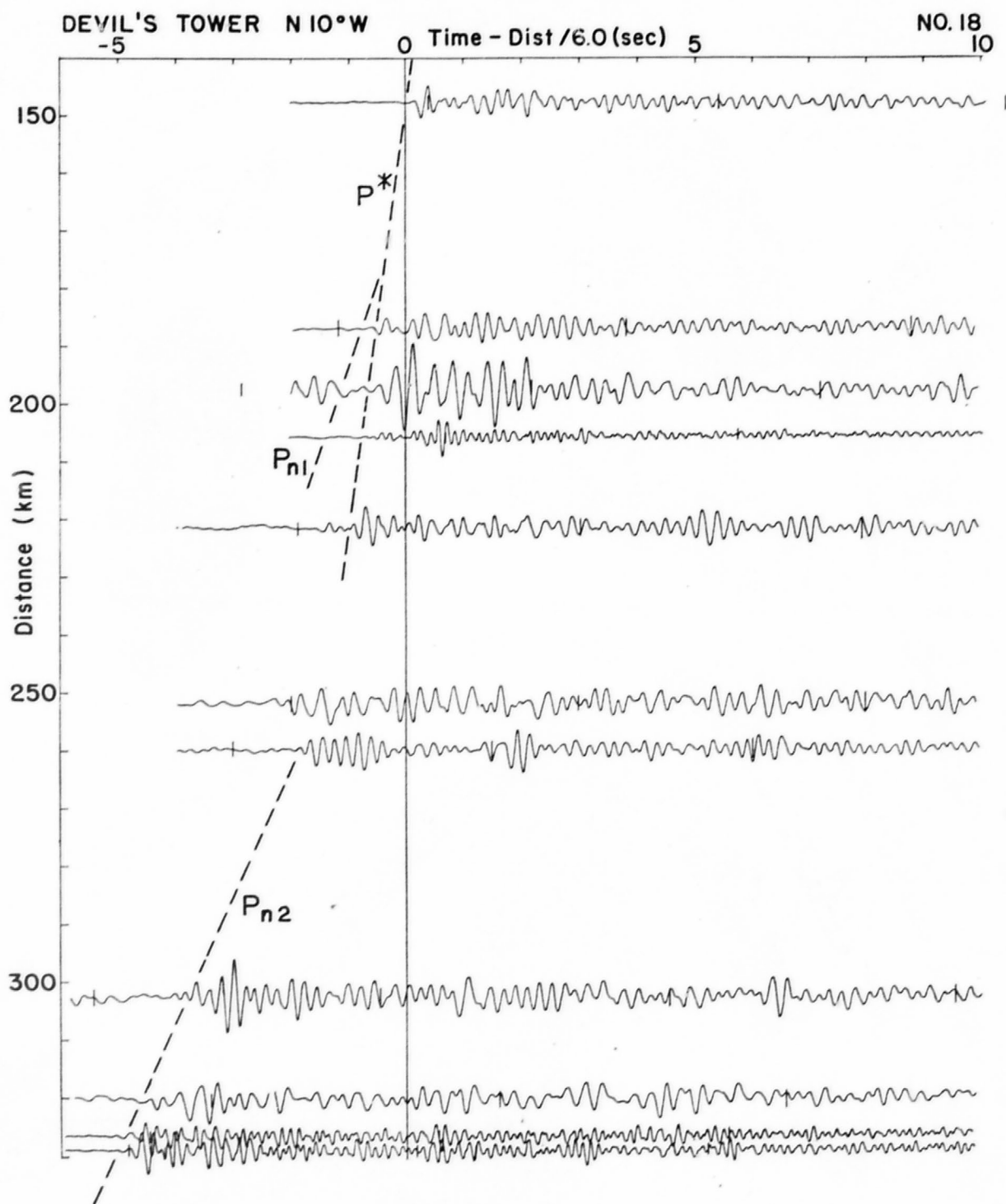


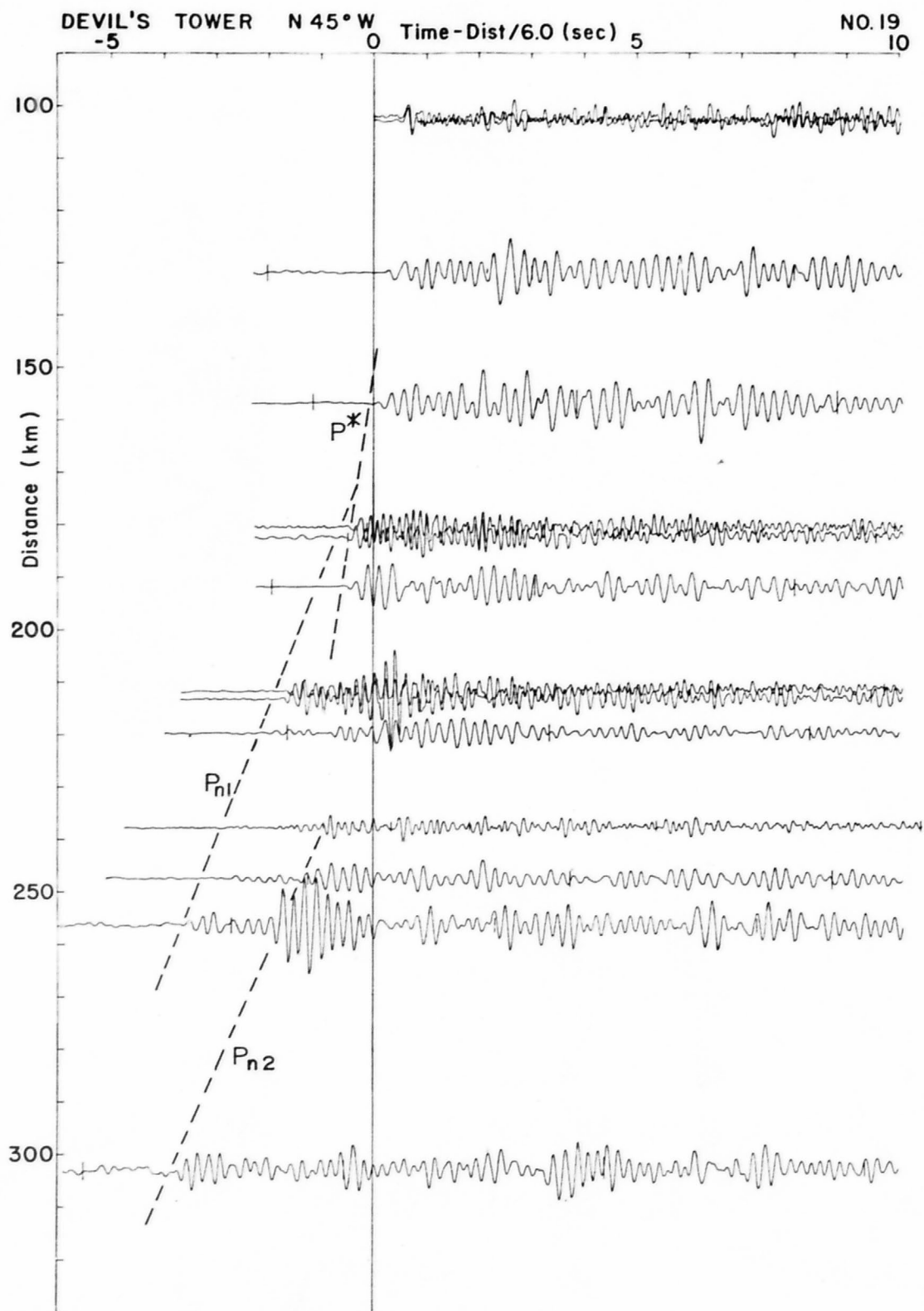
DEVIL'S TOWER N25°W

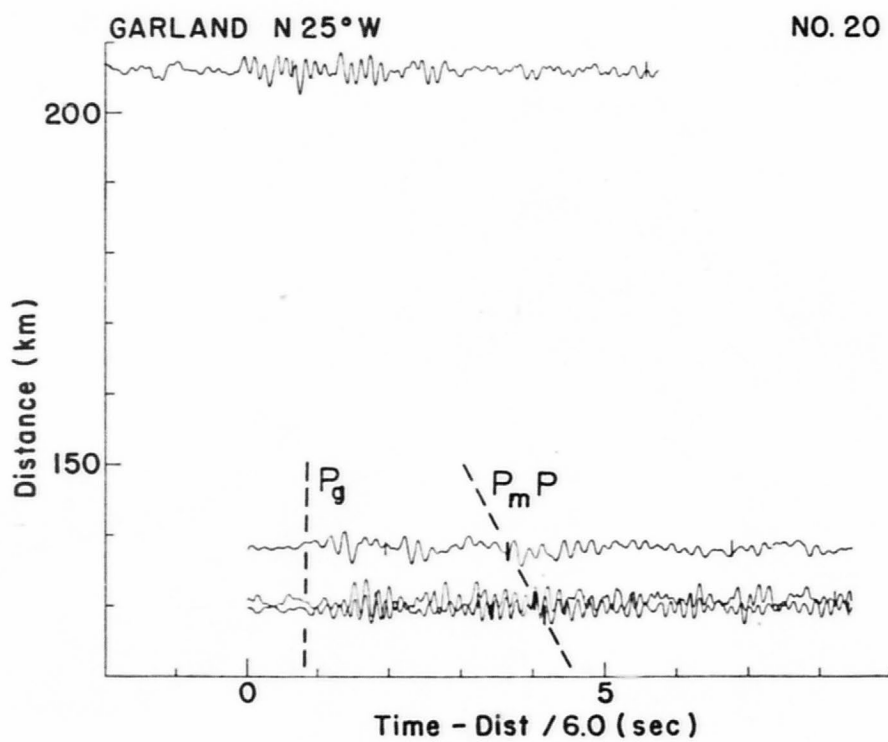
NO. 17





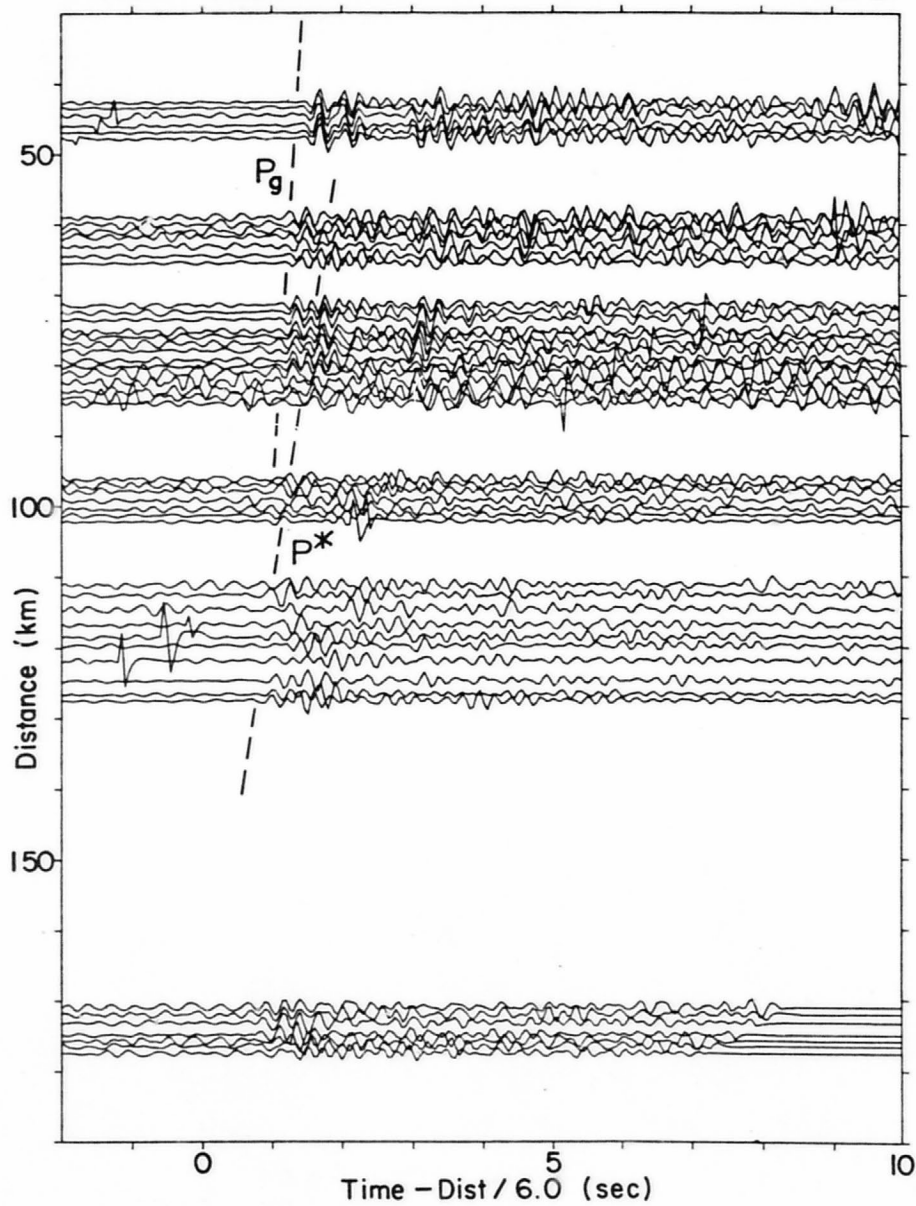


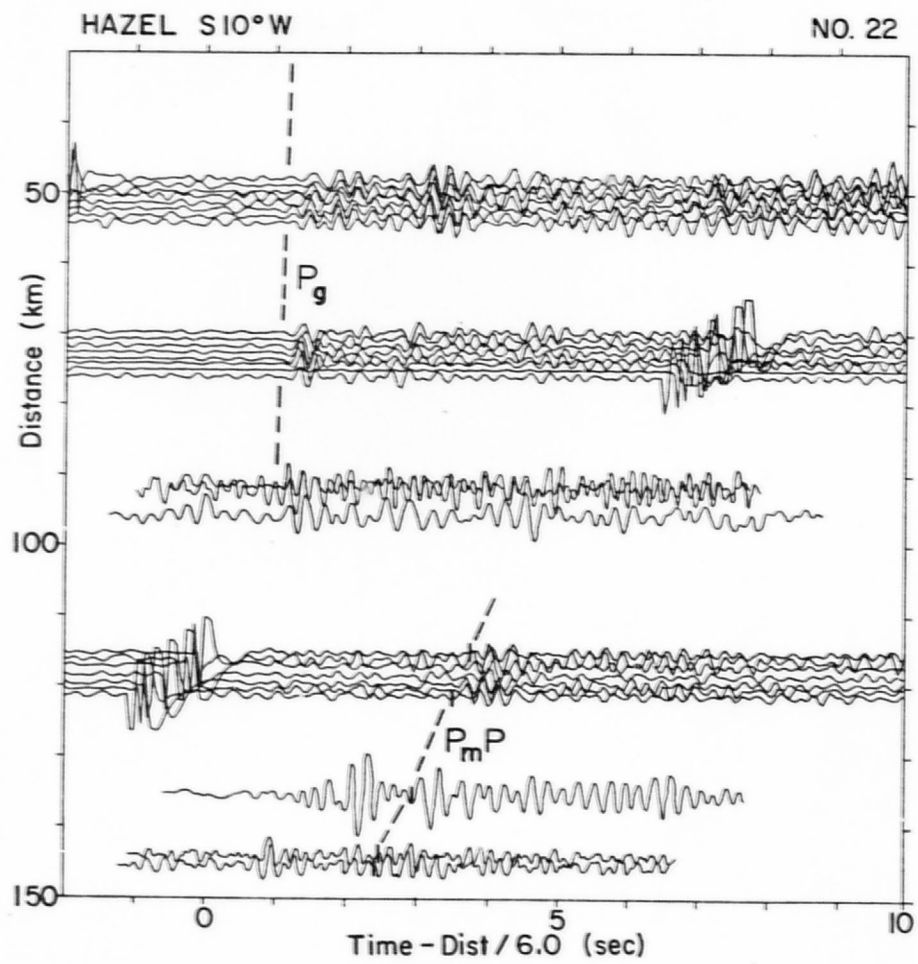


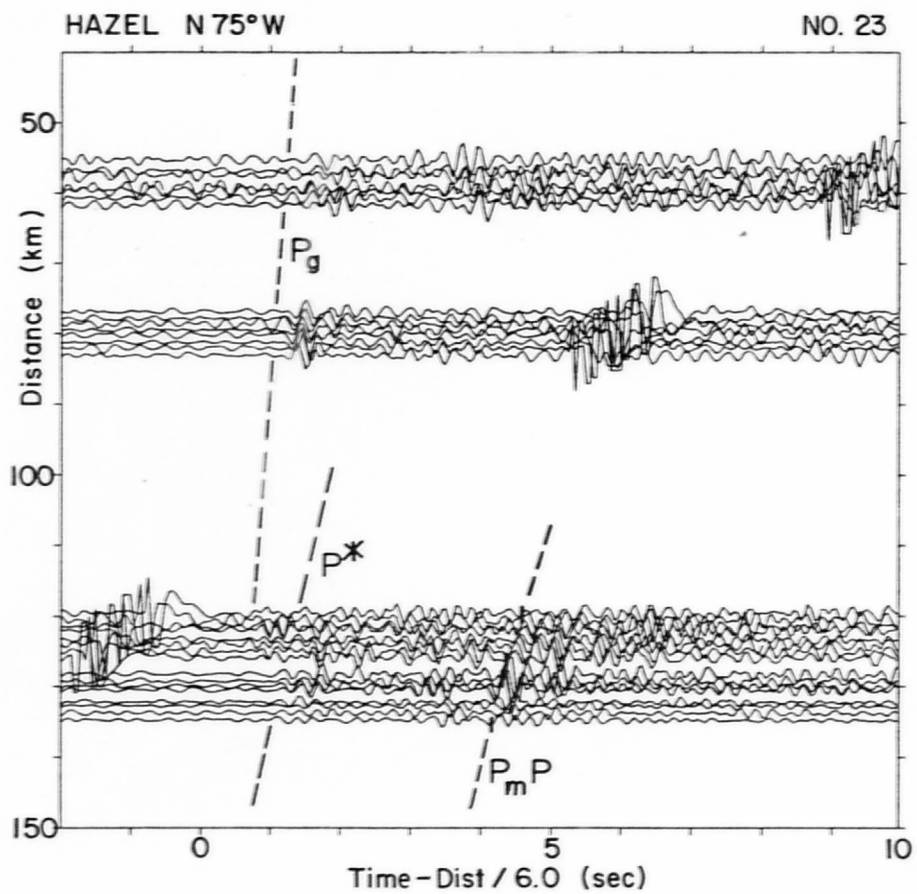


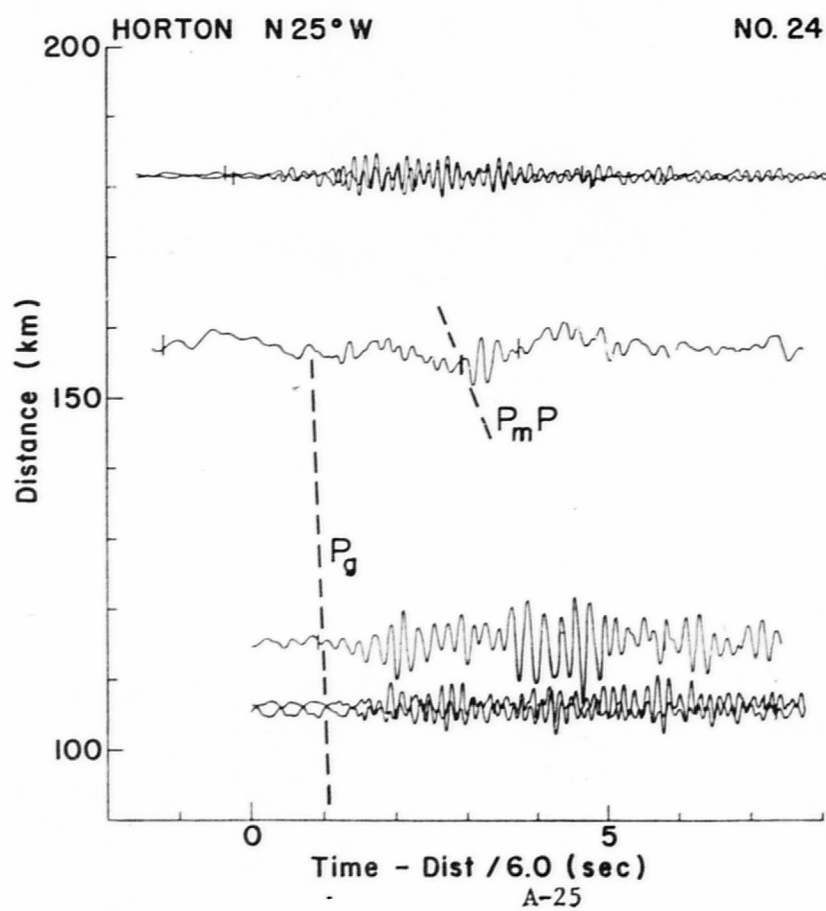
HAZEL S 55° W

NO. 21



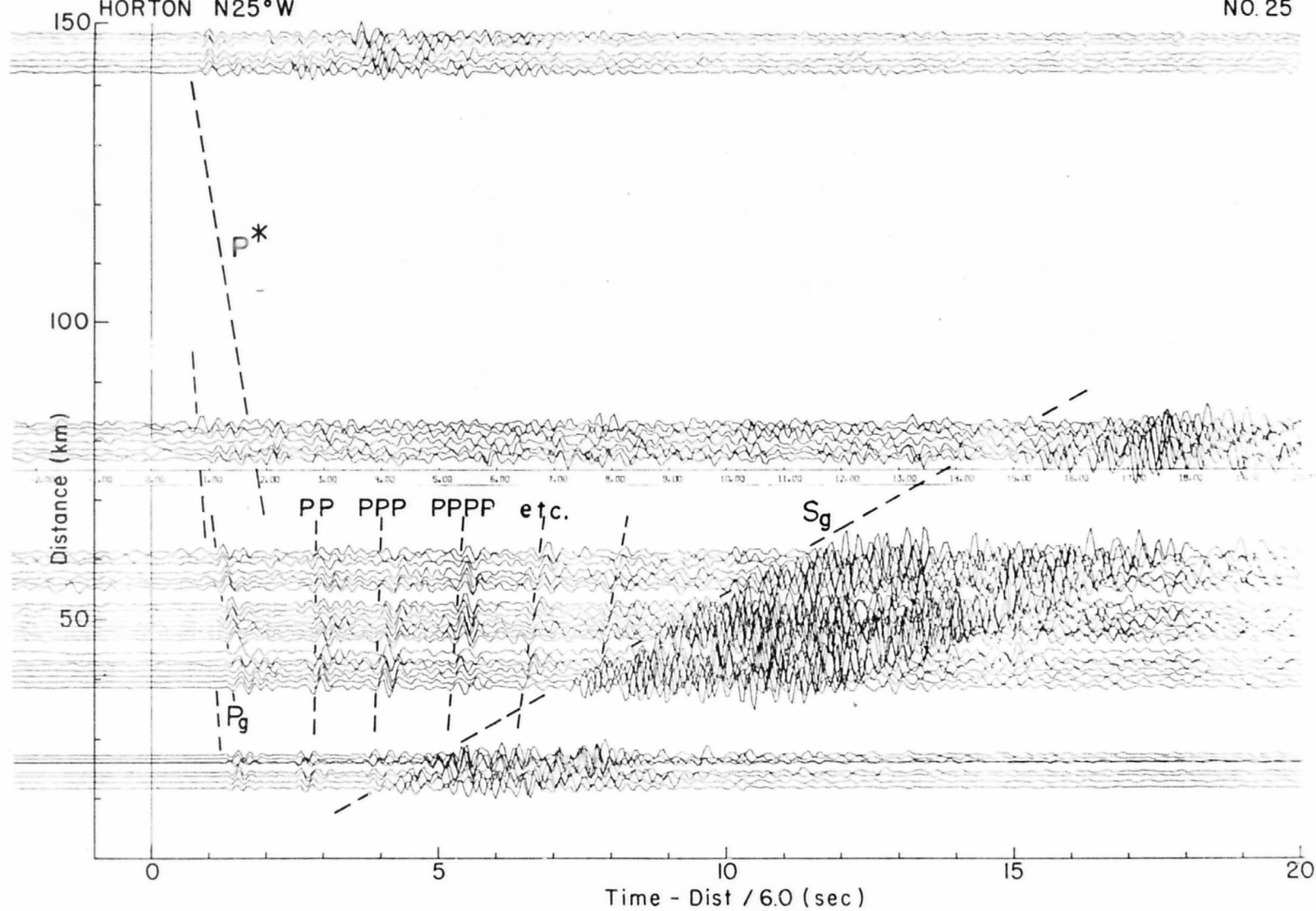




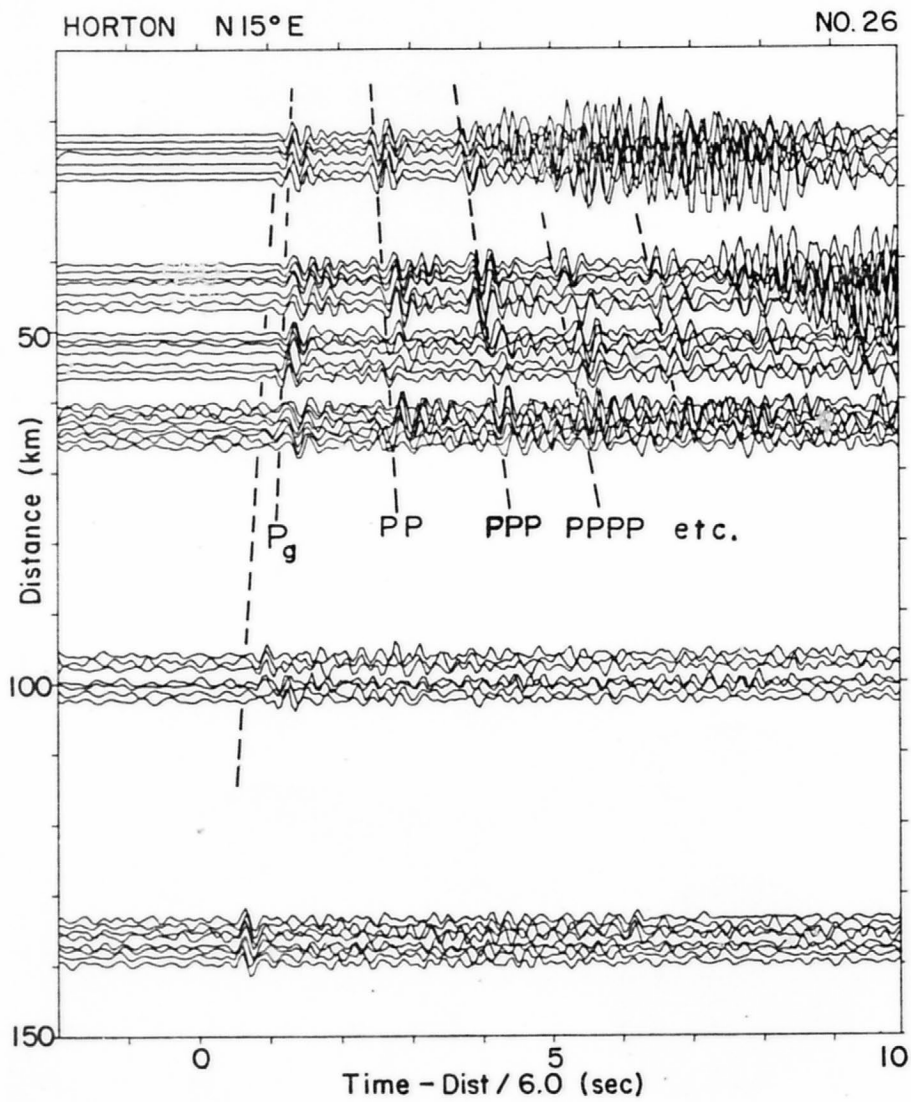


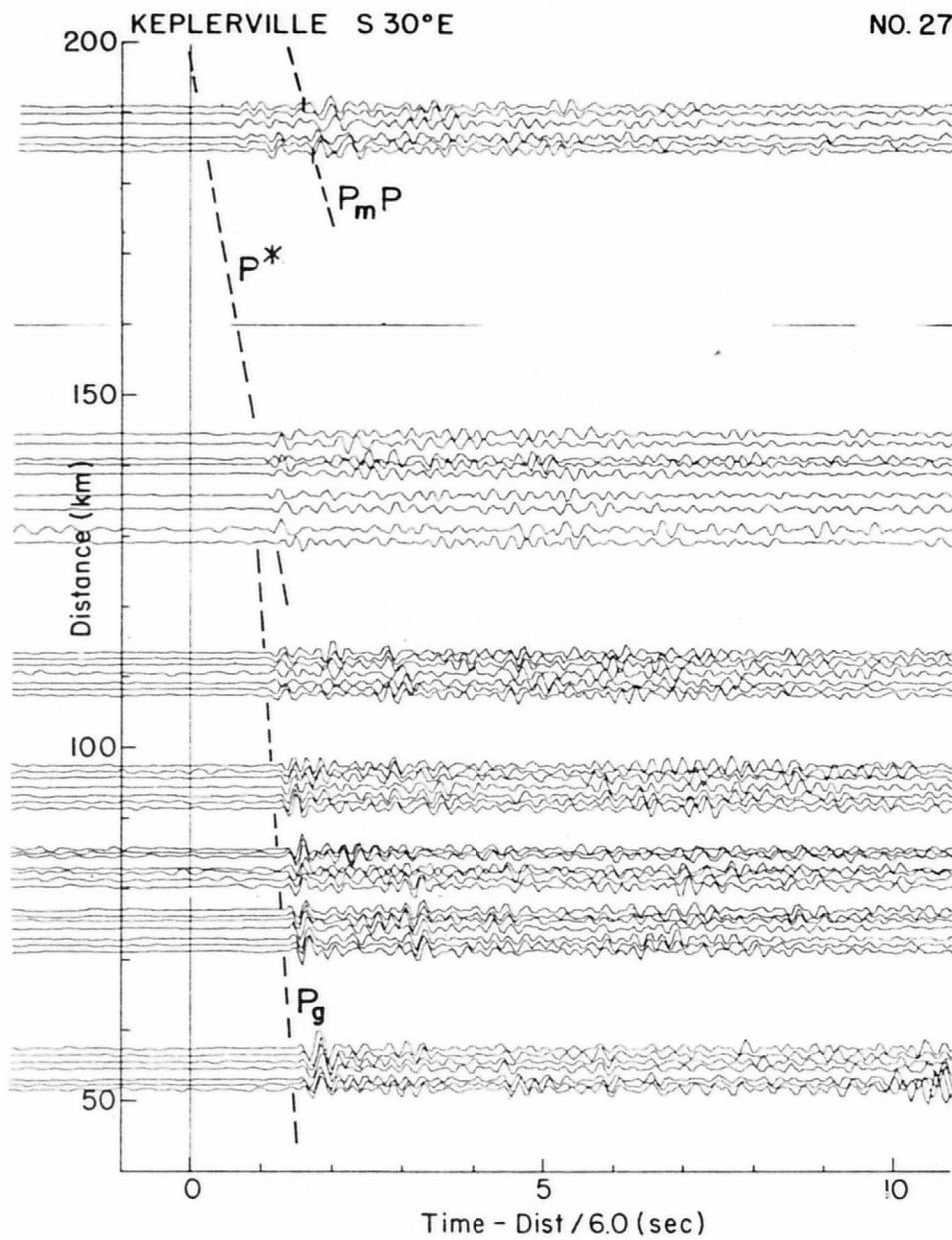
HORTON N25°W

NO. 25



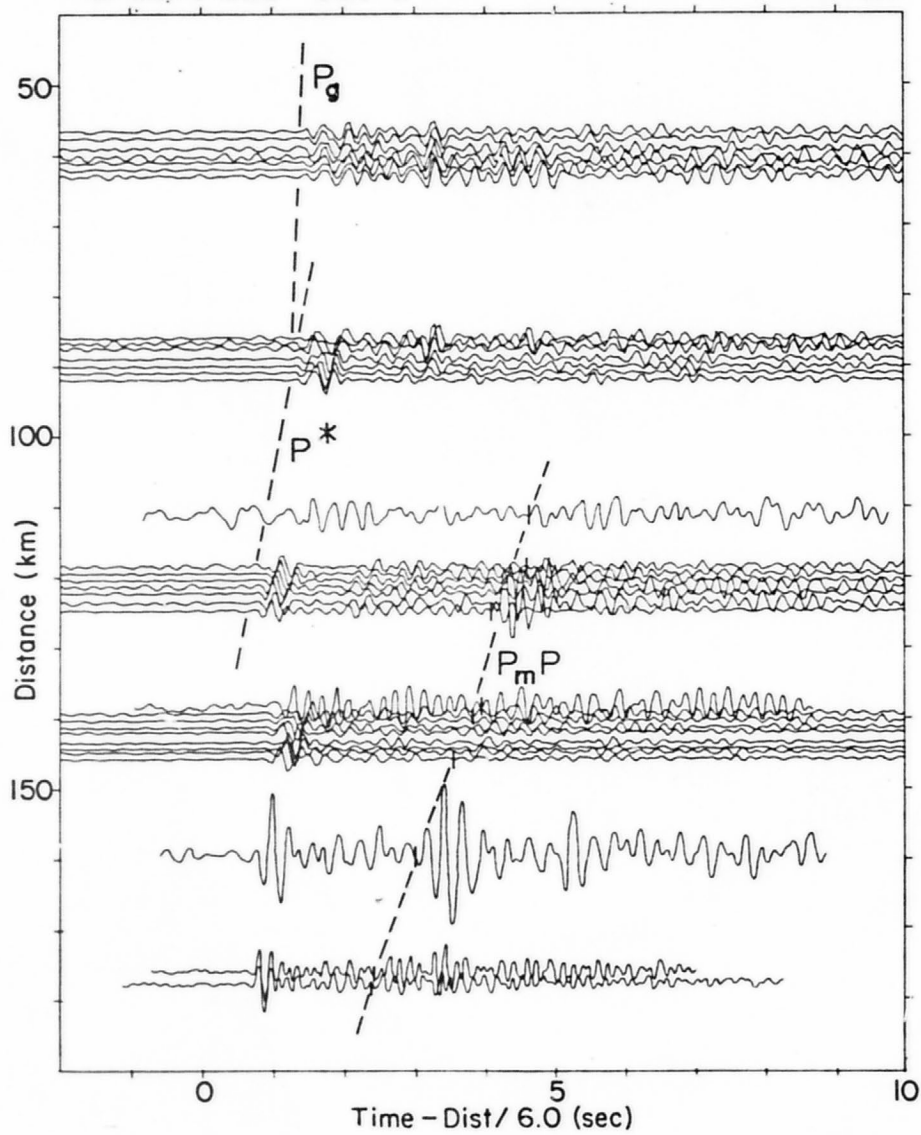
A-26

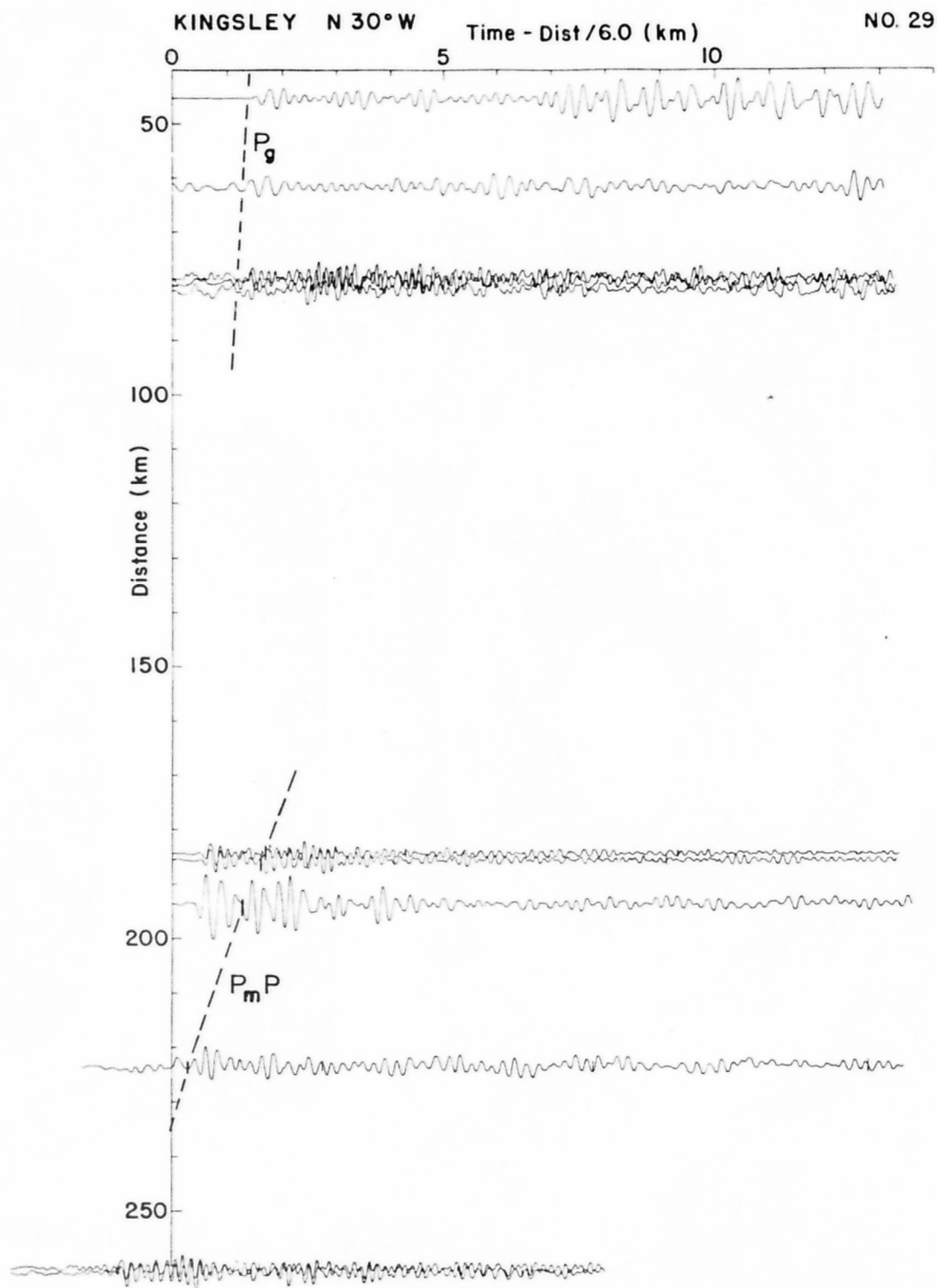


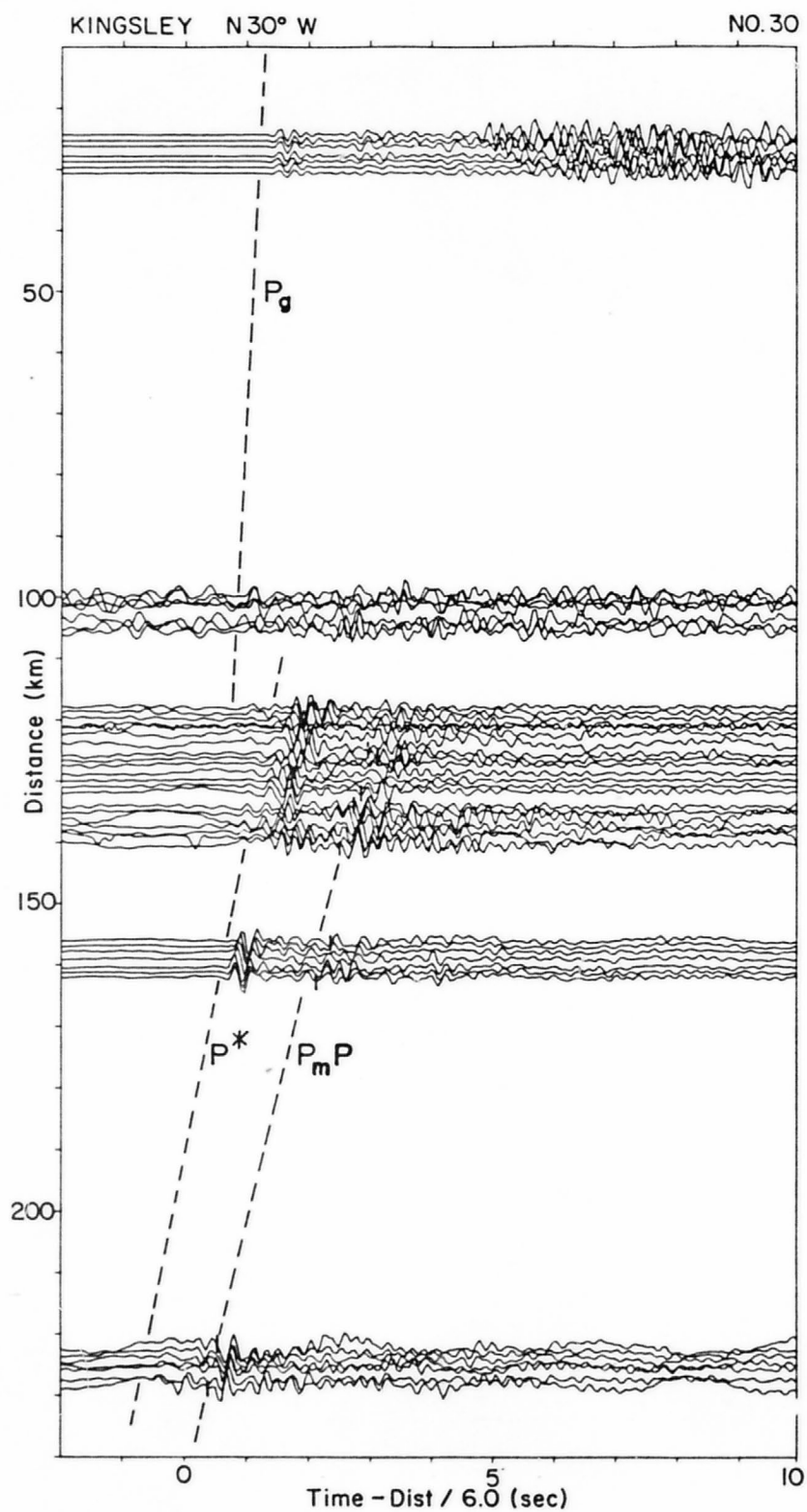


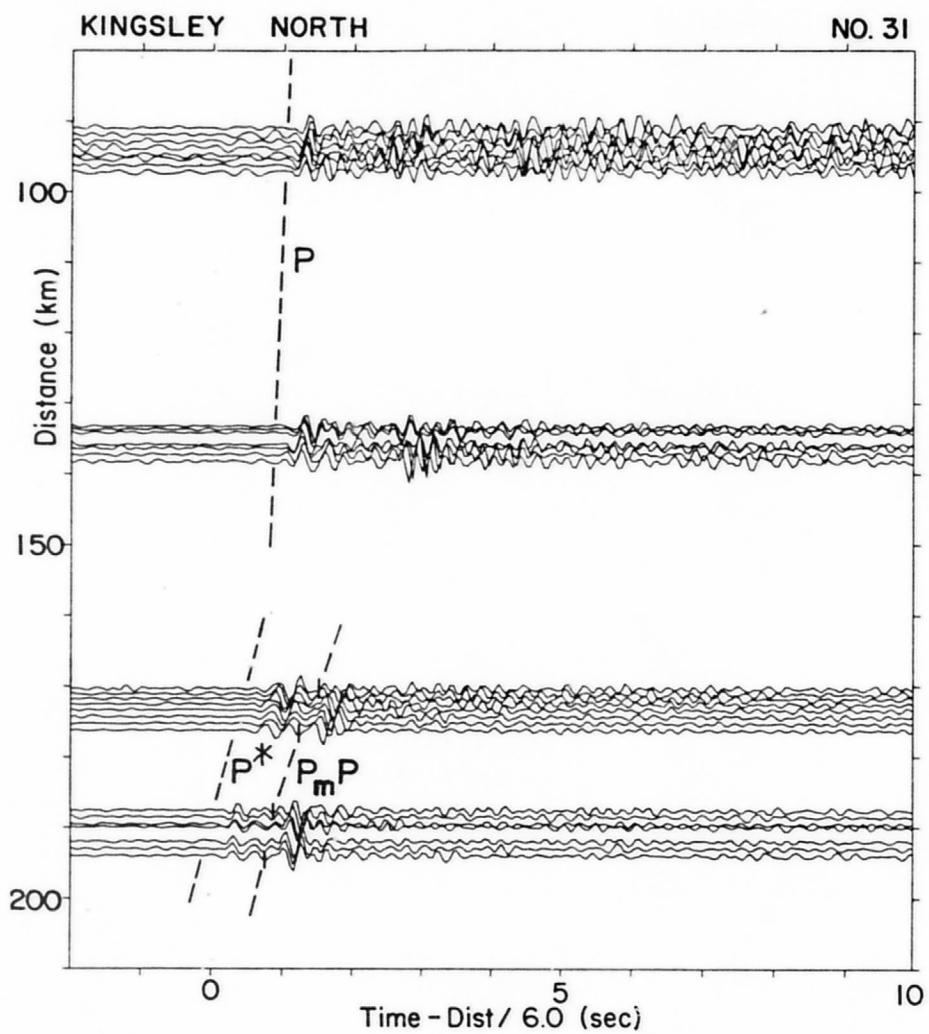
KEPLERVILLE S65°E

NO. 28



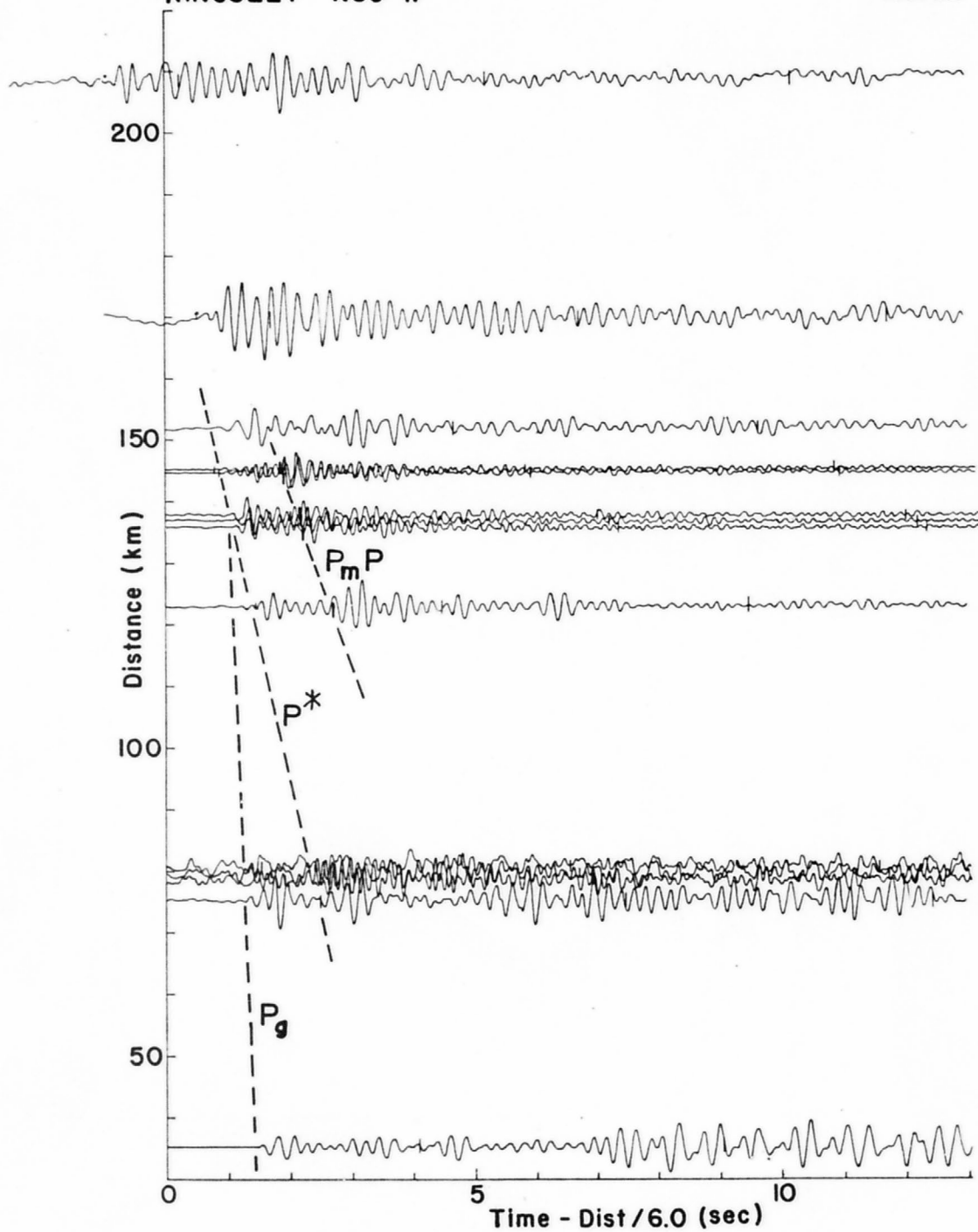


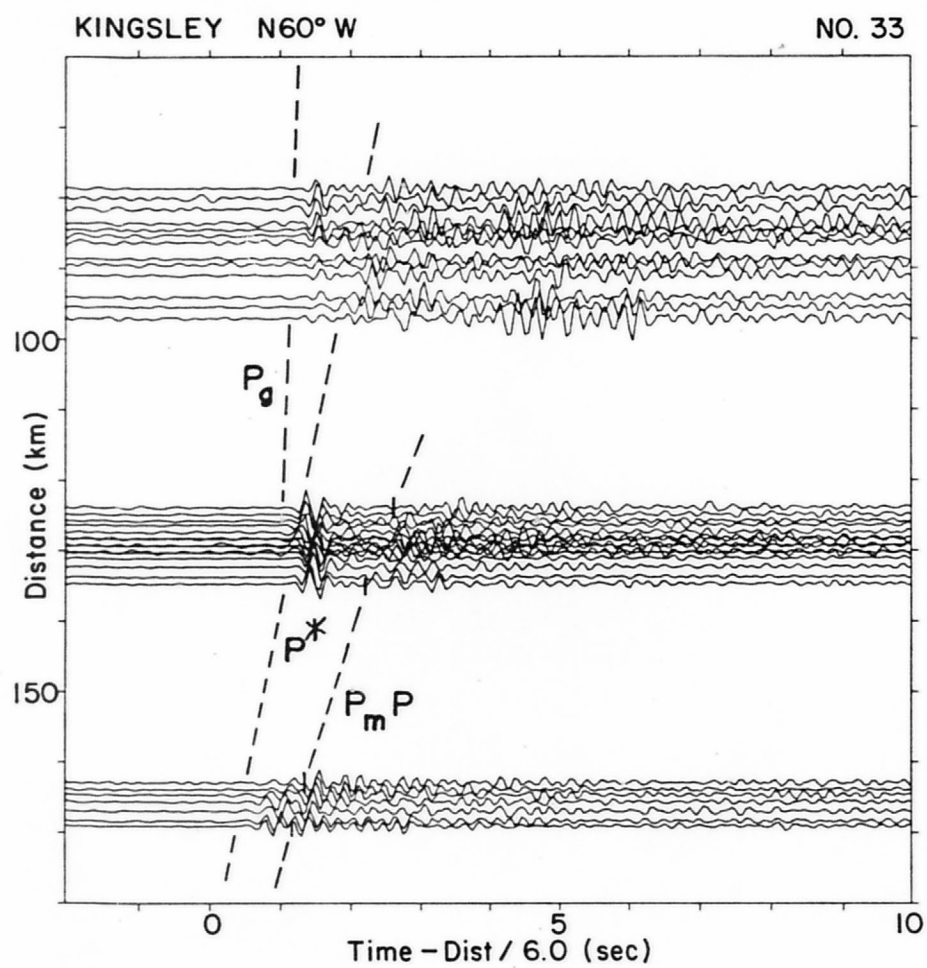


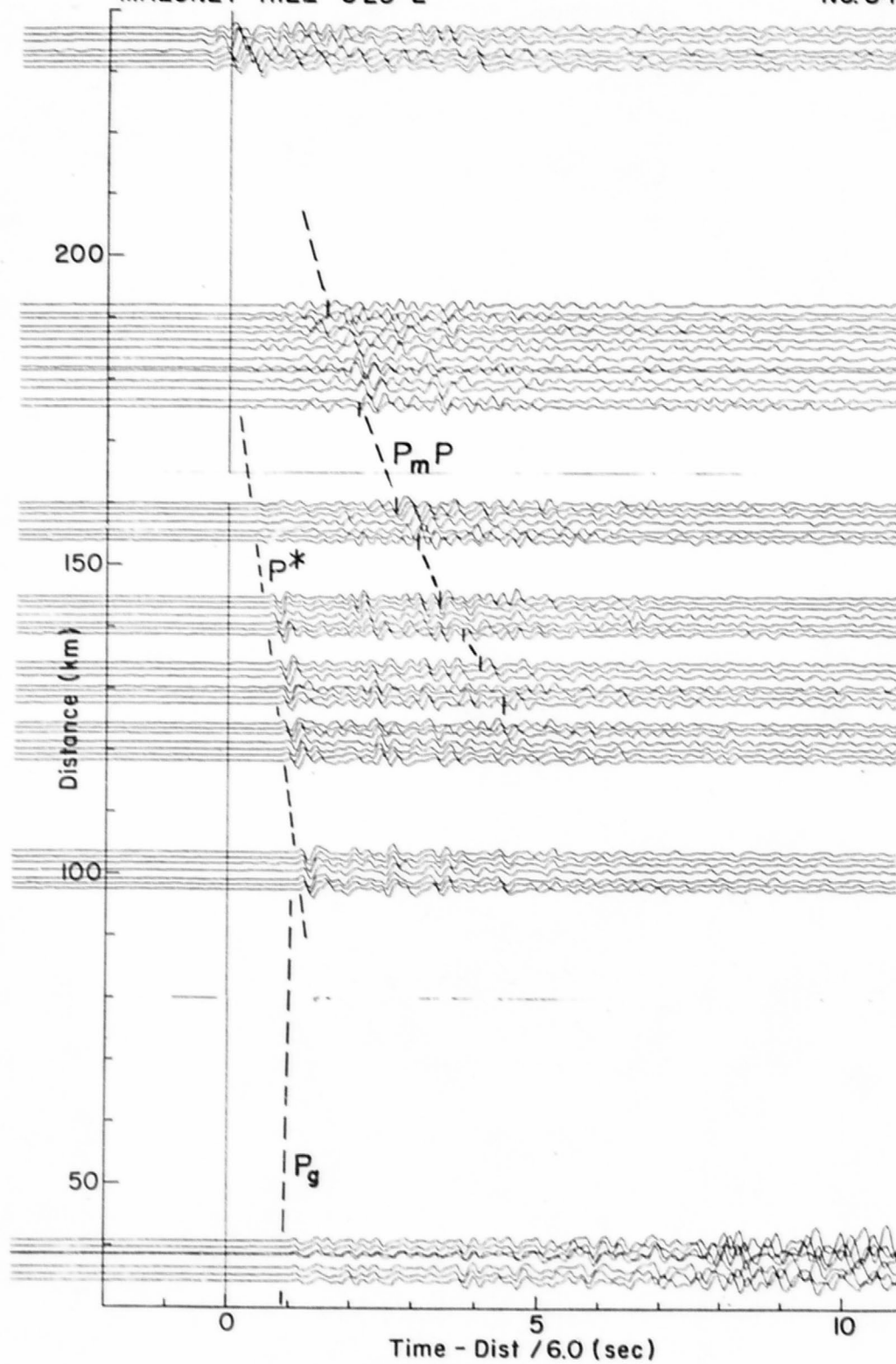


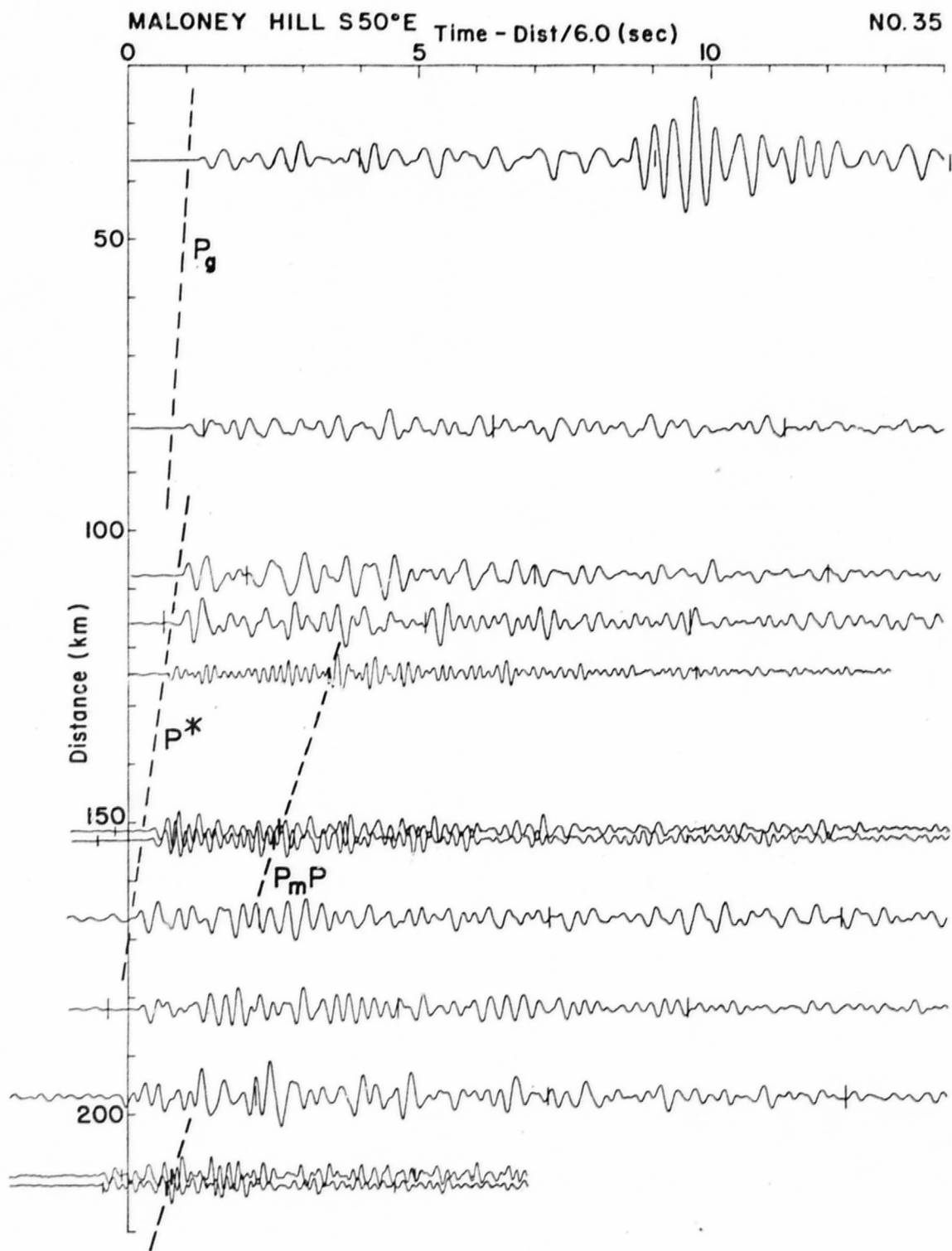
KINGSLEY N60°W

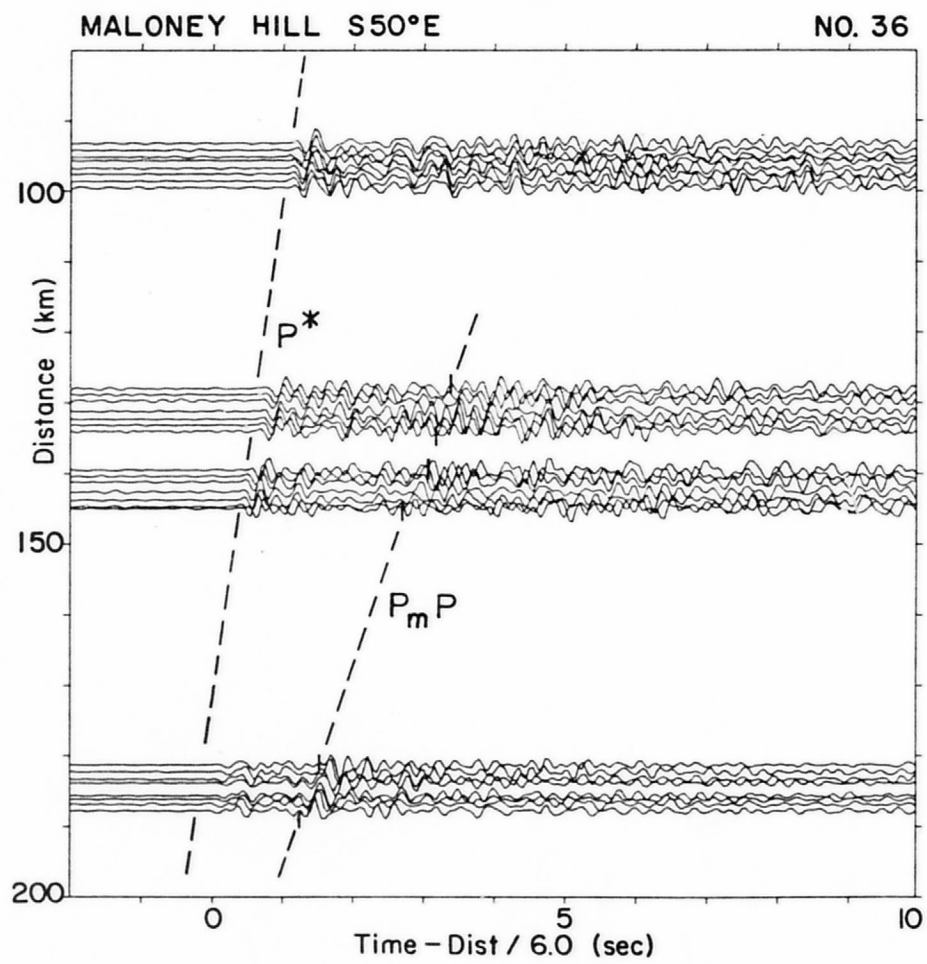
NO. 32

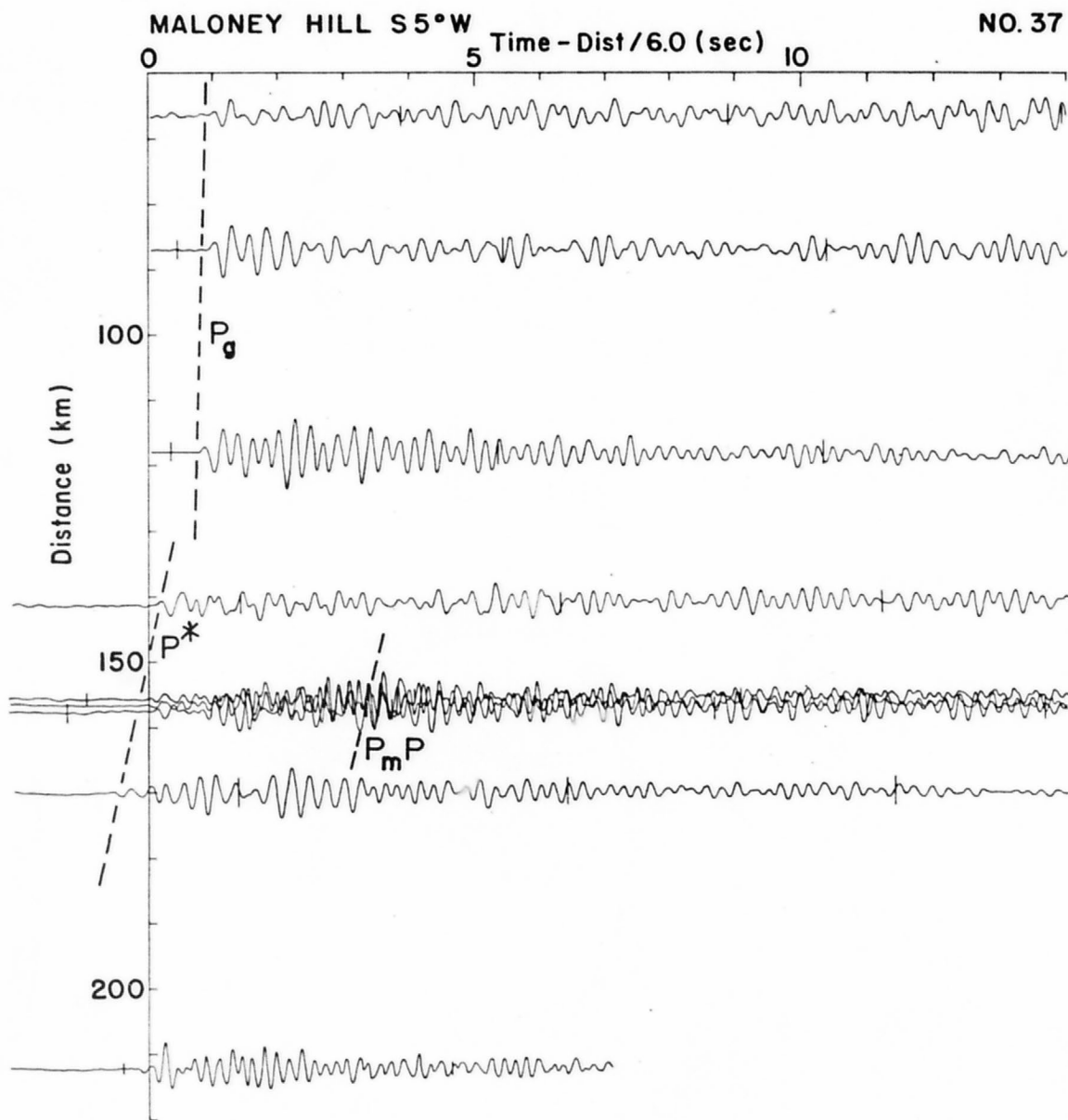


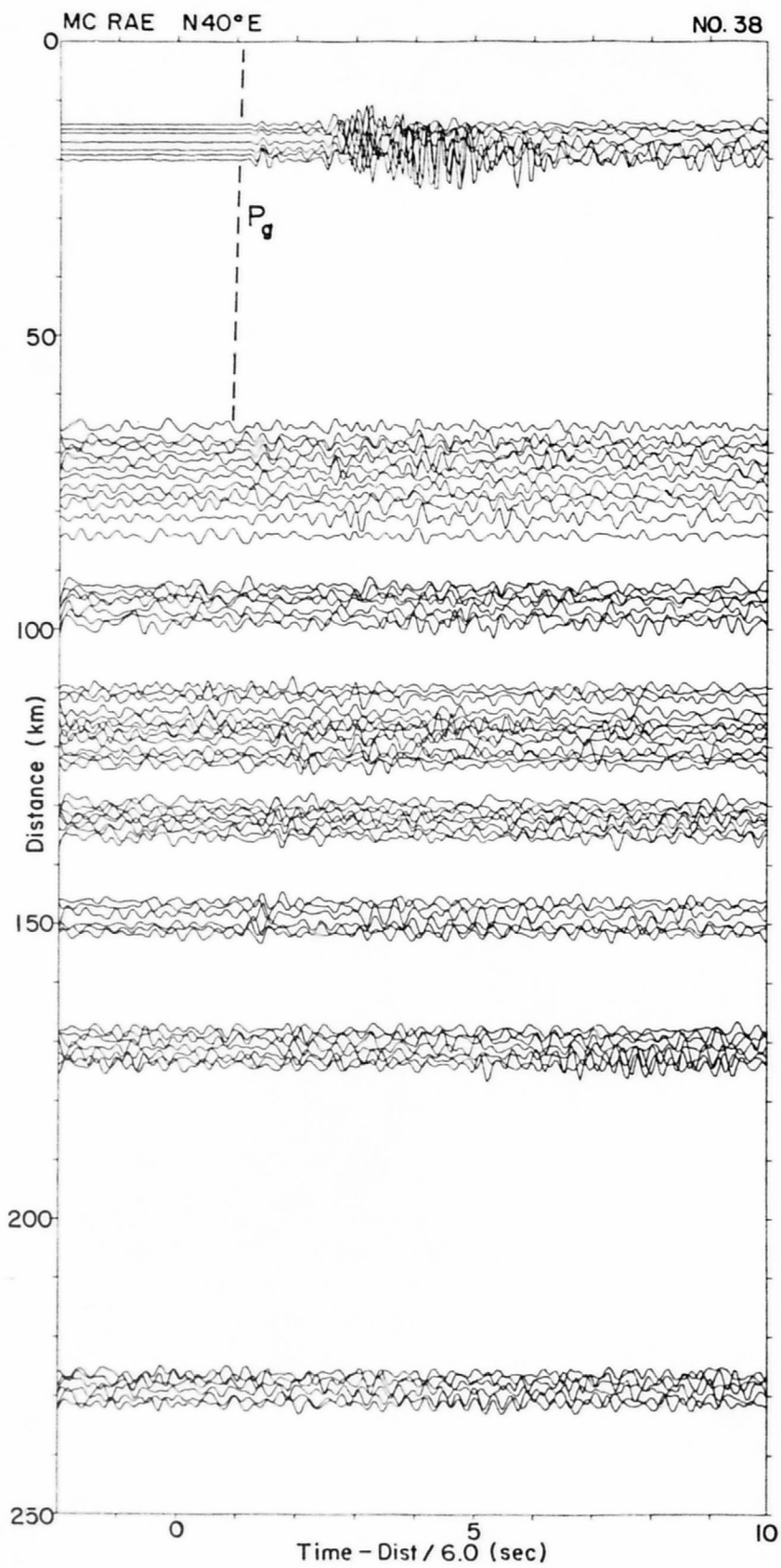


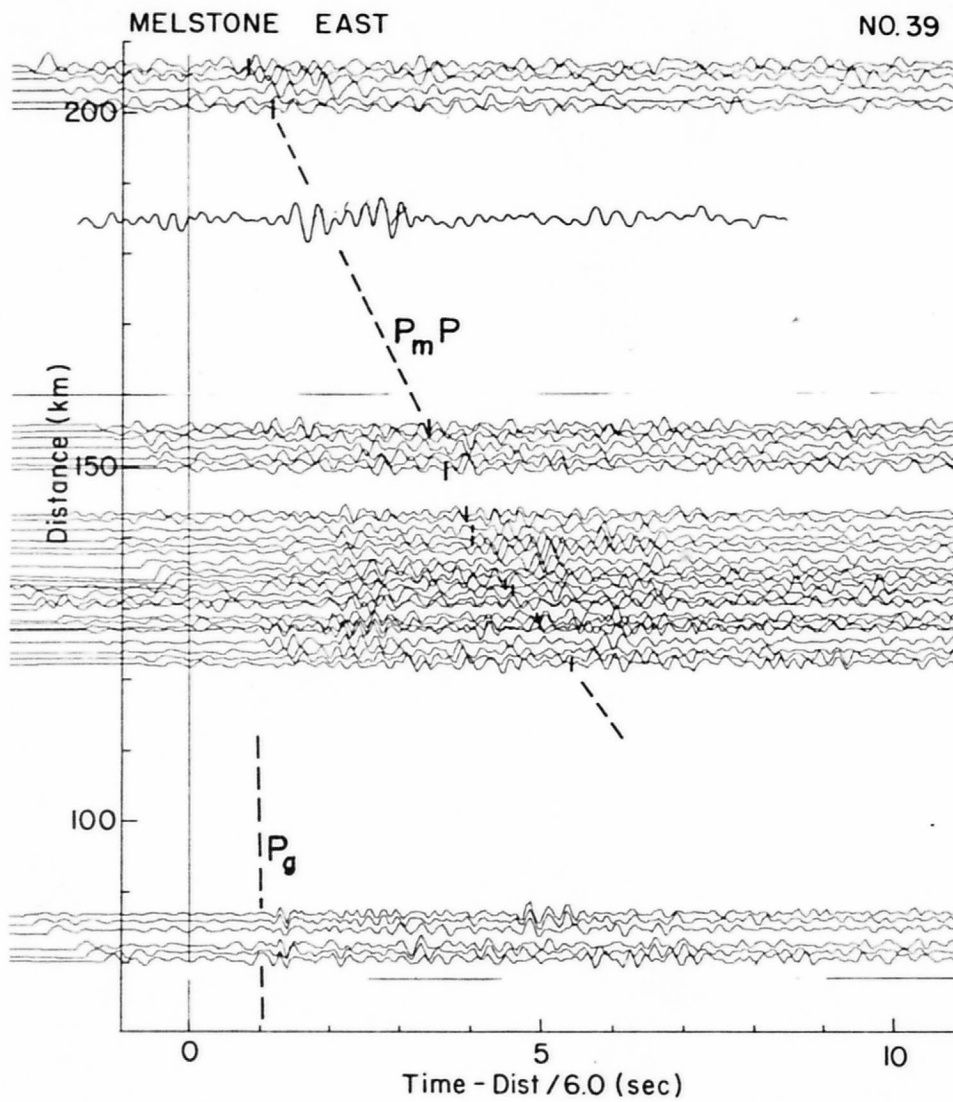


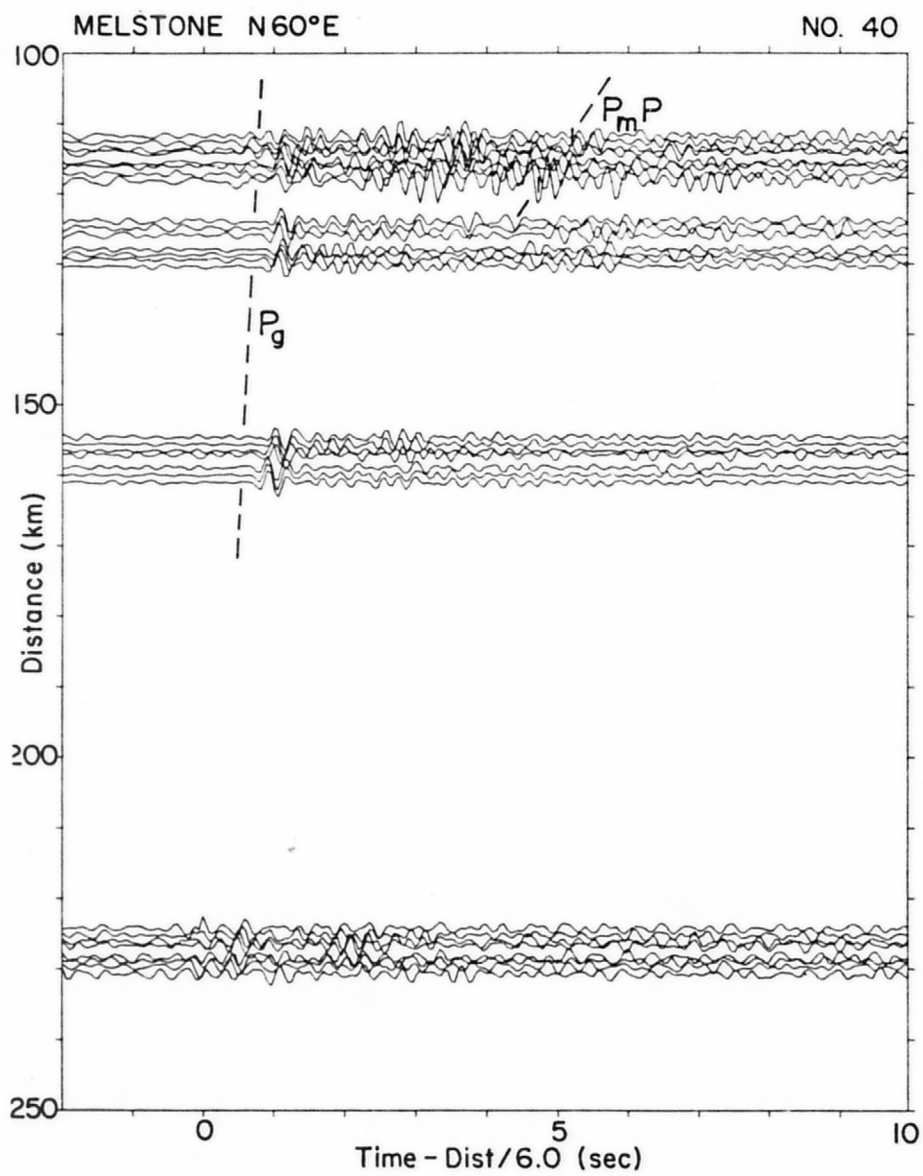


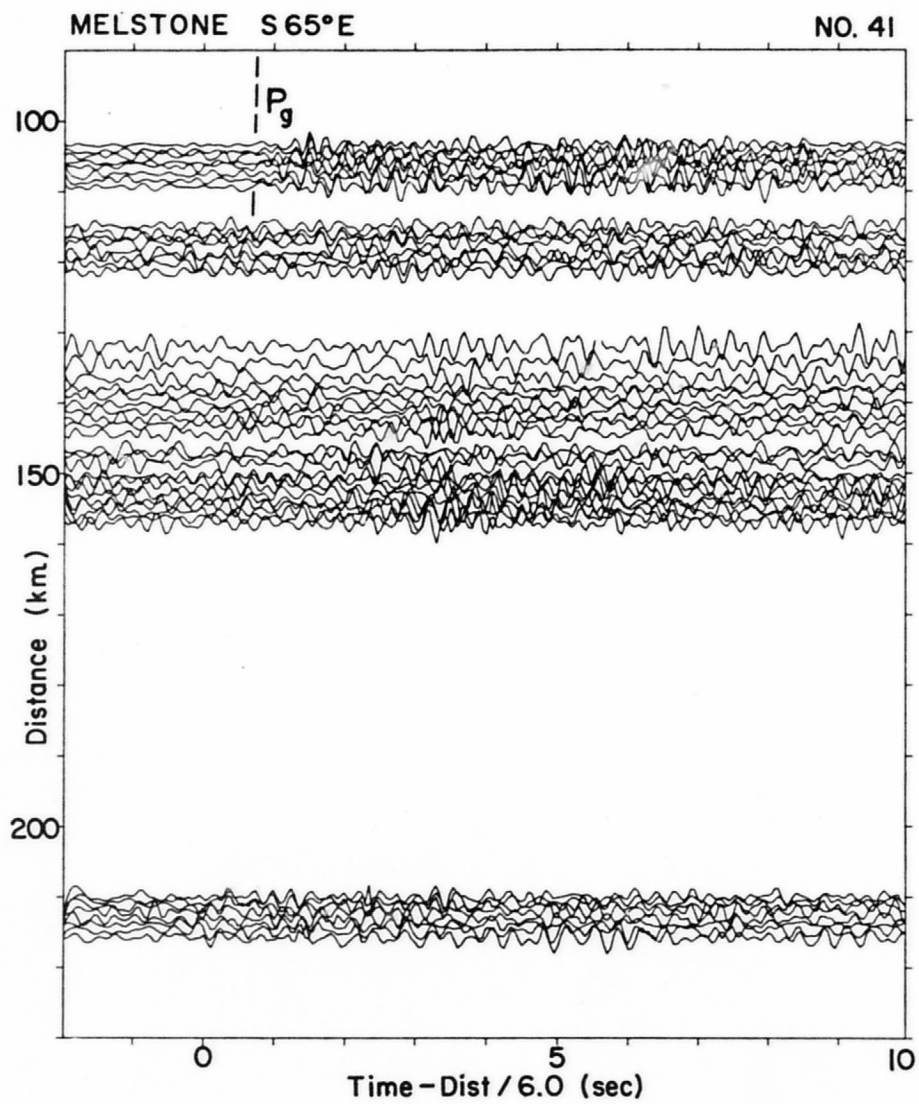


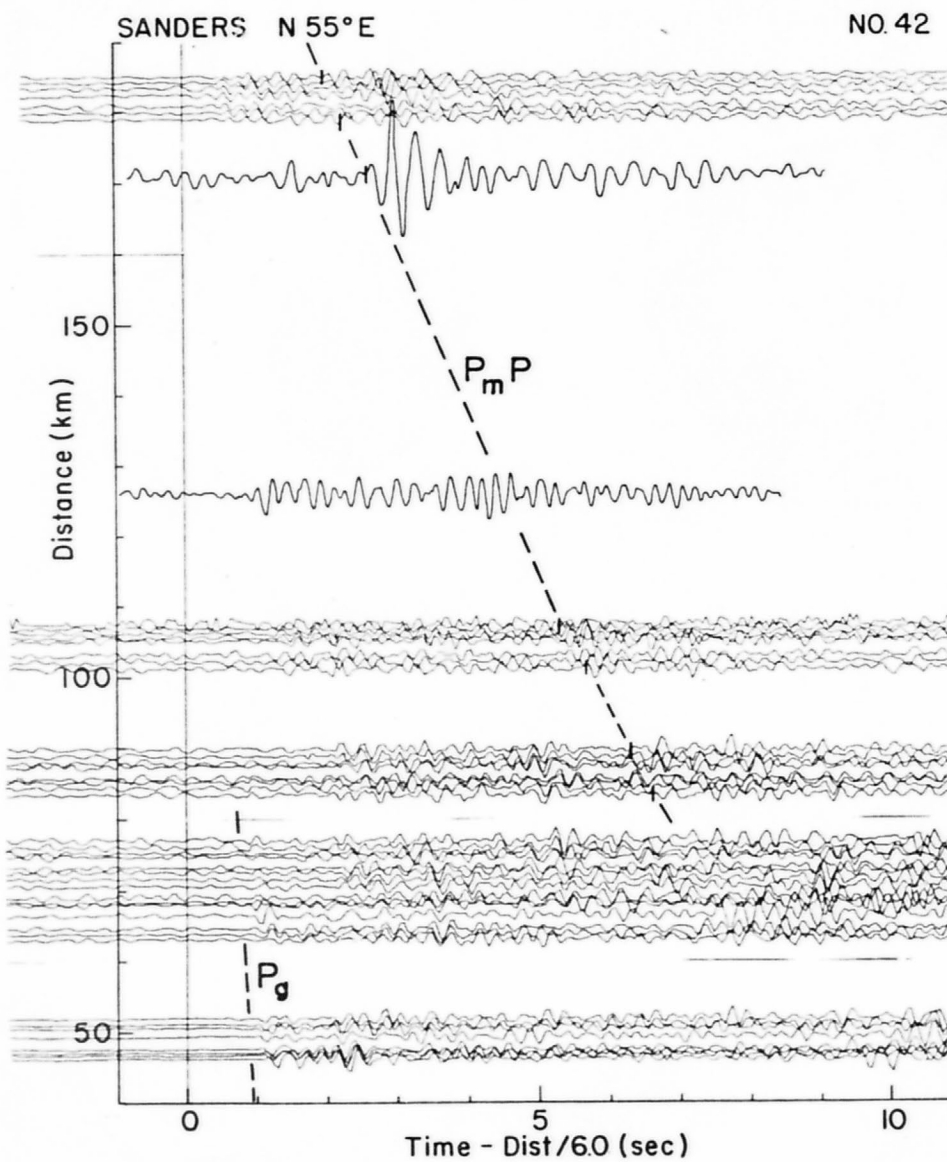


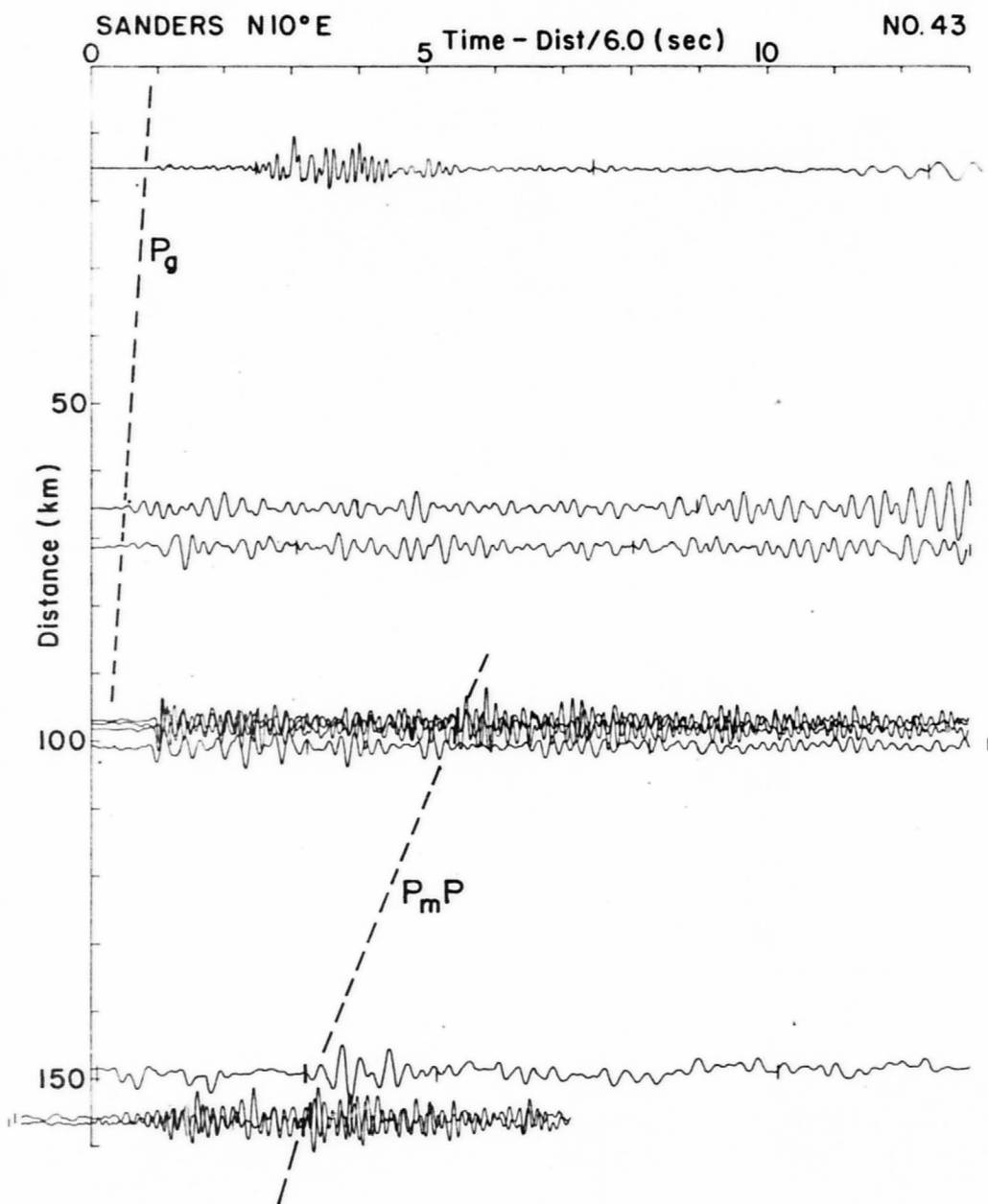


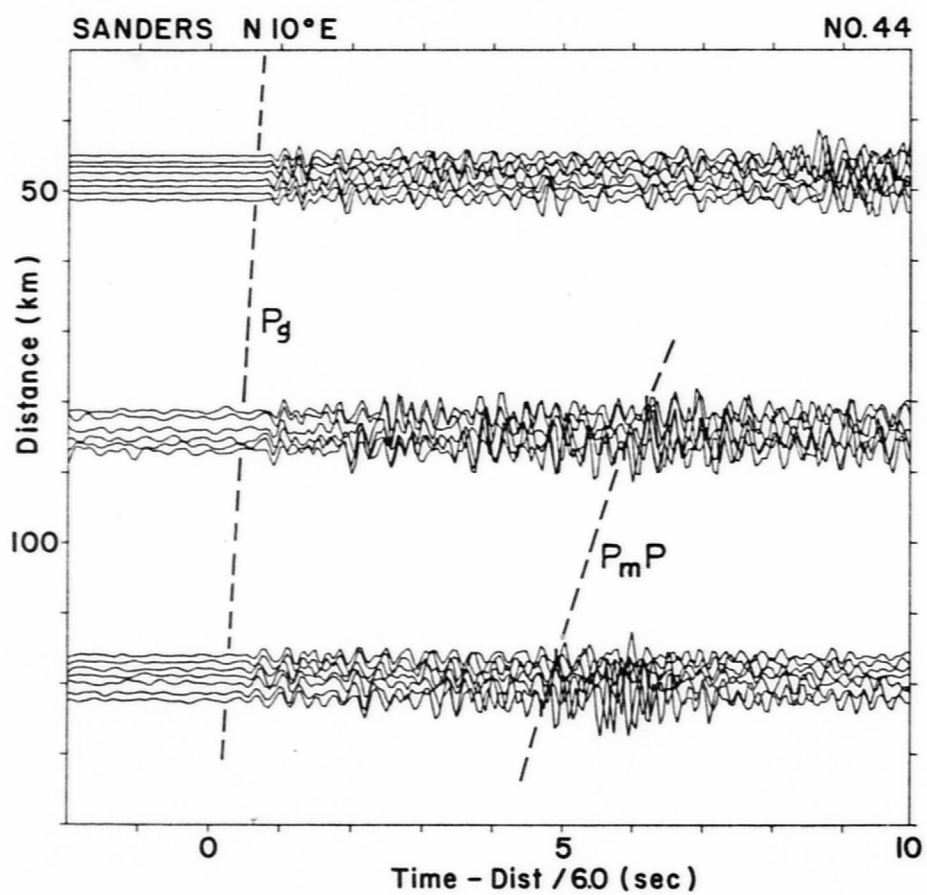


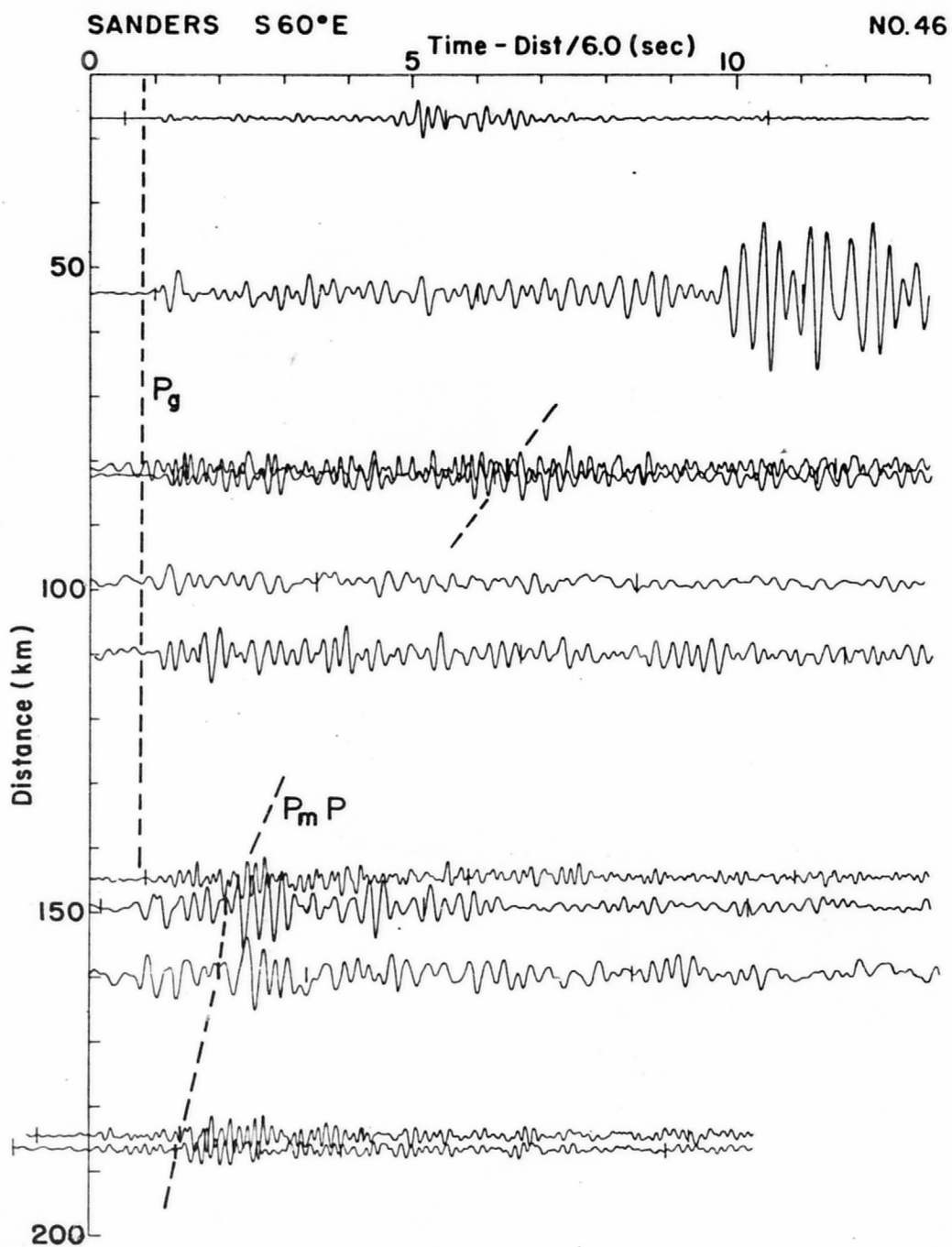


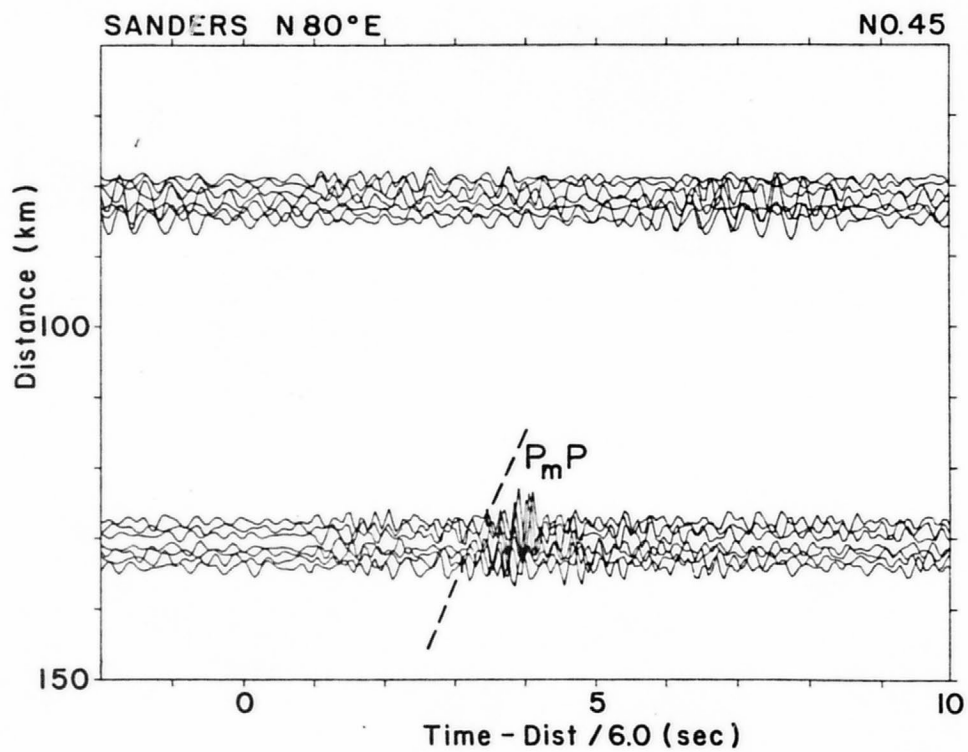


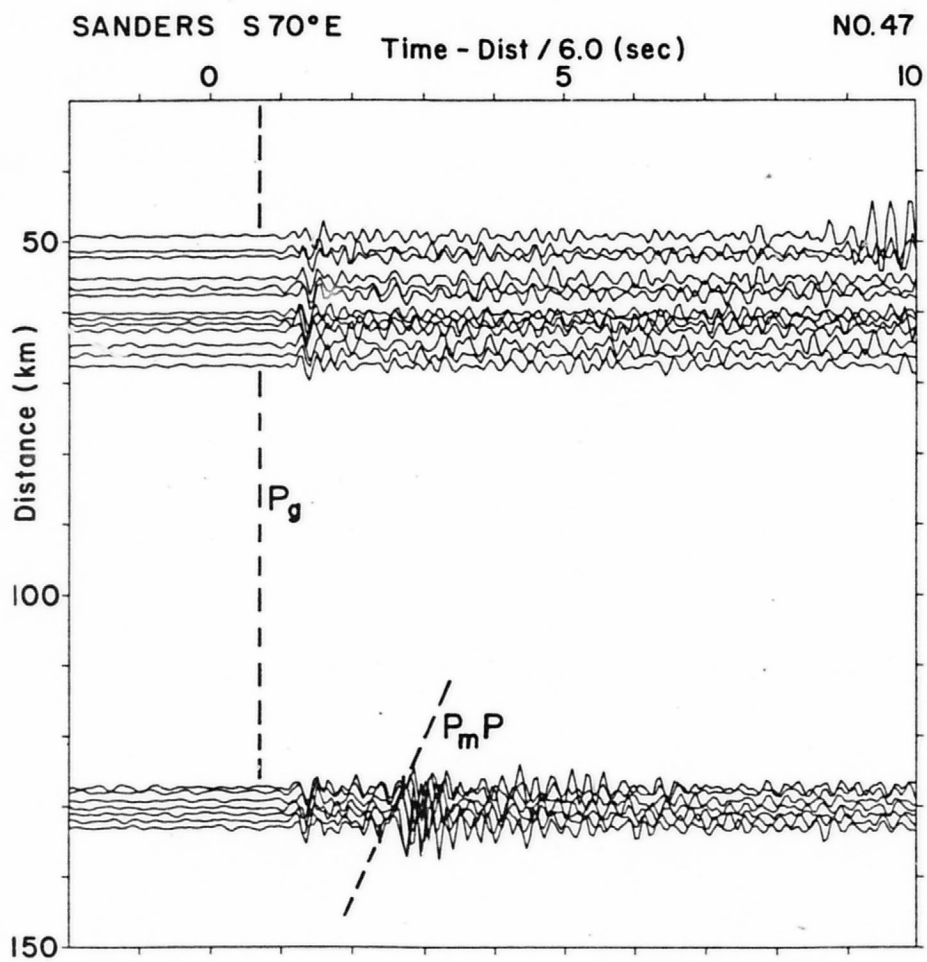












TURNER S 30°E

NO. 48

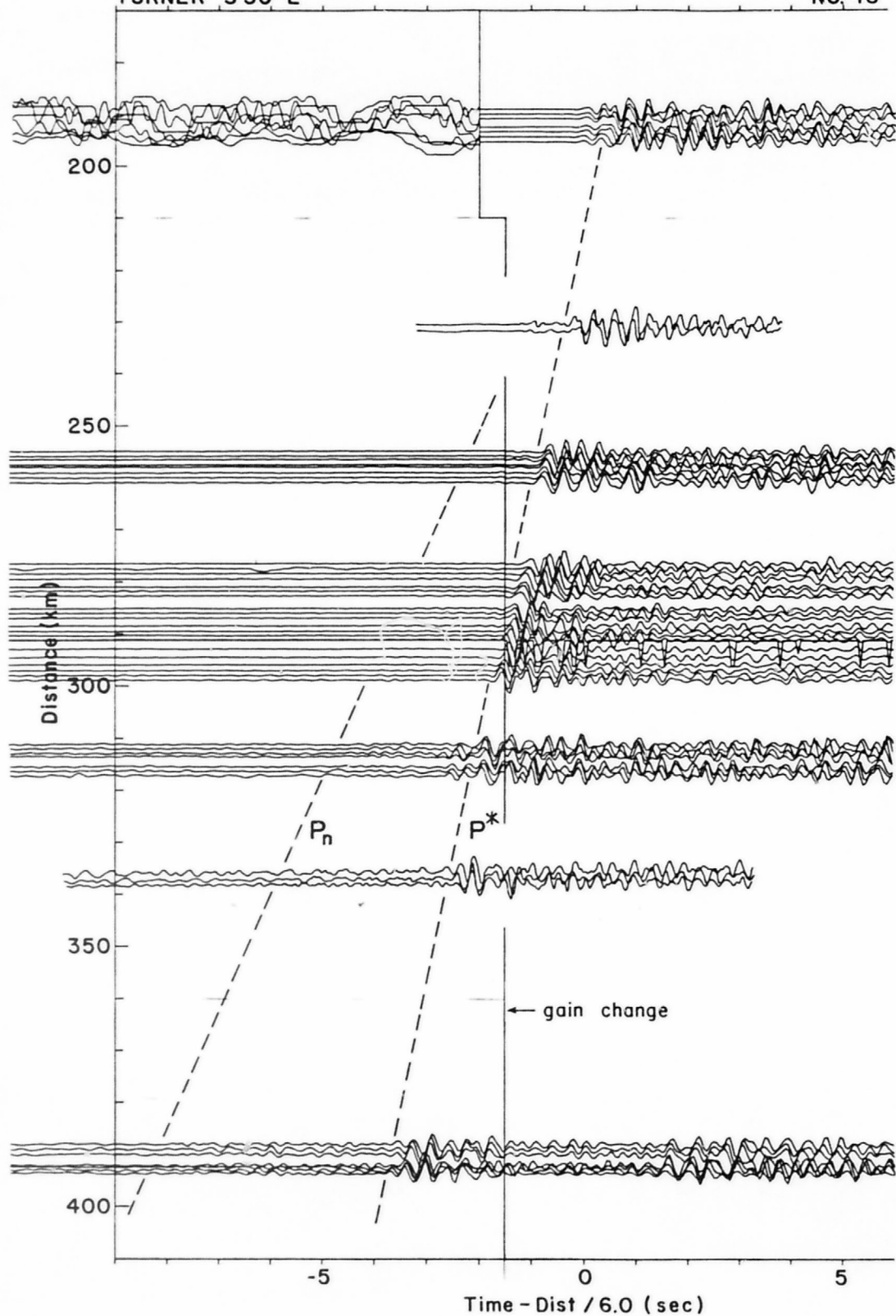


## TABLE FOR SECTION NO. 1

AXTELL S35°W

<u>Trace</u>	<u>Distance (km)</u>	<u>Reduced PmP Time</u>
AXT E1-5	82.4	
AXT E1-4	83.2	
AXT E1-3	83.9	
AXT E1-24	85.4	
AXT E1-19	86.5	
AXT E1-20	87.5	
AXT E1-21	88.4	
AXT C1-5	114.9	
AXT C1-4	115.9	
AXT C1-7	116.9	
AXT C1-15	119.3	
AXT C1-16	120.3	
AXT C1-17	121.3	
AXT B4-5	126.3	
AXT B4-4	127.2	
AXT B4-7	128.0	
AXT B4-15	130.5	
AXT B4-16	131.5	
AXT B4-17	132.5	
AXT A0-5	133.1	
AXT A0-4	133.9	
AXT A0-3	134.8	
AXT A0-24	136.2	
AXT A0-19	137.4	
AXT A0-20	138.3	
AXT A0-21	139.2	
AXT B3-5	139.5	
AXT B3-4	140.5	
AXT B3-7	141.8	
AXT B3-15	144.0	
AXT B3-16	145.0	
AXT B3-17	146.0	3.3
AXT C3-12	148.6	3.22
AXT C3-15	149.7	
AXT C3-16	150.6	
AXT C3-17	151.5	3.11
AXT D3-5	156.4	2.89
AXT D3-4	157.4	
AXT D3-7	158.7	
AXT D3-12	160.5	
AXT D3-15	160.9	
AXT D3-16	161.9	
AXT D3-17	162.9	2.64
AXT E3-4	185.8	1.97
AXT E3-3	188.4	
AXT E3-24	189.4	

TABLE FOR SECTION NO. 1 (Cont'd)

<u>Trace</u>	<u>Distance (km)</u>	<u>Reduced PmP Time</u>
AXT E3-2	191.1	
AXT E3-22	193.5	
AXT E3-18	196.3	
AXT E3-19	198.7	
AXT E3-21	201.1	1.51
AXT F3-5	235.8	0.45
AXT F3-4	236.5	
AXT F3-3	237.3	
AXT F3-24	238.8	
AXT F3-19	239.9	
AXT F3-20	240.8	
AXT F3-21	241.7	0.30

## TABLE FOR SECTION NO. 2

AXTELL S5°W

<u>Trace</u>	<u>Distance (km)</u>	<u>Reduced PmP Time</u>
AXT CIR	33.2	
AXT GLE	76.6	
AXT AGA	82.3	
AXT HUN	111.7	
AXT MIL	129.7	
AXT COT	144.7	
AXT TON	179.9	2.2
AXT VOL	220.2	

## TABLE FOR SECTION NO. 3

AXTELL S5°W

<u>Trace</u>	<u>Distance (km)</u>	<u>Reduced PmP Time</u>
AXT F1-5	41.1	
AXT F1-4	42.0	
AXT F1-3	42.9	
AXT F1-19	44.2	
AXT F1-11	45.4	
AXT F1-12	46.3	
AXT F1-13	47.0	
AXT D1-5	107.1	
AXT D1-4	107.9	
AXT D1-3	108.7	
AXT D1-11	109.8	
AXT D1-19	111.2	
AXT D1-20	112.1	
AXT D1-21	113.1	
AXT C2-9	128.1	
AXT C2-8	128.9	
AXT C2-7	129.8	
AXT C2-23	130.8	
AXT C2-12	131.2	
AXT C2-15	132.3	
AXT C2-16	133.2	
AXT C2-17	134.2	
AXT E2-5	135.2	4.16
AXT E2-4	136.1	
AXT E2-23	136.9	
AXT E2-7	137.7	
AXT E2-20	138.5	
AXT E2-15	139.5	
AXT E2-16	140.5	
AXT E2-17	141.4	3.81
AXT D2-9	145.4	3.65
AXT D2-8	146.2	
AXT D2-7	146.9	
AXT D2-23	147.9	
AXT D2-12	148.5	
AXT D2-15	149.5	
AXT D2-16	150.5	
AXT D2-17	151.4	3.42
AXT F2-5	202.2	1.72
AXT F2-4	203.1	
AXT F2-3	204.0	
AXT F2-24	205.2	
AXT F2-19	206.6	
AXT F2-20	207.4	
AXT F2-21	208.2	1.50

## TABLE FOR SECTION NO. 4

AXTELL S60°W

<u>Trace</u>	<u>Distance (km)</u>	<u>Reduced PmP Time</u>
AXT CIR	33.2	
AXT WEL	45.5	
AXT JOR	91.0	
AXT COH-6	112.2	4.23
AXT COH-3	113.2	
AXT COH-1	114.2	4.22
AXT LAN	115.5	4.0
AXT MAL-6	124.1	
AXT MAL-1	126.3	
AXT HRS	144.3	2.9
AXT SND	163.0	
AXT VAN	191.3	1.5
AXT SUM	204.4	1.3?

## TABLE FOR SECTION NO. 5

AXTELL S60°W

<u>Trace</u>	<u>Distance (km)</u>	<u>Reduced PmP Time</u>
AXT D4-5	116.9	3.73
AXT D4-4	117.8	
AXT D4-3	118.6	
AXT D4-24	120.0	
AXT D4-19	121.2	
AXT D4-20	122.1	
AXT D4-21	123.0	3.47
AXT F4-9	123.3	
AXT F4-8	124.2	
AXT F4-7	125.2	
AXT F4-4	126.3	
AXT F4-23	127.7	
AXT F4-24	128.5	
AXT F4-25	129.3	
AXT E4-5	159.3	2.42
AXT E4-4	160.2	
AXT E4-3	161.1	
AXT E4-24	162.3	
AXT E4-19	163.7	
AXT E4-20	164.5	
AXT E4-21	165.2	2.09

## TABLE FOR SECTION NO. 6

## CABIN CREEK WEST

<u>Trace</u>	<u>Distance (km)</u>	<u>Reduced PmP Time</u>
CAB HUN	80.0	
CAB AGA	96.7	
CAB FOR	159.3	2.6
CAB HRS	169.2	
CAB SAN-1	184.6	1.84?
CAB SAN-6	186.6	1.82?
CAB MYE	219.5	
CAB SUM	225.2	

## TABLE FOR SECTION NO. 7

## CABIN CREEK WEST

<u>Trace</u>	<u>Distance (km)</u>	<u>Reduced PmP Time</u>
CAB E2-9	52.4	
CAB E2-8	53.4	
CAB E2-7	54.4	
CAB E2-12	55.1	
CAB E2-15	56.8	
CAB E2-20	57.9	
CAB E2-21	58.9	
CAB C2-9	98.9	
CAB C2-8	99.8	
CAB C2-7	100.7	
CAB C2-4	101.9	
CAB C2-23	103.3	
CAB C-2-24	104.1	
CAB C2-25	105.0	
CAB B2-9	110.7	
CAB B2-8	111.5	
CAB B2-8	112.3	
CAB B2-4	113.7	
CAB A0-13	114.8	
CAB A0-12	115.7	
CAB A0-11	116.6	
CAB A0-16	117.9	
CAB A0-19	119.2	
CAB A0-20	120.1	
CAB A0-21	120.9	
CAB B3-9	121.8	
CAB B3-8	122.8	
CAB B3-7	123.8	
CAB B3-4	124.1	
CAB C4-13	126.5	
CAB C4-12	127.4	
CAB C4-11	128.3	
CAB C4-16	129.6	
CAB C4-19	130.9	
CAB C4-20	131.8	
CAB C4-21	132.7	
CAB D3-9	135.3	
CAB D3-8	136.3	
CAB D3-7	137.3	
CAB D3-23	139.2	
CAB D3-20	140.7	
CAB D3-21	141.7	
CAB E4-0	168.0	
CAB E4-8	169.0	
CAB E4-11	170.1	
CAB E4-16	171.8	
CAB E4-19	172.5	
CAB E4-20	173.5	
CAB E4-21	174.4	

## TABLE FOR SECTION NO. 8

## CABIN CREEK S60°W

<u>Trace</u>	<u>Distance(km)</u>	<u>Reduced PmP Time</u>
CAB MIL	26.0	
CAB COT	69.0	
CAB TON	103.0	4.9
CAB HOR-6	109.8	4.44
CAB HOR-1	110.5	4.40
CAB VOL	133.2	3.3
CAB FOR	159.3	2.6
CAB GRE	169.0	
CAB SAN-1	184.6	1.84?
CAB SAN-6	186.6	1.82?
CAB MCR-6	213.9	1.25?
CAB MCR-1	216.0	1.21?

## TABLE FOR SECTION NO. 9

## CABIN CREEK S60°W

<u>Trace</u>	<u>Distance (km)</u>	<u>Reduced PmP Time</u>
CAB E2-9	52.4	
CAB E2-8	53.4	
CAB E2-7	54.4	
CAB E2-12	55.1	
CAB E2-23	56.5	
CAB E2-20	57.9	
CAB E2-21	58.9	
CAB D2-9	100.7	
CAB D2-8	101.7	
CAB D2-7	102.6	
CAB D2-4	103.6	
CAB D2-17	104.7	
CAB D2-24	105.9	
CAB D2-25	106.7	
CAB F2-9	103.3	4.25
CAB F2-8	104.3	
CAB F2-3	105.5	
CAB F2-24	107.2	
CAB F2-19	107.8	
CAB F2-2-	108.8	
CAB F2-21	109.8	4.01
CAB E3-9	131.0	3.13
CAB E3-8	133.2	
CAB E3-8	134.0	
CAB E3-6	136.9	
CAB E3-10	138.7	
CAB E3-12	139.9	
CAB E3-14	141.9	
CAB E3-15	143.3	
CAB E3-23	144.4	
CAB E3-19	146.4	
CAB E3-20	147.6	
CAB E3-21	149.5	2.18
CAB F3-9	198.2	0.99
CAB F3-8	199.2	
CAB F3-11	200.1	
CAB F3-3	200.7	
CAB F3-16	201.8	
CAB F3-24	202.5	
CAB F3-20	203.6	
CAB F3-21	204.6	0.68

## TABLE FOR SECTION NO. 10

CABIN CREEK N55°W

<u>Trace</u>	<u>Distance (km)</u>	<u>Reduced PmP Time</u>
CAB F1-13	82.3	
CAB F1-12	83.0	
CAB F1-11	83.9	
CAB F1-9	84.8	
CAB F1-20	85.9	
CAB F1-3	86.5	
CAB F1-4	87.3	
CAB F1-5	88.0	
CAB D1-13	90.5	
CAB D1-12	91.5	
CAB D1-11	92.5	
CAB D1-3	94.6	
CAB D1-20	95.5	
CAB D1-21	96.1	
CAB D1-25	97.0	
CAB E1-13	113.9	
CAB E1-12	114.9	
CAB E1-11	116.0	
CAB E1-16	116.6	
CAB E1-19	118.3	
CAB E1-20	118.9	
CAB E1-21	119.4	
CAB F4-13	186.9	
CAB F4-12	187.9	
CAB F4-15	189.1	
CAB F4-20	190.8	
CAB F4-23	191.4	
CAB F4-24	192.5	
CAB F4-25	193.5	

## TABLE FOR SECTION NO. 11

CHARLSON S55°W

<u>Trace</u>	<u>Distance (km)</u>	<u>Reduced PmP Time</u>
CHA E1-9	243.6	
CHA E1-8	244.3	
CHA E1-3	245.6	
CHA E1-24	247.4	
CHA E1-19	247.8	
CHA E1-20	248.8	
CHA E1-21	249.8	
CHA D1-9	251.1	
CHA D1-8	251.9	
CHA D1-11	253.1	
CHA D1-3	253.4	
CHA D1-16	254.7	
CHA D1-19	255.4	
CHA D1-20	256.4	
CHA D1-21	257.4	
CHA C2-9	269.2	
CHA C2-8	270.2	
Cha C2-7	271.2	
CHA C2-12	271.9	
CHA C2-15	273.6	
CHA C2-20	274.8	
CHA C2-21	275.3	
CHA B2-9	280.7	
CHA B2-8	281.7	
CHA B2-7	282.7	
CHA B2-15	285.0	
CHA B2-20	286.2	
CHA B2-21	287.2	
CHA C3-9	290.2	
CHA C3-8	291.2	
CHA C3-7	292.1	
CHA C3-12	293.1	
CHA C3-15	294.7	
CHA C3-20	295.6	
CHA C3-21	296.5	
CHA D3-9	306.8	
CHA D3-8	307.5	
CHA D3-7	308.3	
CHA D3-12	309.8	
CHA D3-15	310.9	
CHA D3-16	311.8	
CHA D3-17	312.7	
CHA E3-0	319.7	
CHA E3-5	321.5	
CHA E3-7	322.6	
CHA E3-3	325.1	
CHA E3-6	325.6	

TABLE FOR SECTION NO. 11 (Cont'd)

<u>Trace</u>	<u>Distance (km)</u>	<u>Reduced PmP Time</u>
CHA E3-2	327.1	
CHA E3-10	328.1	
CHA E3-22	330.2	
CHA E3-18	331.9	
CHA E3-19	334.9	
CHA E3-16	336.4	
CHA E3-21	337.9	
CHA F3-9	382.4	
CHA F3-8	383.4	
CHA F3-3	384.6	
CHA F3-19	386.9	
CHA F3-20	387.9	
CHA F3-21	389.0	

## TABLE FOR SECTION NO. 12

CHARLSON S55° W

<u>Trace</u>	<u>Distance (km)</u>	<u>Reduced PmP Time</u>
CHA E1-9	243.3	
CHA E1-8	244.2	
CHA E1-3	245.6	
CHA E1-24	247.4	
CHA E1-19	247.8	
CHA E1-20	248.8	
CHA E1-21	249.8	
CHA D1-9	251.1	
CHA D1-8	251.9	
CHA D1-11	253.1	
CHA D1-3	253.4	
CHA D1-16	254.7	
CHA D1-19	255.4	
CHA D1-20	256.4	
CHA D1-21	257.4	
CHA C2-9	269.2	
CHA C2-8	270.3	
CHA C2-7	271.3	
CHA C2-12	271.9	
CHA C2-15	273.6	
CHA C2-20	274.8	
CHA C2-21	275.3	
CHA B2-9	289.7	
CHA B2-8	281.7	
CHA B2-8	282.7	
CHA B2-15	285.0	
CHA B2-20	286.2	
CHA B2-21	287.2	
CHA C3-9	290.2	
CHA C3-8	291.2	
CHA C3-7	292.1	
CHA C3-12	293.1	
CHA C3-15	294.7	
CHA C3-20	295.6	
CHA C3-21	296.5	
CHA D3-9	306.8	
CHA D3-8	307.5	
CHA D3-8	308.3	
CHA D3-12	309.8	
CHA D3-15	310.9	
CHA D3-16	311.8	
CHA D3-17	312.7	
CHA E3-9	319.7	
CHA E3-5	321.5	
CHA E3-7	322.6	
CHA E3-3	325.1	

TABLE FOR SECTION NO. 12 (Cont'd)

<u>Trace</u>	<u>Distance (km)</u>	<u>Reduced PmP Time</u>
CHA E3-6	325.6	
CHA E3-2	327.1	
CHA E3-10	328.1	
CHA E3-22	330.2	
CHA E3-18	331.9	
CHA E3-19	334.9	
CHA E3-16	336.5	
CHA E3-21	337.9	
CHA F3-9	382.4	
CHA F3-8	383.4	
CHA F3-3	384.6	
CHA F3-19	386.9	
CHA F3-20	387.9	
CHA F3-21	388.9	

## TABLE FOR SECTION NO. 13

COHAGEN S25°E

<u>Trace</u>	<u>Distance (km)</u>	<u>Reduced PmP Time</u>
COH HOR-2	105.3	5.67
COH HOR-4	106.3	
COH HOR-6	107.0	5.57
COH TON	123.5	
COH VOL	158.4	2.4
COH KIN-1	184.6	1.50
COH KIN-4	185.3	1.48

## TABLE FOR SECTION NO. 14

## COHAGEN S25°E

(In order of decreasing distance)

<u>Trace</u>	<u>Distance (km)</u>	<u>PmP Time</u>
COH F2-17	162.81	2.61
COH F2-16	161.83	
COH F2-11	160.82	
COH F2- 8	159.17	
COH F2- 3	158.38	
COH F2- 4	157.39	
COH F2- 5	156.45	2.90
COH E3-13	117.65	4.61
COH E3-11	115.75	
COH E3-10	113.88	
COH E3- 6	110.74	
COH E3- 2	109.09	
COH E3- 3	106.12	
COH E3- 5	103.15	5.18
COH D2-17	85.54	
COH D2-16	84.65	
COH D2-15	83.77	
COH D2-20	82.52	
COH D2-23	81.17	
COH D2-24	80.32	
COH D2-25	79.48	
COH B2-13	66.39	
COH B2-12	65.59	
COH B2-20	64.31	
COH B2- 4	62.15	
COH B2-25	61.28	
COH B2- 5	61.23	
COH A0-13	59.42	
COH A0-12	58.62	
COH A0-11	57.82	
COH A0- 8	56.38	
COH A0- 3	55.25	
COH A0- 4	54.32	
COH A0- 5	53.40	
COH B4-13	50.97	
COH B4-12	50.00	
COH B4- 7	48.48	
COH B4-20	47.56	
COH B4-23	46.61	
COH B4-24	45.64	
COH B4-25	44.68	
COH D4-13	29.22	
COH D4-12	28.29	
COH D4-11	27.35	
COH D4- 8	26.29	
COH D4- 3	24.79	
COH D4-24	24.13	
COH D4-25	23.22	

## TABLE FOR SECTION NO. 15

COHAGEN S70°E

<u>Trace</u>	<u>Distance (km)</u>	<u>Reduced PmP Time</u>
COH D1-5	57.9	
COH D1-4	58.6	
COH D1-3	59.3	
COH D1-20	59.9	
COH D1-8	60.9	
COH D1-11	61.8	
COH D1-12	62.8	
COH D1-13	63.7	
COH F1-21	102.2	
COH F1-20	103.2	
COH F1-25	104.1	
COH F1-3	106.4	
COH F1-5	107.4	
COH F1-9	108.7	
COH E2-25	110.8	
COH E2-24	110.8	
COH E2-23	112.8	
COH E2-4	113.6	
COH E2-15	114.9	
COH E2-12	116.3	
COH E2-13	117.3	

## TABLE FOR SECTION NO. 16

COHAGEN S20°W

<u>Trace</u>	<u>Distance (km)</u>	<u>Reduced PmP Time</u>
COH E4-5	47.8	
COH E4-4	48.8	
COH E4-3	49.9	
COH E4-24	50.6	
COH E4-11	52.2	
COH E4-16	53.3	
COH E4-17	54.3	
COH D3-25	63.3	
COH D3-24	64.3	
COH D3-23	65.1	
COH D3-20	66.3	
COH D3-7	66.8	
COH D3-15	67.7	
COH D3-16	68.5	
COH D3-17	69.3	
COH E2-5	103.1	
COH E3-24	104.6	
COH E3-25	106.4	
COH E3-23	108.1	
COH E3-22	109.9	
COH E3-20	111.1	
COH E3-18	113.2	
COH E3-19	114.5	
COH E3-21	115.7	
COH E3-16	118.3	
COH F3-5	133.6	
COH F3-4	134.5	
COH F3-8	135.2	
COH F3-25	136.5	
COH F3-11	137.0	
COH F3-20	138.8	
COH F3-21	139.6	

## TABLE FOR SECTION NO. 17

DEVILS TOWER N25°W

<u>Trace</u>	<u>Distance</u>	<u>Reduced PmP Time</u>
DEV F2-17	125.3	2.44
DEV F2-21	126.7	
DEV F2-19	127.6	
DEV F2-8	129.3	
DEV F2-3	129.8	
DEV F2-4	130.8	
DEV F2-5	131.8	2.18
DEV E3-12	177.2	1.51
DEV E3-11	179.6	
DEV E3-8	180.5	
DEV E3-14	182.4	
DEV E3-6	184.7	
DEV E3-18	185.5	
DEV E3-21	186.7	
DEV E3-22	188.4	
DEV E3-20	190.3	
DEV E3-5	192.5	0.95
DEV D2-17	201.9	0.74?
DEV D2-16	202.9	
DEV D2-15	203.8	
DEV D2-20	204.9	
DEV D2-23	206.4	
DEV D2-24	207.2	
DEV D2-25	208.3	0.59?
DEV B2-17	220.2	
DEV B2-16	221.2	
DEV B2-15	222.1	
DEV B2-20	223.2	
DEV B2-8	223.9	
DEV B2-23	224.6	
DEV B2-4	225.3	
DEV B2-25	226.3	
DEV A0-13	228.1	
DEV A0-12	228.9	
DEV A0-11	229.7	
DEV A0-19	230.7	
DEV A0-3	232.2	
DEV A0-4	223.2	
DEV A0-5	234.1	
DEV B4-17	236.7	
DEV B4-16	237.5	
DEV B4-15	238.2	
DEV B4-8	239.1	
DEV B4-20	239.7	
DEV B4-23	240.8	
DEV B4-5	241.7	
DEV B4-25	242.7	

TABLE FOR SECTION NO. 17 (Cont'd)

<u>Trace</u>	<u>Distance (km)</u>	<u>Reduced PmP Time</u>
DEV D4-13	258.3	
DEV D4-12	259.2	
DEV D4-11	260.2	
DEV D4-8	261.4	
DEV D4-19	261.7	
DEV D4-3	262.8	
DEV D4-4	263.6	
DEV D4-5	264.4	
DEV F4-17	324.4	
DEV F4-16	325.3	
DEV F4-15	326.3	
DEV F4-20	327.3	
DEV F4-4	329.6	
DEV F4-25	330.4	

## TABLE FOR SECTION No. 18

## DEVILS TOWER N10°W

<u>Trace</u>	<u>Distance (km)</u>	<u>Reduced PmP Time</u>
DEV ONE	147.6	
DEV COT	187.0	
DEV MIL	197.2	
DEV CAB-4	205.8	0.45
DEV HUN	221.5	
DEV GLE	252.0	
DEV AGA	260.0	
DEV CIR	302.8	
DEV WEL	320.3	
DEV AXT-6	326.6	
DEV AXT-1	329.0	

## TABLE FOR SECTION NO. 19

## DEVILS TOWER N45°W

<u>Trace</u>	<u>Distance (km)</u>	<u>Reduced PmP Time</u>
DEV KIN-4	102.1	
DEV KIN-1	102.8	
DEV VOL	131.9	2.2
DEV GRE	156.9	
DEV HOR-6	180.7	
DEV HOR-1	182.8	
DEV CAS	191.8	
DEV MCR-6	211.9	
DEV MCR-1	213.4	
DEV FOR	219.8	
DEV SAN-5	237.9	
DEV VAN	247.5	
DEV MYE	256.3	
DEV SUM	303.3	

## TABLE FOR SECTION NO. 20

GARLAND N25°W

<u>Trace</u>	<u>Distance (km)</u>	<u>Reduced PmP Time</u>
GAR COH-6	129.3	4.18?
GAR COH-1	130.4	4.04?
GAR LAN	138.3	3.7?
GAR MAL-1	206.0	

## TABLE FOR SECTION NO. 21

HAZEL S55°W

<u>Trace</u>	<u>Distance (km)</u>	<u>Reduced PmP Time</u>
HAZ D1-8	42.7	
HAZ D1-11	43.4	
HAZ D1-3	44.5	
HAZ D1-19	45.9	
HAZ D1-20	46.9	
HAZ D1-21	47.8	
HAZ B1-9	59.0	
HAZ B18	60.0	
HAZ B1-7	61.0	
HAZ B1-4	61.8	
HAZ B1-15	63.1	
HAZ B1-20	64.5	
HAZ B1-21	65.5	
HAZ A0-9	71.5	
HAZ A0-8	72.5	
HAZ A0-11	73.6	
HAZ A0-16	75.3	
HAZ A0-19	76.0	
HAZ A0-20	77.0	
HAZ A0-21	77.9	
HAZ B3-9	79.4	
HAZ B3-8	80.3	
HAZ B3-7	81.1	
HAZ B3-12	82.5	
HAZ B3-15	83.8	
HAZ B3-16	84.6	
HAZ B3-17	85.5	
HAZ D3-9	96.2	
HAZ D3-8	97.0	
HAZ D3-7	97.9	
HAZ D3-12	99.2	
HAZ D3-15	100.5	
HAZ D3-16	101.3	
HAZ D3-17	102.2	
HAZ E3-5	111.2	
HAZ E3-4	112.6	
HAZ E3-3	114.6	
HAZ E3-2	116.9	
HAZ E3-10	118.6	
HAZ E3-22	119.8	
HAZ E3-18	121.9	
HAZ E3-19	124.8	
HAZ E3-16	126.7	
HAZ E3-21	127.6	
HAZ F3-9	170.9	
HAZ F3-8	172.0	
HAZ F3-3	173.1	
HAZ F3-24	174.8	
HAZ F3-17	175.7	
HAZ F3-20	176.4	
HAZ F3-21	177.5	

## TABLE FOR SECTION NO. 22

HAZEL S10°W

<u>Trace</u>	<u>Distance (km)</u>	<u>Reduced PmP Time</u>
HAZ E2-5	47.9	
HAZ E2-4	48.9	
HAZ E2-23	49.9	
HAZ E2-7	50.5	
HAZ E2-20	51.5	
HAZ E2-15	52.4	
HAZ E2-16	53.3	
HAZ E2-17	54.3	
HAZ D2-9	69.8	
HAZ D2-8	70.8	
HAZ D2-7	71.7	
HAZ D2-12	72.7	
HAZ D2-23	73.6	
HAZ D2-15	74.2	
HAZ D2-20	75.1	
HAZ D2-21	76.1	
HAZ HOR-1	91.6	
HAZ HOR-6	92.2	
HAZ TON	95.9	
HAZ F2-5	115.3	3.73
HAZ F2-4	116.2	
HAZ F2-3	117.1	
HAZ F2-11	118.5	
HAZ F2-19	119.7	
HAZ F2-20	120.5	
HAZ F2-21	121.4	3.52
HAZ VOL	135.5	2.95
HAZ KIN-1	144.3	2.50
HAZ KIN-4	145.5	2.44

TABLE FOR SECTION NO. 23

HAZEL N75°W

<u>Trace</u>	<u>Distance (km)</u>	<u>Reduced PmP Time</u>
HAZ E1-13	55.3	
HAZ E1-9	56.9	
HAZ E1-8	57.5	
HAZ E1-3	59.3	
HAZ E1-19	59.7	
HAZ E1-24	60.7	
HAZ E1-25	61.7	
HAZ D4-9	76.9	
HAZ D4-8	77.9	
HAZ D4-11	78.7	
HAZ D4-3	79.15	
HAZ D4-16	80.2	
HAZ D4-24	81.3	
HAZ D4-25	82.1	
HAZ D4-21	83.1	
HAZ E4-9	119.6	4.59
HAZ E4-8	120.6	
HAZ E4-12	121.6	
HAZ E4-11	122.1	
HAZ E4-24	123.4	
HAZ E4-19	124.1	
HZZ E4-20	125.1	
HAZ E4-21	125.9	4.35
HAZ F4-13	128.3	4.30
HAZ F4-12	129.3	
HAZ F4-16	130.1	
HAZ F4-15	130.6	
HAZ F4-20	132.3	4.17
HAZ F4-23	132.8	
HAZ F4-24	133.9	
HAZ F4-25	134.8	

## TABLE FOR SECTION NO. 24

HORTON N25°W

<u>Trace</u>	<u>Distance (km)</u>	<u>Reduced PmP Time</u>
HOR COH-6	105.5	
HOR COH-1	106.5	
HOR LAN	114.3	
HOR JOR	157.3	2.9
HOR MAL-6	182.1	
HOR MAL-1	181.5	

## TABLE FOR SECTION NO. 25

HORTON N25°W  
(In order of decreasing distance)

<u>Trace</u>	<u>Distance (km)</u>	<u>Reduced PmP Time</u>
HOR F4-25	148.32	3.37
HOR F4-24	147.54	
HOR F4-23	146.77	
HOR F4-20	145.29	
HOR F4-15	144.21	
HOR F4-16	143.27	3.67
HOR F4-17	142.33	
HOR D4- 5	82.92	
HOR D4- 4	82.05	
HOR D4- 3	81.19	
HOR D4- 8	79.89	
HOR D4-11	78.59	
HOR D4-12	77.72	
HOR D4-13	76.86	
HOR B4-25	61.24	
HOR B4-24	60.32	
HOR B4-23	59.39	
HOR B4- 7	57.87	
HOR B4-15	56.82	
HOR B4-16	56.02	
HOR B4-17	55.24	
HOR A0- 5	52.54	
HOR A0- 4	51.58	
HOR A0- 3	50.62	
HOR A0- 8	49.67	
HOR A0-19	48.87	
HOR A0-11	48.10	
HOR A0-12	47.39	
HOR A0-13	46.68	
HOR B2-25	44.51	
HOR B2-23	43.06	
HOR B2- 7	42.49	
HOR B2-20	41.50	
HOR B2-15	40.57	
HOR B2-16	39.60	
HOR B2-17	38.63	
HOR D2-25	27.32	
HOR D2-24	26.71	
HOR D2-23	26.12	
HOR D2- 7	26.01	
HOR D2-20	24.42	
HOR D2-15	23.78	
HOR D2-16	22.78	
HOR D2-17	21.78	

TABLE FOR SECTION NO. 26

HORTON N15°E

<u>Trace</u>	<u>Distance (km)</u>	<u>Reduced PmP Time</u>
HOR D2-17	2210	
HOR D2-16	22.9	
HOR D2-15	23.9	
HOR D2-20	24.7	
HOR D2-7	26.2	
HOR D2-4	27.5	
HOR D2-5	28.5	
HOR C2-17	40.5	
HOR C2-16	41.5	
HOR C2-15	42.5	
HOR C2-20	43.1	
HOR C2-7	44.7	
HOR C2-4	46.0	
HOR C2-5	47.0	
HOR B1-17	50.3	
HOR B1-16	51.3	
HOR B1-13	51.9	
HOR B1-20	53.1	
HOR B1-23	54.7	
HOR B1-4	55.7	
HOR B1-5	56.7	
HOR D1-21	60.6	
HOR D1-20	61.3	
HOR D1-19	62.1	
HOR D1-11	63.0	
HOR D1-25	63.9	
HOR D1-3	64.7	
HOR D1-4	65.5	
HOR D1-5	66.5	
HOR E1-17	95.9	
HOR E1-16	96.9	
HOR E1-20	97.8	
HOR E1-8	99.8	
HOR E1-9	100.3	
HOR E1-4	101.4	
HOR E1-5	102.4	
HOR F1-17	133.4	
HOR F1-16	134.3	
HOR F1-19	135.3	
HOR F1-11	135.8	
HOR F1-25	137.2	
HOR F1-3	137.7	
HOR F1-4	138.7	
HOR F1-5	139.7	

## TABLE FOR SECTION NO. 27

KEPLERVILLE S30°E

(In order of decreasing distance)

<u>Trace</u>	<u>Distance (km)</u>	<u>Reduced PmP Time</u>
KEP F2-17	190.86	1.58
KEP F2-16	189.88	
KEP F2-19	188.40	
KEP F2- 3	186.44	
KEP F2- 4	185.46	1.75
KEP F2- 5	184.53	
KEP E3-12	144.51	
KEP E3-15	143.13	
KEP E3-11	140.98	
KEP E3-14	140.21	
KEP E3-10	138.88	
KEP E3- 6	135.85	
KEP E3- 2	133.89	
KEP E3- 3	130.99	
KEP E3-24	129.14	
KEP D2-17	113.48	
KEP D2-16	112.62	
KEP D2-15	111.76	
KEP D2- 7	110.53	
KEP D2-23	109.17	
KEP D2-24	108.29	
KEP D2-25	107.42	
KEP C3-17	97.55	
KEP C3-16	96.70	
KEP C3-15	95.86	
KEP C3-20	94.51	
KEP C3-23	93.27	
KEP C3-24	92.38	
KEP C3-25	91.49	
KEP B3-17	85.73	
KEP B3-16	85.18	
KEP B3-15	84.65	
KEP B3-20	82.91	
KEP B3-22	82.36	
KEP B3-24	81.36	
KEP B3-25	80.36	
KEP C4-17	77.08	
KEP C4-16	76.16	
KEP C4-11	75.58	
KEP C4-19	74.49	
KEP C4- 3	72.99	
KEP C4- 4	72.09	
KEP C4- 5	71.19	
KEP D4-13	57.46	
KEP D4-12	56.50	
KEP D4-11	55.53	
KEP D4- 8	54.61	
KEP D4- 3	53.02	
KEP D4- 4	52.32	
KEP D4- 5	51.63	

## TABLE FOR SECTION NO. 28

KEPLERVILLE S65°E

<u>Trace</u>	<u>Distance (km)</u>	<u>Reduced PmP Time</u>
KEP E1-25	56.7	
KEP E1-24	57.7	
KEP E1-3	59.2	
KEP E1-16	60.4	
KEP E1-11	61.1	
KEP E1-12	62.1	
KEP E1-13	63.1	
KEP D1-5	86.0	
KEP D1-4	86.8	
KEP D1-3	87.5	
KEP D1-8	89.0	
KEP D1-11	90.1	
KEP D1-12	91.0	
KEP D1-13	92.0	
KEP HUN	111.2	
KEP F1-21	118.5	4.57
KEP F1-20	119.5	
KEP F1-19	120.4	
KEP F1-16	121.4	
KEP F1-3	122.3	
KEP F1-12	123.7	
KEP F1-9	124.8	4.08
KEP COT	138.3	3.9
KEP E2-25	139.3	3.82
KEP E2-24	140.3	
KEP E2-23	141.3	
KEP E2-4	142.0	
KEP E2-15	143.4	
KEP E2-17	144.3	
KEP E2-12	144.9	
KEP E2-13	145.8	3.54
KEP MIL	159.0	3.0
KEP CAB-1	175.9	2.40
KEP CAB-6	178.0	2.39

## TABLE FOR SECTION NO. 29

## KINGSLEY N30°W

<u>Trace</u>	<u>Distance (km)</u>	<u>Reduced PmP Time</u>
KIN VOL	35.2	
KIN TON	61.6	
KIN HOR-6	78.6	
KIN HOR-3	79.6	
KIN HOR-1	80.8	
KIN COH-6	184.5	1.67
KIN COH-1	185.7	1.62
KIN LAN	193.6	1.2
KIN SND	223.5	0.3
KIN MAL-6	260.6	
KIN MAL-1	261.3	

## TABLE FOR SECTION NO. 30

## KINGSLEY N30°W

<u>Trace</u>	<u>Distance(km)</u>	<u>Reduced PmP Time</u>
KIN F2-13	24.363	
KIN F2-12	25.356	
KIN F2-14	26.234	
KIN F2-18	27.873	
KIN F2- 2	28.721	
KIN F2- 3	29.688	
KIN F2- 4	30.660	
KIN D2-13	99.702	
KIN D2-12	100.595	
KIN D2-11	101.501	
KIN D2-15	102.706	
KIN D2-17	104.087	
KIN D2-18	104.908	
KIN D2-19	105.743	
KIN B2-13	117.970	
KIN B2-12	118.884	
KIN B2-11	119.827	
KIN B2-15	120.952	
KIN B2-17	122.370	
KIN B2-18	123.195	
KIN B2-19	124.007	2.99
KIN A0-10	125.782	3.12
KIN A0- 9	126.581	
KIN A0- 8	127.389	
KIN A0- 6	128.809	
KIN A0- 2	129.958	
KIN A0- 3	130.895	
KIN A0- 4	131.793	2.85
KIN B4-10	134.265	2.74
KIN B4- 9	135.197	
KIN B4-11	135.935	
KIN B4-15	137.443	
KIN B4-17	138.475	
KIN B4-18	139.417	
KIN B4-19	140.381	2.52
KIN D4-10	156.042	2.32
KIN D4- 9	156.960	
KIN D4- 8	157.889	
KIN D4- 6	159.061	
KIN D4- 2	160.462	
KIN D4- 3	161.268	
KIN D4- 4	162.077	2.13
KIN F4-13	222.275	0.53
KIN F4-12	223.211	
KIN F4-11	224.160	
KIN F4-15	225.243	
KIN F4- 5	225.628	
KIN F4- 3	227.431	
KIN F4- 4	228.357	0.40

TABLE FOR SECTION NO. 31

## KINGSLEY NORTH

<u>Trace</u>	<u>Distance (km)</u>	<u>Reduced PmP Time</u>
KIN E2-17	90.9	
KIN E2-16	91.9	
KIN E2-15	92.9	
KIN E2-20	93.8	
KIN E2-7	94.8	
KIN E2-23	95.4	
KIN E2-4	96.3	
KIN E2-5	97.3	
KIN D1-21	133.3	
KIN D1-20	133.8	
KIN D1-19	134.2	
KIN D1-8	135.9	
KIN D1-3	136.4	
KIN D1-4	137.3	
KIN D1-5	138.3	
KIN E1-13	170.4	1.51
KIN E1-12	171.1	
KIN E1-11	171.9	
KIN E1-19	172.6	
KIN E1-8	173.4	
KIN E1-3	174.4	
KIN E1-4	175.3	
KIN E1-5	176.3	1.24
KIN F1-17	187.7	0.89
KIN F1-16	188.6	
KIN F1-11	189.6	
KIN F1-19	189.9	
KIN F1-3	192.0	
KIN F1-4	193.0	
KIN F1-5	194.0	0.71

## TABLE FOR SECTION NO. 32

KINGSLEY N60°W

<u>Trace</u>	<u>Distance (km)</u>	<u>Reduced PmP Time</u>
KIN VOL	35.2	
KIN GRE	75.1	
KIN HOR-6	78.6	
KIN HOR-3	79.6	
KIN HOR-1	80.8	
KIN FOR	123.0	2.7
KIN MCR-6	135.9	2.23
KIN MCR-4	136.9	
KIN MCR-1	137.9	2.18
KIN SAN-2	144.7	1.90
KIN SAN-6	145.2	1.85
KIN VAN	151.9	
KIN MYE	169.8	
KIN SUM	208.5	

## TABLE FOR SECTION NO. 33

KINGSLEY N60°W

<u>Trace</u>	<u>Distance (km)</u>	<u>Reduced PmP Time</u>
KIN E3-13	78.7	
KIN E3-12	80.1	
KIN E3-11	81.6	
KIN E3-15	83.6	
KIN E3-10	84.5	
KIN E3-14	85.4	
KIN E3-6	86.3	
KIN E3-18	88.6	
KIN E3-2	89.4	
KIN E3-22	91.0	
KIN E3-23	94.0	
KIN E3-24	95.4	
KIN E3-25	97.1	
KIN D3-13	123.8	
KIN D3-12	124.8	
KIN D3-7	125.8	
KIN D3-15	126.4	
KIN D3-4	127.4	
KIN D3-23	128.3	
KIN D3-24	129.2	
KIN D3-25	130.2	
KIN F3-13	128.3	2.56
KIN F3-12	129.3	
KIN F3-11	130.3	
KIN F3-16	131.1	
KIN F3-3	132.3	
KIN F3-24	133.8	
KIN F3-25	134.7	2.20
KIN E4-13	162.9	1.33
KIN E4-12	163.9	
KIN E4-11	164.6	
KIN E4-16	165.6	
KIN E4-3	166.9	
KIN E4-24	168.4	
KIN E4-25	169.1	1.17

## TABLE FOR SECTION NO. 34

MALONEY HILL S25°E

(In order of decreasing distance)

<u>Trace</u>	<u>Distance (km)</u>	<u>Reduced PmP Time</u>
MAL F2-17	237.10	
MAL F2-16	236.11	
MAL F2-11	235.06	
MAL F2- 8	233.39	
MAL F2- 3	232.64	
MAL F2- 4	231.65	
MAL F2- 5	230.71	
MAL E3-12	192.02	1.59
MAL E3-15	190.61	
MAL E3-16	189.87	
MAL E3-11	188.51	
MAL E3-14	187.70	
MAL E3-10	186.40	
MAL E3-18	185.15	
MAL E3- 6	183.37	
MAL E3-22	181.89	
MAL E3- 2	181.39	
MAL E3-23	179.76	
MAL E3- 3	178.50	
MAL E3-24	176.61	
MAL E3- 5	175.58	2.13
MAL D2-17	159.94	2.71
MAL D2-16	159.04	
MAL D2-15	158.15	
MAL D2-20	156.93	
MAL D2-23	155.55	
MAL D2-24	154.72	
MAL D2-25	153.89	3.05
MAL C3-17	144.80	3.43
MAL C3-16	143.93	
MAL C3-15	143.07	
MAL C3-20	141.77	
MAL C3-23	140.47	
MAL C3-24	139.60	
MAL C3-25	138.74	3.81
MAL B3-13	134.06	4.07
MAL B3-12	133.06	
MAL B3-15	131.92	
MAL B3-20	130.21	
MAL B3-23	129.57	
MAL B3-24	128.58	
MAL B3-25	127.58	4.46
MAL C4-13	124.36	
MAL C4-12	123.56	
MAL C4-11	122.77	
MAL C4- 8	121.32	
MAL C4- 3	120.20	
MAL C4- 4	119.27	
MAL C4- 5	118.35	

TABLE FOR SECTION NO. 34 (cont'd)

<u>Trace</u>	<u>Distance (km)</u>	<u>Reduced PmP Time</u>
MAL D4-13	103.58	
MAL D4-12	102.66	
MAL D4-11	101.75	
MAL D4- 8	100.60	
MAL D4- 3	99.17	
MAL D4- 4	98.36	
MAL D4- 5	97.56	
MAL F4-17	40.82	
MAL F4-16	39.82	
MAL F4-15	38.83	
MAL F4-20	38.51	
MAL F4- 7	36.50	
MAL F4- 4	35.34	
MAL F4- 5	34.34	

## TABLE FOR SECTION NO. 35

## MALONEY HILL S50°E

<u>Trace</u>	<u>Distance (km)</u>	<u>Reduced PmP Time</u>
MAL JOR	36.4	
MAL WEL	82.3	
MAL CIR	107.8	
MAL AGA	116.1	
MAL AXT-6	124.5	3.41
MAL HAZ-1	151.3	2.56
MAL HAZ-5	153.1	2.44
MAL GLE	166.6	
MAL COT	182.0	
MAL MIL	197.1	
MAL CAB-1	210.6	0.71
MAL CAB-6	212.5	0.64

## TABLE FOR SECTION NO. 36

## MALONEY HILL S50°E

<u>Trace</u>	<u>Distance</u>	<u>Reduced PmP Time</u>
MAL E1-25	93.26	5.25?
MAL E1-24	94.26	
MAL E1-21	95.21	
MAL E1-19	95.74	
MAL E1-8	96.81	
MAL E1-11	97.65	
MAL E1-12	98.63	
MAL E1-13	99.61	5.07?
MAL D1-5	128.05	3.39
MAL D1-4	128.94	
MAL D1-3	129.76	
MAL D1-20	131.28	
MAL D1-11	132.36	
MAL D1-12	133.22	
MAL D1-13	134.08	3.17
MAL F1-21	139.58	3.05
MAL F1-20	140.41	
MAL F1-19	141.25	
MAL F1-16	142.63	
MAL F1-11	143.83	
MAL F1-12	144.74	
MAL F1-13	145.03	2.69
MAL E2-25	181.33	1.53
MAL E2-24	182.32	
MAL E2-23	183.32	
MAL E2-20	183.89	
MAL E2-15	185.64	
MAL E2-16	186.17	
MAL E2-12	186.84	
MAL E2-13	187.81	1.25

## TABLE FOR SECTION NO. 37

## MALONEY HILL S5°W

<u>Trace</u>	<u>Distance (km)</u>	<u>Reduced PmP Time</u>
MAL SND	66.7	
MAL HRS	87.1	
MAL SUM	118.0	
MAL VAN	141.3	
MAL SAN-1	155.7	3.39
MAL SAN-4	156.7	3.32
MAL FOR	157.4	
MAL MYE	170.1	
MAL MCR-6	212.3	

## TABLE FOR SECTION NO. 38

MC RAE N40°E

<u>Trace</u>	<u>Distance</u>	<u>Reduced PmP Time</u>
MCR F3-21	14.06	
MCR F3-20	14.91	
MCR F3-16	15.53	
MCR F3-24	17.10	
MCR F3-3	18.39	
MCR F3-4	19.26	
MCR F3-5	20.11	
MCR E3-21	65.55	
MCR E3-20	67.70	
MCR E3-19	68.63	
MCR E3-25	69.91	
MCR E3-23	71.18	
MCR E3-22	72.74	
MCR E3-24	74.13	
MCR E3-2	75.97	
MCR E3-3	77.44	
MCR E3-5	78.77	
MCR E3-7	81.10	
MCR E3-9	84.11	
MCR D3-17	92.67	
MCR D3-16	93.67	
MCR D3-15	94.67	
MCR D3-20	95.13	
MCR D3-7	96.93	
MCR D3-4	98.15	
MCR D3-5	99.15	
MCR B3-17	109.85	
MCR B3-16	110.83	
MCR B3-15	111.83	
MCR B3-23	114.01	
MCR B3-4	115.34	
MCR B3-5	116.33	
MCR A0-21	117.00	
MCR A0-20	117.97	
MCR A0-19	118.92	
MCR A0-11	120.71	
MCR A0-3	121.45	
MCR A0-8	122.27	
MCR A0-9	123.23	
MCR B1-21	129.33	
MCR B1-20	130.27	
MCR B1-15	131.02	
MCR B1-23	131.91	
MCR B1-12	132.53	
MCR B1-7	133.59	
MCR B1-8	134.54	
MCR B1-9	135.47	

## TABLE FOR SECTION NO. 38 (Cont'd)

MC RAE N40°E

<u>Trace</u>	<u>Distance</u>	<u>Reduced PmP Time</u>
MCR D1-21	146.14	
MCR D1-20	147.14	
MCR D1-25	148.38	
MCR D1-11	150.24	
MCR D1-4	150.98	
MCR D1-8	151.74	
MCR E1-21	167.94	
MCR E1-20	168.83	
MCR E1-19	169.70	
MCR E1-25	170.98	
MCR E1-3	172.31	
MCR E1-4	173.17	
MCR E1-5	174.02	
MCR F1-21	226.22	
MCR F1-20	227.04	
MCR F1-19	227.90	
MCR F1-11	229.13	
MCR F1-3	230.50	
MCR F1-4	231.38	

## TABLE FOR SECTION NO. 39

## MELSTONE EAST

(In order of decreasing distance)

<u>Trace</u>	<u>Distance (km)</u>	<u>Reduced PmP Time</u>
MEL E2- 9	206.63	0.85
MEL E2- 8	205.69	
MEL E2- 7	204.74	
MEL E2-15	203.05	
MEL E2-20	201.44	
MEL E2-21	200.50	1.21
MEL HUN	184.27	
MEL C2- 9	155.59	3.42
MEL C2- 8	154.74	
MEL C2- 7	153.88	
MEL C2- 4	152.56	
MEL C2-23	151.29	
MEL C2-24	150.41	3.68
MEL C2-25	149.53	
MEL B2- 9	143.23	
MEL B2- 8	142.43	
MEL B2- 4	140.99	
MEL A0-13	139.70	4.05
MEL A0-12	138.79	
MEL A0-11	137.89	
MEL A0- 3	136.42	
MEL A0-19	135.30	
MEL A0-20	134.48	
MEL A0-21	133.67	
MEL B3- 9	132.84	4.61
MEL B3- 8	131.84	
MEL B3- 7	130.85	
MEL B3- 4	130.40	
MEL B3-23	128.63	
MEL C4-13	128.01	
MEL C4-12	127.15	
MEL C4- 8	126.78	
MEL C4- 3	125.07	
MEL C4-19	123.70	
MEL C4-20	122.82	
MEL C4-21	121.95	
MEL E4- 9	86.76	7.57?
MEL E4- 8	85.76	
MEL E4- 3	84.51	
MEL E4-19	82.26	
MEL E4-20	81.26	
MEL E4-21	80.26	
		8.04?

## TABLE FOR SECTION NO. 40

## MELSTONE N60°E

<u>Trace</u>	<u>Distance (km)</u>	<u>Reduced PmP Time</u>
MEL F4-21	111.74	5.23
MEL F4-20	112.71	
MEL F4-24	113.70	
MEL F4-23	114.12	
MEL F4-12	115.62	
MEL F4-7	116.11	
MEL F4-8	117.24	
MEL F4-9	118.22	4.73
MEL D4-21	123.93	
MEL D4-20	124.91	
MEL D4-19	125.92	
MEL D4-3	127.95	
MEL D4-5	128.71	
MEL D4-8	129.38	
MEL D4-9	130.38	
MEL E1-21	154.64	
MEL E1-20	155.64	
MEL E1-19	156.61	
MEL E1-17	157.15	
MEL E1-4	158.95	
MEL E1-8	160.04	
MEL E1-9	161.05	
MEL F1-21	224.28	
MEL F1-20	225.27	
MEL F1-17	226.19	
MEL F1-16	226.68	
MEL F1-11	228.44	
MEL F1-12	228.92	
MEL F1-5	229.71	
MEL F1-9	230.77	

## TABLE FOR SECTION NO. 41

## MELSTONE S65°E

<u>Trace</u>	<u>Distance (km)</u>	<u>Reduced PmP Time</u>
MEL F3-25	103.40	
MEL F3-24	104.29	
MEL F3-3	104.92	
MEL F3-20	105.90	
MEL F3-8	106.38	
MEL F3-11	107.53	
MEL F3-12	108.42	
MEL F3-13	109.35	
MEL D3-21	114.92	
MEL D3-20	115.93	
MEL D3-24	116.54	
MEL D3-15	117.27	
MEL D3-4	118.82	
MEL D3-7	119.42	
MEL D3-8	120.42	
MEL D3-9	121.42	
MEL E3-25	131.99	
MEL E3-20	134.37	
MEL E3-21	136.55	
MEL E3-22	138.07	
MEL E3-3	138.97	
MEL E3-2	140.23	
MEL E3-16	141.18	
MEL E3-4	142.26	
MEL E3-14	143.16	
MEL E3-15	144.45	
MEL E3-9	146.93	
MEL E3-11	147.56	
MEL E3-8	148.70	
MEL E3-13	150.52	
MEL D2-25	151.05	
MEL D2-24	151.98	
MEL D2-23	152.92	
MEL D2-4	154.01	
MEL D2-15	154.56	
MEL D2-7	155.48	
MEL D2-8	156.27	
MEL D2-13	157.15	
MEL F2-5	209.99	
MEL F2-4	210.61	
MEL F2-3	211.32	
MEL F2-15	212.02	
MEL F2-9	213.15	
MEL F2-11	213.84	
MEL F2-12	214.79	
MEL F2-13	215.77	

## TABLE FOR SECTION NO. 42

SANDERS N55°E

(In order of decreasing distance)

<u>Trace</u>	<u>Distance (km)</u>	<u>Reduced PmP Time</u>
SAN F1- 5	185.04	1.98
SAN F1- 4	184.23	
SAN F1- 3	183.42	
SAN F1-11	182.39	
SAN F1-19	180.84	
SAN F1-20	179.92	
SAN F1-21	179.01	2.23
SAN CIR	170.69	2.6
SAN AGA	125.93	
SAN D1- 9	107.52	5.28
SAN D1-13	106.85	
SAN D1-12	106.19	
SAN D1-11	105.54	
SAN D1- 3	105.09	
SAN D1-19	103.09	
SAN D1-20	102.11	
SAN D1-21	101.12	5.70
SAN B1- 9	89.82	6.30
SAN B1- 8	88.82	
SAN B1- 7	87.82	
SAN B1- 4	87.39	
SAN B1-23	85.62	
SAN B1-24	85.17	
SAN B1-20	84.32	
SAN B1-21	83.32	6.62
SAN A0- 9	77.11	
SAN A0- 8	76.11	
SAN A0- 4	75.28	
SAN A0- 3	74.81	
SAN A0-16	73.23	
SAN A0-19	72.62	
SAN A0-20	71.62	
SAN A0-21	70.62	
SAN B3- 9	69.12	
SAN B3- 8	68.29	
SAN B3- 4	68.05	
SAN B3-24	66.50	
SAN B3-20	64.60	
SAN B3-21	63.80	
SAN B3-17	63.07	
SAN D3- 5	51.95	
SAN D3- 4	51.06	
SAN D3- 7	50.59	
SAN D3-23	49.35	
SAN D3-20	47.60	
SAN D3-16	47.12	
SAN D3-21	46.76	
SAN D3-17	46.26	

TABLE FOR SECTION NO. 43

SANDERS N10°E

<u>Trace</u>	<u>Distance (km)</u>	<u>Reduced Pmp Time</u>
SAN VAN	15.2	
SAN SUM	65.6	
SAN HRS	71.4	
SAN COH-1	97.2	5.43
SAN SND	97.5	
SAN COH-6	98.2	5.41
SAN LAN	100.8	
SAN JOR	149.4	3.2
SAN MAL-1	156.9	3.26
SAN MAL-6	157.3	3.18

## TABLE FOR SECTION NO. 44

## SANDERS N10°E

<u>Trace</u>	<u>Distance (km)</u>	<u>Reduced PmP Time</u>
SAN E4-17	45.02	
SAN E4-16	45.97	
SAN E4-11	46.58	
SAN E4-19	47.48	
SAN E4-8	48.56	
SAN E4-3	49.39	
SAN E4-4	50.39	
SAN E4-5	51.35	
SAN D4-17	81.34	6.20
SAN D4-16	82.22	
SAN D4-11	84.02	
SAN D4-3	85.35	
SAN D4-4	86.23	
SAN D4-5	87.11	5.90
SAN F4-17	116.03	4.92
SAN F4-16	116.99	
SAN F4-15	118.00	
SAN F4-12	118.94	
SAN F4-23	119.92	
SAN F4-4	121.42	
SAN F4-5	122.39	4.73

## TABLE FOR SECTION NO. 45

## SANDERS N80°E

<u>Trace</u>	<u>Distance (km)</u>	<u>Reduced PmP Time</u>
SAN D2-25	78.99	
SAN D2-24	79.71	
SAN D2-17	80.96	
SAN D2-4	82.00	
SAN D2-12	83.10	
SAN D2-8	83.96	
SAN D2-9	84.92	
SAN E2-21	127.61	3.45
SAN E2-20	128.63	
SAN E2-16	129.61	
SAN E2-4	131.43	
SAN E2-7	132.12	
SAN E2-8	133.10	
SAN E2-9	134.10	3.10

## TABLE FOR SECTION NO. 46

SANDERS S60°E

<u>Trace</u>	<u>Distance (km)</u>	<u>Reduced PmP Time</u>
SAN FOR	26.9	
SAN CAS	54.0	
SAN HOR-1	81.1	
SAN GRE	82.3	
SAN TON	98.8	
SAN VOL	109.9	
SAN KIN-3	144.9	2.3
SAN ONE	149.2	2.1
SAN MIL	159.8	2.0
SAN CAB-1	184.5	1.40
SAN CAB-6	186.8	1.33

## TABLE FOR SECTION NO. 47

SANDERS S70°E

<u>Trace</u>	<u>Distance (km)</u>	<u>Reduced PmP Time</u>
SAN E3-25	49.27	
SAN E3-20	51.38	
SAN E3-23	52.23	
SAN E3-22	55.28	
SAN E3-3	56.70	
SAN E3-2	57.64	
SAN E3-14	60.18	
SAN E3-6	60.93	
SAN E3-10	61.74	
SAN E3-7	62.65	
SAN E3-11	64.71	
SAN E3-8	66.15	
SAN E3-13	67.66	
SAN F2-5	127.38	2.72
SAN F2-4	127.96	
SAN F2-19	129.23	
SAN F2-8	130.24	
SAN F2-11	131.12	
SAN F2-12	132.09	
SAN F2-13	133.07	2.40

TABLE FOR SECTION NO. 48

TURNER S30°E

<u>Trace</u>	<u>Distance (km)</u>	<u>Reduced PmP Time</u>
TUR F4-5	189.04	
TUR F4-4	189.99	
TUR F4-23	190.86	
TUR F4-20	192.48	
TUR F4-15	193.39	
TUR F4-16	194.37	
TUR F4-17	195.35	
TUR D4-25	254.88	
TUR D4-24	255.79	
TUR D4-3	256.45	
TUR D4-19	257.47	
TUR D4-8	257.88	
TUR D4-11	259.01	
TUR D4-12	259.95	
TUR D4-13	260.88	
TUR B4-25	276.50	
TUR B4-24	277.47	
TUR B4-23	278.42	
TUR B4-20	279.44	
TUR B4-15	280.95	
TUR B4-12	281.73	
TUR B4-13	282.67	
TUR A0-5	285.09	
TUR A0-4	285.99	
TUR A0-3	286.92	
TUR A0-19	288.45	
TUR A0-11	289.49	
TUR A0-12	290.30	
TUR A0-13	291.11	
TUR B2-25	292.89	
TUR B2-24	293.69	
TUR B2-23	294.51	
TUR B2-20	295.94	
TUR B2-15	297.06	
TUR B2-16	298.00	
TUR B2-17	298.92	
TUR D2-25	311.17	
TUR D2-24	312.02	
TUR D2-23	312.86	
TUR D2-20	314.20	
TUR D2-15	315.46	
TUR D2-16	316.34	
TUR D2-17	317.22	
TUR F2-5	388.05	
TUR F2-4	389.00	

## TABLE FOR SECTION NO. 48 (Cont'd)

TURNER S30°E

<u>Trace</u>	<u>Distance (km)</u>	<u>Reduced PmP Time</u>
TUR F2-3	389.99	
TUR F2-19	392.05	
TUR F2-11	392.38	
TUR F2-12	392.98	
TUR F2-13	393.61	
TUR F4-5	189.04	
TUR F4-4	189.99	
TUR F4-23	190.86	
TUR F4-20	192.48	
TUR F4-15	193.39	
TUR F4-16	194.37	
TUR F4-17	195.35	
TUR D4-25	254.88	
TUR D4-24	255.79	
TUR D4-3	256.45	
TUR D4-19	257.47	
TUR D4-8	257.88	
TUR D4-11	259.01	
TUR D4-12	259.95	
TUR D4-13	260.88	
TUR B4-25	276.50	
TUR B4-24	277.47	
TUR B4-23	278.42	
TUR B4-20	279.44	
TUR B4-15	280.95	
TUR B4-12	281.73	
TUR B4-13	282.67	
TUR A0-5	285.09	
TUR A0-4	285.99	
TUR A0-3	286.92	
TUR A0-19	288.45	
TUR A0-11	289.49	
TUR A0-12	290.30	
TUR A0-13	291.11	
TUR B2-25	292.89	
TUR B2-24	293.69	
TUR B2-23	294.51	
TUR B2-20	295.94	
TUR B2-15	297.06	
TUR B2-16	298.00	
TUR B2-17	298.92	
TUR D2-25	311.17	
TUR D2-24	312.02	
TUR D2-23	312.86	
TUR D2-20	314.20	
TUR D2-15	315.46	
TUR D2-16	316.34	
TUR D2-17	317.22	

## TABLE FOR SECTION NO. 48 (Cont'd)

TURNER S30°E

<u>Trace</u>	<u>Distance (km)</u>	<u>Reduced PmP Time</u>
TUR F2-5	388.05	
TUR F2-4	389.00	
TUR F2-3	389.99	
TUR F2-19	392.05	
TUR F2-11	392.38	
TUR F2-12	392.98	
TUR F2-13	393.61	